

Dissertation
submitted to the
Combined Faculties of the Natural Sciences and Mathematics
of the Ruperto-Carola University of Heidelberg, Germany
for the degree of
Doctor of Natural Sciences

Put forward by
Sarah J. Müller
born in Buchen, Germany
Oral examination: December 11th, 2013

Electroweak Processes in Laser-Boosted Lepton Collisions

Referees: Hon.-Prof. Dr. Christoph H. Keitel
 Prof. Dr. Carlo Ewerz

Zusammenfassung

In dieser Arbeit werden verschiedene Prozesse der elektroschwachen Wechselwirkung bei relativistischen Lepton–Antilepton-Stößen in starken Laserfeldern untersucht. In einem solchen Szenario kann die Energie der vorbeschleunigten Teilchen durch deren Wechselwirkung mit dem intensiven Laserfeld deutlich erhöht werden. Den Hauptteil der vorliegenden Arbeit bildet die Untersuchung der gemeinsamen Produktion von Higgs- und Z^0 -Bosonen. Weil in typischen Laser-Experimenten hauptsächlich Laser mit zirkularer oder linearer Polarisierung verwendet werden, werden die totalen Wirkungsquerschnitte sowie die Energiespektren der erzeugten Higgs-Bosonen für beide Polarisierungen ausführlich diskutiert. Die Ergebnisse werden mit feldfreien Kollisionen vergleichbarer Stoßenergie verglichen. Besonderes Augenmerk wird auf die lineare Polarisierung gerichtet, denn dieses Szenario erweist sich als vielversprechender im Hinblick auf eine experimentelle Umsetzung. Die benötigten Laserparameter für eine solche Umsetzung sowie die zu überwindenden experimentellen Herausforderungen werden ausführlich behandelt. Als weiteres Beispiel eines Laser-beschleunigten Prozesses wird die Erzeugung von Myon-Antimyon-Paaren bei im Laserfeld stattfindenden Elektron-Positron-Stößen untersucht. Dieser Prozess ist prinzipiell mit heutiger Technologie experimentell umsetzbar und könnte daher zum Studium der dieser Arbeit zugrundeliegenden Prinzipien dienen.

Abstract

In this thesis, electroweak processes in relativistic lepton-antilepton collisions taking place inside strong laser fields are studied. The energy of the pre-accelerated particles can be vastly enhanced by their interaction with the intense laser field in such a scenario. The main effort of the investigations presented in this work lies in the examination of the associated production of Higgs and Z^0 bosons. Since laser experiments most commonly employ lasers of either circular or linear polarization, the total cross section of the reaction as well as the energy distribution of the produced Higgs boson are discussed in detail for both of these polarizations. The findings are related to field-free collisions of comparable collision energies. Special attention is paid to the linear polarization case since it is more appealing in view of an experimental implementation. The required laser parameters for such an implementation and the experimental challenges that need to be overcome are specified. As another example for a laser-boostered reaction, the production of muon-antimuon pairs in electron-positron collisions taking place in a laser field is studied. This process can in principle be experimentally realized using present-day technology and thus might serve as a proof-of-principle experiment for the concepts underlying this work.

In connection with the work on this thesis, the following article has been submitted for publication in a refereed journal:

- S. J. Müller, C. H. Keitel, and C. Müller,
Higgs Boson Creation in Laser-Boosted Lepton Collisions,
submitted to Physics Letters B.
Preprint: arXiv:1307.6751 [hep-ph]

Contents

I	Introduction and Fundamental Concepts	1
1	Motivation	3
2	History of the Higgs Boson	7
3	Notation and Units System	13
4	Charged Particles in Plane Electromagnetic Waves	17
4.1	Classical Considerations	17
4.2	Quantum Mechanical Description	20
II	Higgs Boson Creation in Lepton Collisions	23
5	Higgs Boson Creation Without a Laser Field	27
6	Higgs Boson Creation in a Circularly Polarized Laser Field	37
6.1	Analytical Calculation	37
6.1.1	Expansion of the Leptonic Current	39
6.1.2	The Differential Cross Section	41
6.1.3	The Total Cross Section	43
6.1.4	Reproduction of the Field-Free Cross Section	44
6.2	Numerical Results	47
6.2.1	Setup and Collision Momenta in the Laser Field	47
6.2.2	Maximum Cross Section	48
6.2.3	Produced Higgs Boson's Energy Distribution	48
6.2.4	Small Energy Excess	52
6.2.5	Below-Threshold Creation	53
6.3	Required Laser Parameters and other Experimental Demands	54
7	Higgs Boson Creation in a Linearly Polarized Laser Field	59
7.1	Analytical Calculation	59
7.2	Numerical Results	63
7.2.1	Partial Cross Sections	63
7.2.2	Differential Cross Sections	67
7.3	Required Laser Parameters and other Experimental Demands	69
8	Conclusion of Part II	75

III	Muon Pair Creation in Electron-Positron Collisions	77
9	Muon Pair Creation Without a Laser Field	81
10	Muon Pair Creation in a Circularly Polarized Laser Field	85
10.1	Analytical Calculation	85
10.1.1	Reproduction of the Field-Free Cross Section	90
10.2	Numerical Results	90
10.2.1	Partial Cross Sections	91
10.2.2	Differential Cross Sections	92
11	Muon Pair Creation in a Linearly Polarized Laser Field	95
11.1	Analytical Calculation	95
11.2	Numerical Results	98
11.2.1	Partial Cross Sections	99
11.2.2	Differential Cross Sections	100
12	Required Laser Parameters and Other Experimental Demands	103
13	Conclusion of Part III	105
IV	Summary and Outlook	107
V	Appendices	113
A	Feynman Rules and S-Matrix Formalism	115
B	Properties of the γ-matrices	119
C	Properties of the Bessel Functions	121
	Bibliography	127
	Acknowledgments	139

Part I

Introduction and Fundamental Concepts

Chapter 1

Motivation

Among many important achievements of the Large Hadron Collider (LHC) at CERN, the recent detection of the Higgs boson is possibly its most groundbreaking feat [ATL12b; CMS12b]. This particle has been a missing puzzle piece for the Standard Model of elementary particles for the past half century and has been sought for experimentally for the past few decades. The analysis of LHC collision data has now established the existence of a Higgs particle with a mass of $M_H \approx 125 \text{ GeV}/c^2$ [CER13]. However, further investigations of its properties are necessary in order to find out if it is indeed the Higgs boson of the Standard Model or rather a different kind of Higgs boson. High-precision measurements of a vast variety of different properties of the boson and its couplings to fundamental particles and to itself require TeV-scale lepton collisions (see also Ch. 2).

Due to limiting effects such as synchrotron radiation, such high collision energies cannot be obtained in ring accelerators, and therefore, a new generation of linear e^+e^- [ILC; CLIC] or $\mu^+\mu^-$ [Ale12] colliders is necessary. Building such large-scale facilities is very costly. In addition, the dimensions of such high-power accelerator facilities are very large. For these reasons, there is ongoing research towards alternative acceleration techniques.

In view of the ever increasing intensities and pulse energies that are attainable at modern laser facilities¹, laser acceleration appears to be a very promising candidate [Mal12]. There already exist a number of experiments on laser-plasma acceleration where a super-intense laser field generates a plasma in an atom gas or solid-state target. The wake field of the laser then induces plasma waves with very large electric fields ($\sim 100 \text{ GeV/m}$). For sufficiently large amplitudes of these plasma waves, electrons from the plasma can be accelerated with energy gradients on the GeV/cm scale [TD79]. This is three orders of magnitude larger than obtained at conventional particle accelerators. With this technique, electrons have been accelerated to GeV-order energy along a 3 cm acceleration capillary [LNG⁺06]. Such plasma waves can also be induced by particle beams instead of laser beams, as has been done in [BCD⁺07]. There, the energy of some of the electrons from a 42-GeV beam has been doubled in a meter-scale plasma wakefield accelerator. Thus,

¹Laser intensities of up to $2 \times 10^{22} \text{ W/cm}^2$ have been obtained at the HERCULES laser in Michigan [YCK⁺08], while the most powerful laser to date, the National Ignition Facility in Livermore, has reached pulse powers of up to 500 TW [NIF].

by combining the plasma-wakefield acceleration principle with existing acceleration techniques, there are good prospects to obtain comparatively compact high-power lepton colliders (see e.g. [LE09]).

Another scenario involving high-intensity lasers for lepton acceleration exploits the fact that, while traveling inside a plane electromagnetic wave, charged particles may temporarily gain vast amounts of energy [MS99]. Therefore, the center-of-mass (c.m.) energy of a lepton collision may be substantially enhanced if the collision takes place inside a laser field [HMK06; EZL98]. There have been a number of experiments studying high-energy quantum electrodynamics (QED) processes in the presence of intense laser fields [BFHS⁺97; CPK⁺99; SLS⁺06; CWB⁺09; CWM⁺10]. Detailed reviews on current state-of-the-art experiments as well as the underlying theoretical predictions can be found e.g. in [EKK09; DPMHK12]. With the very high laser intensities that are to be reached at the Extreme Light Infrastructure (ELI), a new generation of experiments involving laser-matter interactions will become possible [ELIa], allowing for studies of fundamental physics beyond the Standard Model [RRS06; Gie09; ML09; Dun09].

In this thesis, the latter laser-acceleration scheme is employed for studying different kinds of particle production processes in laser-boosted lepton collisions. Since the lepton may gain a large amount of energy while moving inside the laser field, a high collision energy can be obtained even if the *free* lepton energy, i.e. the energy the lepton has gained from conventional acceleration before entering the laser field, is comparatively small. Therefore, if the laser field is strong enough and the experimental setup fulfills certain conditions, very high collision energies can be obtained by combining powerful conventional accelerators with high-intensity lasers. Against this background we study the associated production of a Higgs and a Z^0 boson in the collision of relativistic leptons inside a plane laser wave, $\ell^+\ell^- \rightarrow HZ^0$. We investigate the total cross section for different laser polarizations and examine the effect of the laser field on the total as well as differential cross sections. Due to the large masses of the Higgs and Z^0 bosons, a very large laser pulse energy is necessary. A possible experimental realization of the studied process therefore requires further technical progress, as we will show. The QED process $e^+e^- \rightarrow \mu^+\mu^-$, i.e. the production of muon-antimuon pairs in electron-positron collisions inside a plane laser wave, could in principle be experimentally implemented with present-day technology and might serve as a proof-of-principle experiment. Therefore, we also study this process in detail and compare the laser field's effects to those found in the preceding weak interaction process.

In Ch. 2, we outline the historical cornerstones that led from the first theoretical prediction to the recent detection of the Higgs boson. After introducing the notation and units system used throughout this work in Ch. 3, we present the fundamental theoretical concepts describing the motion of charged particles in electromagnetic fields in Ch. 4 which concludes the introductory Part I.

Part II, where we examine the associated production of a Higgs and a Z^0 boson in lepton collisions, is the first main part of this thesis. After a review of the well-known field-free process $e^+e^- \rightarrow HZ^0$ in Ch. 5, we consider different setups involving laser fields. In Ch. 6, we examine the process $\ell^+\ell^- \rightarrow HZ^0$ inside a plane

laser wave of circular polarization. We investigate the same process taking place inside a laser field of linear polarization in Ch. 7. There are certain important differences between the two kinds of polarization studied in this work. While the analytical and numerical evaluation of the process in the circularly polarized field are less complex than in a linearly polarized one, the latter case may be of more relevance with regard to a possible experimental implementation. We briefly outline the conclusions of Part II in Ch. 8.

Part III is the second main part of this work, describing the production of muon-antimuon pairs in electron-positron collisions, again for different setups: like in Part II, we start by reviewing the field-free process (Ch. 9), then study the process inside a circularly polarized plane laser field (Ch. 10), and finally in a linearly polarized one (Ch. 11). We specify the required laser parameters and other experimental demands in Ch. 12 and then conclude Part III in Ch. 13.

In Part IV, we summarize the findings of this thesis and put them into perspective with respect to a possible experimental realization. In the Appendices (Part V), we list some relations and properties that are often used in this work: In Appx. A, we state the Feynman rules used in this thesis and outline the S -matrix formalism we employed. In Appx. B, we list some important properties of the Dirac matrices that are used for the evaluation of the cross sections in Parts II and III. In Appx. C, we discuss the properties of the Bessel functions occurring throughout this work and give a few notes on their numerical implementation.

Chapter 2

History of the Higgs Boson

The elementary particles constituting all visible¹ matter and the interactions between them are described by the Standard Model of particle physics [Alt05]. It contains three families of spin-1/2 particles, each consisting of a doublet of quarks, a lepton and the corresponding neutrino. The quarks – the constituents of the protons, neutrons and all other hadrons – carry electroweak as well as strong charges, while the leptons are endowed with electroweak charges only and therefore underly the electromagnetic and weak forces only. The interactions between the spin-1/2 particles are mediated by the exchange of the corresponding gauge bosons, i.e. the spin-1 vector bosons that carry the fundamental forces. They are the gluons for strong interactions, the photon for electromagnetic interactions, and the W^\pm and Z^0 bosons for weak interaction processes. The electromagnetic and weak forces are considered different aspects of the same basic force and thus united into the so-called electroweak interaction. The fact that the eight gluons (and the photon as well) are massless stems from the fact that the corresponding gauge symmetries as generated by the eight color charges (resp. the electric charge) are conserved. However, the gauge bosons of the weak interaction are very massive: the mass of the W^\pm bosons is $M_W \approx 80.4 \text{ GeV}/c^2$ and the Z^0 mass is $M_Z \approx 91.2 \text{ GeV}/c^2$. This indicates that the gauge symmetry underlying the electroweak force is broken. This spontaneous symmetry breaking and the resulting masses of the gauge bosons is governed by the Higgs mechanism which manifests in the existence of a scalar (i.e. spin-0) particle, the so-called Higgs boson. A detailed introduction into spontaneous symmetry breaking and the mechanism that supplies the fundamental particles, in particular the heavy gauge bosons, with their masses can be found e.g. in [Nac86; DGH96]. We will now give a brief overview of the historical development of the basic ideas.

The phenomenon that, in some cases, the vacuum (i.e. the lowest-energy state of a physical system) may partially lack the symmetry of the equations describing the physical system, is called *spontaneous symmetry breaking*. It was first observed in the 1950s, when superconductivity was discovered [BCS57]. In 1964, spontaneous

¹Note that the Standard Model does not contain gravitational interactions according to the General Theory of Relativity, whose influence on fundamental particle processes is negligible on the experimentally available energy scale. Therefore, it also has no concept of dark energy or matter, hence the Standard Model describes *visible* matter.

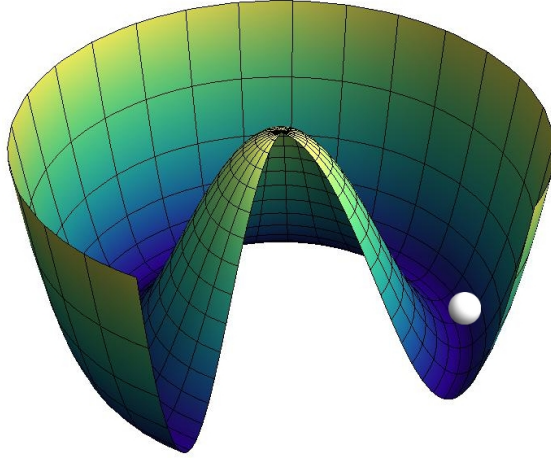
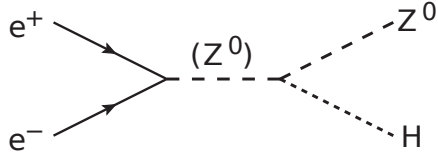


Figure 2.1: Model potential of spontaneous symmetry breaking. The vacuum corresponds to a randomly chosen point with minimal energy, i.e. at the bottom of the brim of the Mexican hat. The phase is chosen freely, and the rotation around the brim corresponds to a massless degree of freedom.

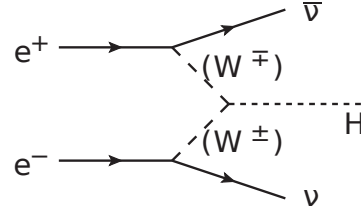
symmetry breaking of the electroweak gauge symmetry was introduced into particle physics [EB64; GHK64; Hig64a; Hig64b]. Spontaneous breaking of the $U(1)$ symmetry is commonly modeled by an effective potential of the shape of a *Mexican hat*, as can be seen in Fig. 2.1. The potential $V(\phi)$ with an arbitrary phase ϕ is unstable at the origin and has a stable minimum all around the bottom of the brim of the Mexican hat. The state of lowest energy, i.e. the vacuum, is an arbitrary point at this bottom of the brim. Rotational movement along the brim corresponds to a massless degree of freedom. The Higgs boson, a massive scalar (spin-0) particle, is associated with an oscillation in radial direction; among the 1964 papers mentioned above, [Hig64a] is the only one to explicitly postulate such a massive scalar boson. In 1967, it was first stated that this scalar field could equip the fundamental fermions with their masses [Wei67; Sal68]. The Higgs mechanism was shown to lead to a unification of the weak and electromagnetic interactions in 1971 [tH71; tHV72].

After its prediction, phenomenological descriptions of the Higgs boson, by then considered a crucial constituent of the Standard Model of particle physics, arose in the early 1970s. The first calculation of the process $e^+e^- \rightarrow HZ^0$, i.e. the associated production of a Higgs and a Z^0 boson in electron-positron collisions, was carried out in 1975 [EGN76]. At that time, the possibility of an experimental Higgs boson search seemed unrealistic to such an extent that the authors concluded their work with an apology

to experimentalists for having no idea what is the mass of the Higgs boson (...) and for not being sure of its couplings to other particles, except that they are probably all very small. For these reasons, we do not want to encourage big experimental searches for the Higgs boson, but we do feel that people doing experiments vulnerable to the Higgs boson should know how it may turn up.

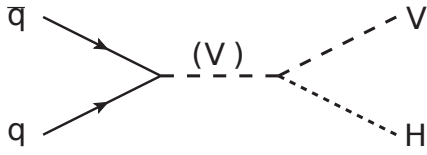


(a)

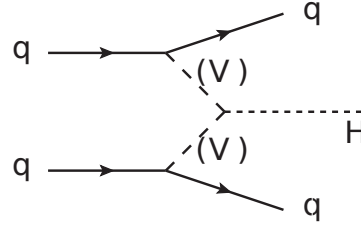


(b)

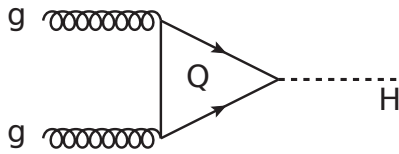
Figure 2.2: The two dominant Higgs boson creation processes in an e^+e^- collision: The Higgs-strahlung process involving the associated production of a Z^0 boson (a) and W^+W^- fusion with a neutrino pair in the final state (b).



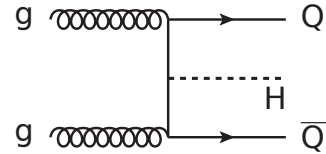
(a)



(b)



(c)



(d)

Figure 2.3: Dominant Higgs creation processes in a $\bar{p}p$ collider: associated production with a W^\pm or a Z^0 boson (denoted by “V”) (a), weak vector fusion processes (b), gluon-gluon fusion (c), and associated production with heavy top or bottom quark (“Q”) (d).

Despite this somewhat pessimistic assessment, the following decades saw a remarkable progress in accelerator physics. After discussions about building an electron-positron collider at CERN had already begun in the late 1970s, the proposal for the Large Electron-Positron Collider (LEP) was officially approved in 1981 [CER]. To date, it is the most powerful lepton collider ever built. It began operating in mid 1989 and was in use until the end of the year 2000, when it was finally shut down in order to make room for the Large Hadron Collider (LHC). At first, search for the Higgs boson was not on the primary agenda of LEP experimentalists, but from the mid 1980s onwards, CERN reports continuously included studies on this issue, for the first time in [BBB⁺86]. The LEP delivered experimental data of very high precision, confirming many of the theoretical predictions of the Standard Model. Detailed investigation of the weak gauge bosons, previously discovered at CERN in proton-antiproton collisions [UA183a; UA183b], allowed for a number of conclusions regarding different aspects of the Standard Model to be drawn [ALE06; ALE13].

In e^+e^- colliders, Higgs bosons can be produced via several processes, among which the most prominent ones correspond to the Feynman diagrams in Fig. 2.2: firstly, the so-called Higgs-strahlung, i.e. the associated production of a Higgs and a Z^0 boson via² $e^+e^- \rightarrow (Z^0) \rightarrow HZ^0$ involving a virtual Z^0 boson [EGN76; Bjo76; JP79; IK78; LQT77a; LQT77b; MO79; Fin80], and secondly the Higgs boson production via W^+W^- fusion, $e^+e^- \rightarrow \bar{\nu}\nu(W^+W^-) \rightarrow \bar{\nu}\nu H$ [JP79; CD84; DW85; AMP87; KKZ96]. Although the LEP never discovered the Higgs boson, the high-precision electroweak data it obtained vastly reduced the range of possible Higgs boson masses by establishing a lower bound of $114 \text{ GeV}/c^2$ [ALE03]. Fermilab's Tevatron collider, which after LEP's shutdown and until the LHC started operating was the leading instance in search for the Higgs boson, excluded a Higgs boson mass between 156 and 177 GeV/c^2 [CDF13]. Despite the fact that the Tevatron collider had not yet fully exploited its potential, it was shut down in 2011. During the three decades of its operation, the Tevatron made many important contributions to the progress of particle physics, among which we would like to point out the discovery of the top quark [DO 95; CDF95].

Unlike the LEP, the Tevatron was a proton-antiproton collider. The Feynman diagrams of the most dominant Higgs production processes in such a hadron collider are shown in Fig. 2.3. Figure 2.3a shows the associated production with a vector boson V , i.e. either a Z^0 or a W^\pm boson, $\bar{q}q \rightarrow (V) \rightarrow VH$ [GNY78; FGS79; EHLQ84]. In Fig. 2.3b, the weak vector boson fusion process $qq \rightarrow (VV) \rightarrow qqH$ is shown [JP79; CD84; DW85; AMP87; KKZ96]. The gluon-gluon fusion process $gg \rightarrow H$ via anomalous triangle diagrams involving heavy quarks Q as shown in Fig. 2.3c was first discussed in [GGMN78]. And finally, Fig. 2.3d shows the associated production of a Higgs boson and a top [RW79; Kun84; BEGM87; NZ84] or bottom [BHS87; OT88; DW89] quark (denoted by a capital Q because of their large mass) $gg, \bar{q}q \rightarrow \bar{Q}QH$. A review on the production channels in the different kinds of particle colliders as well as the dominant decay channels can be found in [Djo08; GHKD00].

²We mark virtual particles by parenthesizing them instead of giving them an asterisk in order to keep their upper indices denoting their electric charge.

The LHC started operating in late 2009 and produced the first 7-TeV $\bar{p}p$ collision in March 2010. From then on, the possible mass range for the Higgs boson has been continuously narrowed down, until it was established that the Higgs mass must be either between 115 and 127 GeV/ c^2 or larger than 600 GeV/ c^2 [CMS12a; ATL12a]. In mid 2012, the detection of a new particle with a mass of approximately 125 GeV/ c^2 has been confirmed by both the ATLAS and the CMS collaborations [ATL12b; CMS12b].

In the spring of 2013, it was announced that this particle is most probably a Higgs boson, as it shows Higgs boson-like properties in all the aspects that have been examined to date [CER13]. These “Higgs boson-like properties” include that the discovered particle must have zero spin and positive parity [BFMvdB04]. In addition, its interactions with other particles should coincide with theoretical predictions. The coupling between a Standard Model-like Higgs boson and a fundamental fermion must be proportional to the mass of the latter, while for the massive gauge bosons (W^\pm and Z^0), the coupling must be proportional to the square of their masses. Finally, all of these couplings must be inversely proportional to the Higgs vacuum expectation value $V \approx 246$ GeV [GHKD00].

While some of the underlying properties of the discovered particle may be deduced from LHC data [DHL⁺04], further investigation in lepton collisions is necessary for a more detailed study. The collision of two leptons such as e^+e^- or $\mu^+\mu^-$ is somewhat easier to describe than a hadron collision. In the latter case, the respective initial state of the quarks that constitute the colliding particles are not accessible, whereas the initial lepton states in the former collision are well-known. In addition, the possible final states are less complicated (cf. Figs. 2.2 and 2.3). A future linear lepton collider, like the International Linear Collider (ILC) or the Compact Linear Collider (CLIC) offers several additional opportunities [ILC; CLIC]. For instance, besides very high-precision measurements of the Higgs boson mass and its couplings to other particles, measurement of its self-coupling is possible [CLI04; CLI13]. Furthermore, a linear e^+e^- collider can be easily modified to operate in different collision schemes; for instance, by replacing the positron beam with another electron beam, one obtains an e^-e^- collider which can be converted into an $e\gamma$ or $\gamma\gamma$ collider by superposition with a laser field [GKST81; GKST83; Tel01; GKP⁺84]. In the latter case, Higgs bosons can be produced as s -channel resonance [GH93; BBC93; BZ95; DDHI98; MSK00; SRJ01]. Investigating this process offers insight into the Higgs boson’s couplings to photons and its charge–parity symmetries [Djo08]. Muon-antimuon colliders, as compared to electron-positron colliders, offer even more opportunities [BCE⁺04; BBGH97; BBGH95]. For instance, the direct coupling to the Higgs boson (without an intermediate virtual particle) is much larger than for electrons and therefore, Higgs boson production in a direct s -resonance $\mu^+\mu^- \rightarrow H$ is possible. For an overview over the Higgs production and decay mechanisms in such a $\mu^+\mu^-$ collider see [Djo08]. Like e^+e^- colliders, muon colliders can be turned into $\gamma\gamma$ colliders as well. In Part II we study a different scenario that combines a muon collider with a laser beam.

The Higgs boson discovered at the LHC is consistent with a Standard Model-like Higgs boson as far as it has been studied up to now. However, from its comparatively small mass (as compared e.g. to the mass of the top quark) arise certain problems with regard to the stability of the electroweak vacuum [EEG⁺09]. The discovered Higgs particle might in fact still be just one of e.g. five different Higgs bosons, as predicted by simple supersymmetric models [WZ74a; WZ74b]. In any case, aside from the need for further examination of the boson's compatibility with the Standard Model, it will be accompanied by some sort of new physics, be it supersymmetry [ER01], extra dimensions [CHL07], new strongly-interacting particles [Wei76] or something that has not even been thought of yet. This can only be found out about in deeper and more detailed investigations of the Higgs boson.

Chapter 3

Notation and Units System

We now constitute the notation and units system employed throughout this thesis.

Units System

Unless otherwise stated, we use natural units with $\hbar = c = 4\pi\epsilon_0 = 1$ and $e = \sqrt{\alpha}$ [PS95]. The values of these fundamental constants in SI units are [MTN08]

Fundamental Constant	Symbol	Value
Elementary Charge	e	$1.602 \times 10^{-19} \text{ C}$
Speed of Light	c	$2.998 \times 10^8 \text{ m/s}$
Planck Constant	\hbar	$1.055 \times 10^{-34} \text{ Js}$
Vacuum Permittivity	ϵ_0	$8.854 \times 10^{-12} \text{ F/m}$
Finestructure Constant	α	$1/137$

In our units system, mass and energy have the same dimension and are measured in units of eV, while the unit of time and distance is eV^{-1} . The conversion factors needed to obtain the corresponding SI units are given by

Dimension	Unit	SI Unit
Energy	eV	$1.602 \times 10^{-19} \text{ J}$
Mass	eV/c^2	$1.783 \times 10^{-36} \text{ kg}$
Momentum	eV/c	$5.344 \times 10^{-28} \text{ kg}\cdot\text{m/s}$
Time	\hbar/eV	$6.582 \times 10^{-16} \text{ s}$
Distance	$\hbar c/\text{eV}$	$1.973 \times 10^{-7} \text{ m}$

Einstein Notation

Throughout this work, Einstein summation convention [PS95] is used, i.e. wherever an index appears twice, summation over this index is implied:

$$a^\mu b_\mu = \sum_\mu a^\mu b_\mu.$$

Covariant Notation

Components of four-vectors are denoted by Greek letters, spatial components are indicated with either $\{x, y, z\}$ or $\{1, 2, 3\}$, and spatial vectors are written in bold face, $(a^\mu) = (a^0, \mathbf{a})$. Products of four-vectors are indicated by parentheses, $(ab) = a^\mu b_\mu$. We employ the metric tensor in its representation [PS95]

$$g^{\mu\nu} = \begin{pmatrix} 1 & 0 & 0 & 0 \\ 0 & -1 & 0 & 0 \\ 0 & 0 & -1 & 0 \\ 0 & 0 & 0 & -1 \end{pmatrix}.$$

With this, covariant vectors are obtained from contravariant vectors via

$$a_\mu = g_{\mu\nu} a^\nu$$

and thus, for $(a^\mu) = (a^0, \mathbf{a})$, the contravariant vector is $(a_\mu) = (a^0, -\mathbf{a})$. Thus, the four-product of a and b is given by

$$(ab) = a^\mu b_\mu = a^0 b^0 - \mathbf{a}\mathbf{b}$$

and the square of a four-vector reads

$$a^2 = a^\mu a_\mu = (a^0)^2 - |\mathbf{a}|^2.$$

The volume element of a vector \mathbf{a} is denoted by $d\mathbf{a}$ and we write ∂_μ for the partial derivative with respect to the μ -component of the spacetime coordinate. Where explicitly written down, the unit matrix is written as 1; there is no distinction between its symbol and the symbol for the number 1.

Electrodynamics

In order to avoid confusion with energies often denoted by E , we denote the electric field with \mathcal{E} . The electrodynamic four-potential is $A^\mu = (A^0, \mathbf{A})$, and the tensor of the electromagnetic field is $F^{\mu\nu} = \partial^\mu A^\nu - \partial^\nu A^\mu$. We use the Lorentz gauge [LL91], i.e.

$$(\partial A) = \partial_\mu A^\mu = 0,$$

and

$$A^0 = 0.$$

With this, the electric field is

$$\mathcal{E} = -\partial^0 \mathbf{A}.$$

With the magnetic field \mathbf{B} , the intensity I of an electromagnetic wave is given by

$$I = \frac{1}{8\pi} (\overline{\mathcal{E}^2} + \overline{\mathbf{B}^2}) = \frac{\overline{\mathcal{E}^2}}{4\pi},$$

where the overline indicates the average in time.

Dirac Formalism

The γ -matrices are used in the Dirac realization [BD64],

$$\gamma^0 = \begin{pmatrix} 1 & 0 \\ 0 & -1 \end{pmatrix}, \quad \gamma^i = \begin{pmatrix} 0 & \sigma^i \\ -\sigma^i & 0 \end{pmatrix} \quad (3.1)$$

with the Pauli matrices σ_i . Note that in the definition of γ^0 , the “1” denotes the 2x2 identity matrix. The fifth γ -matrix reads

$$\gamma^5 = i\gamma^0\gamma^1\gamma^2\gamma^3. \quad (3.2)$$

We employ Feynman slash notation for four-products of four-vectors with γ -matrices, $\gamma^\mu a_\mu = \not{a}$. For future usage, we introduce four-component vectors $\mu = (\delta_{0\mu}, \delta_{1\mu}, \delta_{2\mu}, \delta_{3\mu})$ with the Kronecker symbol $\delta_{\nu\mu}$ for which $\not{\mu} = \gamma^\nu \mu_\nu = \gamma_\mu$. Adjoint spinors (or four-vectors) $\bar{\psi}$ are defined as

$$\bar{\psi} = \psi^\dagger \gamma^0$$

and adjoint matrices are

$$\bar{\Gamma} = \gamma^0 \Gamma^\dagger \gamma^0.$$

Some major properties of the γ -matrices that are often used in this work are listed in Appx. B.

Chapter 4

Charged Particles in Plane Electromagnetic Waves

In this Chapter, we will briefly summarize the behavior of electrically charged spin-1/2 particles inside a plane electromagnetic field with the four-potential A . We will first consider the classical particle motion and then, in Sec. 4.2, outline its quantum mechanical description by the Volkov states.

4.1 Classical Considerations

Along the lines of [IZ80] and [Mül04], we will now consider the motion of a (spinless) charged elementary particle of mass m and charge $-e$ inside a monochromatic plane laser wave with the four-potential

$$A^\mu = A^\mu(\kappa) \quad (4.1)$$

which depends only on the phase $\kappa = (kx)$, with the wave vector k and the space-time coordinate x . We assume the Lorenz gauge, $(\partial A) = 0$, and $A^0 = 0$. For the sake of simplicity, we assume that the plane wave is linearly polarized and can thus be written as

$$A^\mu(\kappa) = \epsilon^\mu f(\kappa) \quad (4.2)$$

with an arbitrary function $f(\kappa)$ and a polarization vector ϵ which fulfills $\epsilon^2 = -1$. The square of the wave vector is $k^2 = (\epsilon k) = 0$ which is equivalent to the condition $(\partial A) = 0$ and signifies the transversality of the plane wave. The components of the electromagnetic field tensor are given by

$$F^{\mu\nu} = \partial^\mu A^\nu - \partial^\nu A^\mu \quad (4.3)$$

and, with (4.2), can be written as

$$F^{\mu\nu} = (k^\mu \epsilon^\nu - k^\nu \epsilon^\mu) f'(\kappa). \quad (4.4)$$

For the electric and magnetic field of the plane wave, \mathcal{E} and \mathcal{B} , respectively, follows $\mathcal{E} = -\partial^0 \mathbf{A}$ and $|\mathcal{E}| = |\mathcal{B}|$ with $\mathcal{E}\mathcal{B} = 0$.

With this, the relativistic equation of motion for an electron of charge $-e$ is

$$m \frac{du^\mu}{d\tau} = -e F_\nu^\mu u^\nu \quad (4.5)$$

with the electron's four-velocity $u^\mu = dx^\mu/d\tau$ and the proper time τ . Because of $k_\mu F^{\mu\nu} = 0$, this leads to $(ku(\tau)) = (ku(0)) = \text{constant}$. Therefore, if we choose the coordinate of the electron at $\tau = 0$ to be the origin, i.e. $x^\mu(0) = 0$, we can write $\kappa = (kx) = (ku(0))\tau$ and replace τ by κ in Eq. (4.5):

$$\frac{du^\mu}{d\kappa} = -\frac{e}{m} f'(\kappa) \left[\frac{(\epsilon u(\kappa))}{(ku(0))} k^\mu - \epsilon^\mu \right]. \quad (4.6)$$

This equation is multiplied by ϵ^μ and then integrated, resulting in

$$(\epsilon u(\kappa)) = (\epsilon u(0)) - \frac{e}{m} [f(\kappa) - f(0)]. \quad (4.7)$$

Inserted in (4.6), this leads to

$$\frac{du^\mu}{d\kappa} = -\frac{e}{m} f'(\kappa) \left\{ \left[\frac{(\epsilon u(0))}{(ku(0))} - \frac{e}{m} \frac{f(\kappa) - f(0)}{(ku(0))} \right] k^\mu - \epsilon^\mu \right\} \quad (4.8)$$

which can be integrated, yielding the velocity

$$\begin{aligned} u^\mu(\kappa) = & u^\mu(0) - \frac{e}{m} [f(\kappa) - f(0)] \left[\frac{(\epsilon u(0))}{(ku(0))} k^\mu - \epsilon^\mu \right] \\ & + \frac{e^2}{2m^2} [f(\kappa) - f(0)]^2 \frac{k^\mu}{(ku(0))}. \end{aligned} \quad (4.9)$$

Under the assumption that for $\kappa \rightarrow \infty$, the wave is damped adiabatically, $f(\infty) = 0$, we find the asymptotic velocity

$$u^\mu(\infty) = u^\mu(0) - \frac{e}{m} f(0) \epsilon^\mu + \frac{e}{m} \left[f(0) \frac{(\epsilon u(0))}{(ku(0))} + \frac{e}{2m} \frac{f^2(0)}{(ku(0))} \right] k^\mu. \quad (4.10)$$

As an example, we consider a linearly polarized wave with $f(\kappa) = a \sin \kappa$ and integrate (4.9) in order to obtain x^μ ,

$$\begin{aligned} x^\mu(\kappa) = & u^\mu(0)\tau + 2 \frac{ea \sin^2 \kappa/2}{m (ku(0))} \epsilon^\mu \\ & - \frac{ea}{m (ku(0))^2} \left\{ 2(\epsilon u(0)) \sin^2 \frac{\kappa}{2} - \frac{e^2 a^2}{2m} (2\kappa - \sin(2\kappa)) \right\}. \end{aligned} \quad (4.11)$$

The first term in (4.11) corresponds to the free electron motion without the electromagnetic wave. The second term describes its oscillations along the polarization direction of the field. The non-periodic part of the third term corresponds to a drift in the propagation direction of the electromagnetic wave. Besides this drift, the electron undergoes oscillations in that direction. Without the drift motion, the superposition of the oscillations in the polarization and propagation directions of the electromagnetic wave describe a figure-8 motion. If the particle is initially at

rest, $u^\mu(0) = (1, 0, 0, 0)$, its trajectory inside the laser field is confined to the plane spanned by the directions of \mathbf{k} and $\boldsymbol{\epsilon}$. The amplitude of the oscillation in the direction of $\boldsymbol{\epsilon}$ is given by $ea/m\omega$ with the angular frequency ω of the electromagnetic wave. The amplitude of the oscillation along the wave's propagation direction is proportional to $e^2 a^2 / 2m^2 \omega$. For comparison, we note that inside an electromagnetic wave of circular polarization, the electron travels along a circular-shaped trajectory in the plane perpendicular to the propagation direction of the wave. The radius of this circle is $ea/m\omega$ [Nol93].

With the Lagrangian $L = -m + e(Au)$ and Eqs. (4.9) and (4.10), we can write for the classical action

$$\begin{aligned} S(\kappa) &= \int_0^\tau d\tilde{\tau} L \\ &= \int_0^\kappa \frac{d\tilde{\kappa}}{(ku(0))} \left\{ -m + ef(\tilde{\kappa}) \left((\epsilon u(0)) - \frac{e}{m} [f(\tilde{\kappa}) - f(0)] \right) \right\} \\ &= -m(u(\infty)x) + \int_0^\kappa \frac{d\tilde{\kappa}}{(ku(\infty))} \left\{ e(A(\tilde{\kappa})u(\infty)) + \frac{e^2}{2m} A^2(\tilde{\kappa}) \right\}. \end{aligned} \quad (4.12)$$

In the last step, (4.10) has been used under the assumption that $f(\infty) = 0$, leading to

$$(u(\infty)x) = \frac{1}{(ku(0))} \int_0^\kappa d\tilde{\kappa} (u(\infty)u(\tilde{\kappa})) = \frac{\kappa}{(ku(0))} - \frac{e^2}{2m^2} \int_0^\kappa d\tilde{\kappa} \frac{A^2(\tilde{\kappa})}{(ku(\infty))}. \quad (4.13)$$

The conjugate momentum of the electron is given by

$$p^\mu = \partial^\mu S(\kappa) = mu^\mu(\infty) - \frac{k^\mu}{(ku(0))} \left[e(A(\kappa)u(\infty)) - \frac{e^2}{2m} A^2(\kappa) \right]. \quad (4.14)$$

The asymptotic momentum $mu(\infty)$ is the momentum of the electron after leaving the electromagnetic wave.

The short-time oscillatory movements of the electron can be averaged over so that one obtains an effective momentum q^μ . In periodic fields, the time average over A is $\overline{A} = 0$ and therefore the quasi-momentum reads

$$q^\mu = \overline{p^\mu} = mu^\mu(\infty) - \frac{e^2 \overline{A^2}}{2m(ku(\infty))} k^\mu. \quad (4.15)$$

The invariant effective mass m_* corresponding to this effective momentum is given by $q^2 = m^2 - e^2 \overline{A^2}$. With the dimensionless intensity parameter¹

$$\xi := \frac{e}{m} \sqrt{-\overline{A^2}}, \quad (4.16)$$

the effective mass can be expressed as

$$m_* = m \sqrt{1 + \xi^2}. \quad (4.17)$$

¹Note that we set $A^0 = 0$ and therefore $-A^2 = \mathbf{A}^2 > 0$.

Note that the validity of the expressions for the classical action (4.12), for the effective momentum (4.15), and for the effective electron mass (4.17) is independent of the polarization of the electromagnetic wave (4.1).

4.2 Quantum Mechanical Description

We now study the behavior of an electron in a plane electromagnetic wave from a quantum mechanical point of view following [IZ80; LL91]. The electron state Ψ must solve the Dirac equation

$$(i\partial\!\!\!/ + e\mathcal{A} - m)\Psi = 0 \quad (4.18)$$

with the wave's four-potential $A^\mu(\kappa)$ from Eq. (4.2). Like in § 40 of [LL91], we consider solutions to the second-order Dirac equation

$$(i\partial\!\!\!/ + e\mathcal{A} + m)(i\partial\!\!\!/ + e\mathcal{A} - m)\Psi = (-\partial^2 + 2ie(A\partial) + e^2 A^2 - m^2 + ie\not{k}\mathcal{A}')\Psi = 0 \quad (4.19)$$

and later omit those solutions that do not solve (4.18). The prime denotes the derivative with respect to $d\kappa$. We now make the ansatz

$$\Psi_p = e^{-i(p x)} \varphi_p(\kappa) \quad (4.20)$$

with a constant four-vector p^μ satisfying $p^2 = m^2$. Inserting this ansatz in (4.19) leads to

$$2i(kp)\varphi_p' + [2e(pA) + e^2 A^2 + ie\not{k}\mathcal{A}']\varphi_p = 0 \quad (4.21)$$

for the function φ_p . Integration gives

$$\varphi_p(\kappa) = N_p \exp\left(\frac{ie}{(kp)} \int^\kappa d\tilde{\kappa} \left[(pA(\tilde{\kappa})) + \frac{e}{2} A^2(\tilde{\kappa})\right]\right) \exp\left(-\frac{e}{2(kp)} \not{k}\mathcal{A}\right) w_p \quad (4.22)$$

with a normalization factor N_p and a spinor w_p that will be determined later on. The Lorenz gauge condition leads to the relations

$$(\not{k}\mathcal{A})^2 = 2(kA)\not{k}\mathcal{A} - \not{k}^2 A^2 = k^2 A^2 = 0. \quad (4.23)$$

Therefore, the second exponential function in (4.22) can be written as

$$\exp\left(-\frac{e}{2(kp)} \not{k}\mathcal{A}\right) = 1 - \frac{e}{2(kp)} \not{k}\mathcal{A}. \quad (4.24)$$

The requirement that for vanishing electromagnetic field, the wave function (4.20) must solve the free Dirac equation, determines the spinor w_p and disposes of solutions to (4.19) which do not solve (4.18). The spinor $w_p = u(p, s)$ must therefore be a free Dirac spinor corresponding to the momentum p and spin projection s (A.1). With this, we find the solution to the Dirac equation (4.18)

$$\Psi_p = \Psi_{p,s}^{(-)} = N_p \left(1 - \frac{e\not{k}\mathcal{A}}{2(kp)}\right) u(p, s) e^{iS^{(-)}} \quad (4.25)$$

with

$$S^{(-)} = -(px) + \frac{e}{(kp)} \int^{\kappa} d\tilde{\kappa} \left[(pA(\tilde{\kappa})) + \frac{e}{2} A^2(\tilde{\kappa}) \right] \quad (4.26)$$

which, for $p^\mu = mu^\mu(\infty)$ from Eq. (4.10), corresponds to the classical action (4.12).

The solutions (4.25) of the Dirac equation in a plane electromagnetic wave have first been calculated by Volkov in 1935 [Vol35] and are therefore called Volkov states. The Volkov state for a positron inside the electromagnetic wave is obtained by replacing p^μ by $-p^\mu$ and $u(p, s)$ by $v(p, s)$:

$$\Psi_{p,s}^{(+)} = N_p \left(1 + \frac{e\not{A}}{2(kp)} \right) v(p, s) e^{iS^{(+)}} \quad (4.27)$$

with

$$S^{(+)} = (px) + \frac{e}{(kp)} \int^{\kappa} d\tilde{\kappa} \left[(pA(\tilde{\kappa})) - \frac{e}{2} A^2(\tilde{\kappa}) \right]. \quad (4.28)$$

The current density j^μ [BD64] corresponding to the electronic Volkov state (4.25) reads

$$j^\mu = \bar{\Psi}_{p,s}^{(-)} \gamma^\mu \Psi_{p,s}^{(-)} = |N_p|^2 \left(p^\mu + eA^\mu - e \left[\frac{(pA)}{(kp)} + \frac{e}{2} \frac{A^2}{(kp)} \right] k^\mu \right). \quad (4.29)$$

Its time average is

$$\bar{j}^\mu = |N_p|^2 \left(p^\mu - \frac{e^2 \overline{A^2}}{2(kp)} k^\mu \right). \quad (4.30)$$

We can therefore, like in the classical case, associate the electron motion inside the electromagnetic wave with an effective momentum

$$q^\mu = p^\mu - \frac{e^2 \overline{A^2}}{2(kp)} k^\mu = p^\mu + \frac{m^2 \xi^2}{2(kp)} k^\mu \quad (4.31)$$

and an effective mass $m_* = m\sqrt{1 + \xi^2}$ with ξ from Eq. (4.16). Eq. (4.31) also holds for the positronic states (4.27). The energy difference

$$E_{\text{pond}} := q^0 - p^0 \quad (4.32)$$

is called *ponderomotive energy*. In the non-relativistic limit, it is $E_{\text{pond}} \approx -e^2 \overline{A^2}/2m$. The effective energy and momentum are related in the usual way,

$$(q^0)^2 = \mathbf{q}^2 + m_*^2. \quad (4.33)$$

We now set the normalization constant to

$$N_p = \sqrt{\frac{1}{2Vq^0}} \quad (4.34)$$

with the effective momentum (4.31) and a unit volume V . With this choice, the 0-component of the current density is normalized to $\bar{j}^0 = 1/V$ and the normalization of the Volkov states leads to

$$\int d^3\mathbf{x} (\Psi_{p,s}^{(\pm)})^\dagger \Psi_{p',s}^{(\pm)} = \int d^3\mathbf{x} \bar{\Psi}_{p,s}^{(\pm)} \gamma^0 \Psi_{p',s}^{(\pm)} = \frac{(2\pi)^3}{V} \delta(\mathbf{p} - \mathbf{p}'). \quad (4.35)$$

The Volkov states, being solutions of the (time-dependent) Dirac equations, are not stationary states; in particular, their energy is not a good quantum number. For an electromagnetic wave propagating in z -direction, it can be shown that the Volkov states are eigenstates to the operators $i\partial_x$, $i\partial_y$, and $i(\partial^0 - \partial_z)$. Therefore, the good quantum numbers are p_x , p_z , and the difference $p^0 - p_z$, in accordance with (4.14).

Part II

Higgs Boson Creation in Lepton Collisions

In this part, we will present our calculations and numerical results for the process $\ell^+\ell^- \rightarrow HZ^0$ for different setups. Here, the ℓ^\pm denote leptons and can be either muon and antimuon or electron and positron. In the first chapter of this part, we re-derive the well-known cross section for the process $\ell^+\ell^- \rightarrow HZ^0$ without a laser field and briefly summarize its main properties. In the following chapters, we investigate the same process inside a laser field of circular (Ch. 6) and linear (Ch. 7) polarization. In Ch. 8, we briefly summarize the findings of this part.

Where ambiguities are possible, we will specify physical quantities with an index ff, c, or l, referring to a field-free, circularly polarized or linearly polarized setup, respectively. However, for the sake of better readability, we will mostly omit these indices where it is clear that the quantities refer to the setup of the respective chapter.

Chapter 5

Higgs Boson Creation Without a Laser Field

In this chapter, we calculate the cross section for the associated creation of a Higgs boson and a Z^0 boson in an e^+e^- collision without a laser field and briefly summarize the results. This process is well-understood and can be found in many textbooks, e.g. in [DGH96]. However, the crucial techniques employed in the derivation of its cross section re-occur in all the other calculations treated in this work, and therefore, it is presented in great detail here.

Following the standard procedure as found e.g. in [Nac86], one can derive the Feynman diagram of Fig. 5.1. We consider a symmetric setup where the momenta of the incoming electron and positron are

$$p_- = (E, 0, 0, E), \quad p_+ = (E, 0, 0, -E), \quad (5.1)$$

respectively. Note that, since the created bosons have very large masses and therefore the lepton energy E has to be very large, the electron mass m may be neglected. The c.m. energy is $\sqrt{s} = \sqrt{(p_+ + p_-)^2} = 2E$. We assume that \sqrt{s} vastly exceeds the Z^0 resonance so that the finite decay width of the Z^0 boson is negligible. Along the lines of Appxs. B and G of [Nac86], we can now describe the

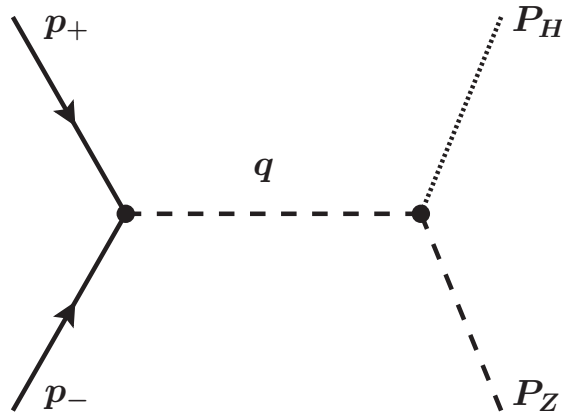


Figure 5.1: Feynman graph of the process $\ell^+ \ell^- \rightarrow H Z^0$.

particles and vertices in momentum space (cf. Appx. A). The electron and positron are described by free Dirac spinors $u_- = u(p_-, s_-)$ and $u_+ = v(p_+, s_+)$ as described in Ch. 3, depending on the four-momenta p_\pm and spins s_\pm , respectively. The Z^0 boson is given by a polarization state $\epsilon(P_Z)$ depending on its four-momentum P_Z . Since the Higgs boson is a scalar particle, it is represented by 1. The lepton vertex reads

$$\frac{-ig}{2 \cos \theta_W} (g_V \gamma^\mu - g_A \gamma^\mu \gamma^5), \quad (5.2)$$

where $g = e/\sin \theta_W$ is the weak coupling constant with the Weinberg angle θ_W and g_V and g_A are the weak neutral coupling constants (cf. Appx. A). The boson vertex is

$$\frac{igM_Z g^{\nu\rho}}{\cos \theta_W} \quad (5.3)$$

with the mass M_Z of the Z^0 boson and the metric tensor $g^{\mu\rho}$. The propagator of the virtual Z^0 boson that propagates between the two vertices is given in Appx. A. We now obtain the transition amplitude \mathcal{T} in momentum space

$$\mathcal{T} = \underbrace{\bar{u}_+}_{e^+} \underbrace{\frac{-ig}{2 \cos \theta_W} (g_V \gamma^\mu - g_A \gamma^\mu \gamma^5)}_{e^+ e^- \text{ vertex}} \underbrace{u_-}_{e^-} \underbrace{\frac{-4\pi i g_{\mu\nu} + \frac{4\pi i q_\mu q_\nu}{M_Z^2}}{q^2 - M_Z^2}}_{\text{virtual } Z^0 \text{ boson}} \underbrace{1}_H \underbrace{\frac{igM_Z g^{\nu\rho}}{\cos \theta_W}}_{ZH \text{ vertex}} \underbrace{\epsilon_\rho^*(P_Z)}_{Z^0}, \quad (5.4)$$

with the virtual Z^0 boson's momentum $q = p_+ + p_- = (2E, 0, 0, 0)$.

All terms in Eq. (5.4) that are of order m/\sqrt{s} , m/M_Z , or m/M_H , M_H being the Higgs boson mass, can be neglected. We now consider

$$\bar{u}_+ \gamma^\mu (g_V - g_A \gamma^5) u_- q_\mu = \bar{u}_+ \not{q} (g_V - g_A \gamma^5) u_- \quad (5.5)$$

from the second summand in the Z^0 propagator. From Eqs. (A.2) and (A.3) follows

$$\begin{aligned} \bar{u}_+ \not{p}_+ &= \not{p}_+ \bar{u}_+ = -m \bar{u}_+, \\ \not{p}_- u_- &= m u_-. \end{aligned} \quad (5.6)$$

Therefore, we can neglect

$$\begin{aligned} \bar{u}_+ \not{q} (g_V - g_A \gamma^5) u_- &= g_V (\bar{u}_+ \not{p}_+ u_- + \bar{u}_+ \not{p}_- u_-) \\ &\quad - g_A (\bar{u}_+ \not{p}_+ \gamma^5 u_- + \bar{u}_+ \not{p}_- \gamma^5 u_-) \\ &= -g_A (\bar{u}_+ \not{p}_+ \gamma^5 u_- - \bar{u}_+ \gamma^5 \not{p}_- u_-) \\ &= 2g_A m \bar{u}_+ \gamma^5 u_- \sim \mathcal{O}(m). \end{aligned} \quad (5.7)$$

With this, we find the transition amplitude in momentum space to be

$$\begin{aligned} \mathcal{T} &= \frac{g^2 M_Z}{2 \cos^2 \theta_W} [\bar{u}_+ \gamma^\mu (g_V - g_A \gamma^5) u_-] \frac{-4\pi i g_{\mu\nu} g^{\nu\rho}}{q^2 - M_Z^2} \epsilon_\rho^*(P_Z) \\ &= \frac{2\pi g^2 M_Z}{\cos^2 \theta_W} [\bar{u}_+ \gamma^\mu (g_V - g_A \gamma^5) u_-] \frac{-i \delta_{\mu\rho}}{q^2 - M_Z^2} \epsilon_\rho^*(P_Z) \\ &= \frac{-2\pi i g^2 M_Z}{\cos^2 \theta_W} \frac{1}{q^2 - M_Z^2} [\bar{u}_+ \not{\epsilon}^*(P_Z) (g_V - g_A \gamma^5) u_-]. \end{aligned} \quad (5.8)$$

From this, the differential cross section can be derived by averaging the square of the amplitude over the incoming leptons' spins and summing it over the outgoing Z^0 boson's polarization. Instead, we will now consider the transition amplitude in position space and derive the cross section from that, so that the calculation is compared more easily with the one inside a laser field in the following chapters.

The transition amplitude \mathcal{S} in position space is given by

$$\begin{aligned} \mathcal{S} = & \frac{-ig}{2 \cos \theta_W} \iiint \frac{1}{2V \sqrt{p_+^0 p_-^0}} \bar{u}_+ \gamma_\mu (g_V - g_A \gamma_5) u_- e^{-i(p_+ + p_-)x} \\ & \cdot \frac{4\pi e^{iq(x-y)} - ig^{\mu\nu} + \frac{iq^\mu q^\nu}{M_Z^2}}{(2\pi)^4 \quad q^2 - M_Z^2} \\ & \cdot \frac{ig M_Z g_{\nu\rho}}{\cos \theta_W} \frac{1}{2V \sqrt{E_Z E_H}} \epsilon_\rho^*(P_Z) e^{i(P_Z + P_H)y} d^4 q d^4 x d^4 y, \end{aligned} \quad (5.9)$$

where the first line describes the electron-positron vertex, the second line is the propagator of the virtual Z^0 boson and the third line is for the outgoing particles. V denotes an arbitrary normalization volume. The integrations over the spacetime coordinates x and y for the leptons and bosons, respectively, can be performed yielding four-dimensional δ -functions:

$$\begin{aligned} \int d^4 x e^{i(q - p_+ - p_-)x} \int d^4 y e^{-i(q - P_Z - P_H)y} &= (2\pi)^4 \delta(q - p_+ - p_-) (2\pi)^4 \delta(q - P_Z - P_H) \\ &= (2\pi)^8 \delta(q - p_+ - p_-) \delta(p_+ + p_- - P_Z - P_H) \end{aligned} \quad (5.10)$$

where we made use of the relation [BD64]

$$\delta(a - b) \delta(a + c) = \delta(a - b) \delta(b + c). \quad (5.11)$$

This allows for the integration over the virtual Z^0 boson's momentum q to be performed. With $p_\pm^0 = E$, $q_0 = p_+ + p_-$ and $(q_0)^2 = s$, the transition amplitude becomes

$$\begin{aligned} \mathcal{S} &= \frac{i(2\pi)^5 g^2 M_Z}{4V^2 E \cos^2 \theta_W \sqrt{E_Z E_H}} \bar{u}_+ \gamma_\mu (g_V - g_A \gamma_5) u_- \frac{\frac{q^\mu q^\nu}{M_Z^2} - g^{\mu\nu}}{(s - M_Z^2)} \epsilon_\nu^*(P_Z) \delta(q_0 - P_Z - P_H) \\ &= \frac{-i(2\pi)^5 g^2 M_Z}{4V^2 E \cos^2 \theta_W \sqrt{E_Z E_H} (s - M_Z^2)} \bar{u}_+ \not{\epsilon}^*(P_Z) (g_V - g_A \gamma_5) u_- \delta(q_0 - P_Z - P_H), \end{aligned} \quad (5.12)$$

where we again neglected the $q^\mu q^\nu$ term in the virtual Z^0 boson's propagator (cf. Eq. (5.7)). In order to obtain a cross section, the square of the transition amplitude has to be averaged over the initial spins and summed over the outgoing polarizations, divided by a time unit¹ τ and the incoming particle flux $|\mathbf{j}|$, and finally integrated

¹Please note that we denote the unit time with the symbol τ in order to avoid ambiguities with the trace product T_n occurring in the following. It is not to be confused with the proper time we briefly used in Ch. 4.

over the final particles' momenta,

$$d^6\sigma = \frac{1}{4} \sum_{\text{pol. spins}} \sum_{\mathbf{j}} \frac{|\mathcal{S}|^2}{\tau|\mathbf{j}|} \frac{V d^3\mathbf{P}_Z}{(2\pi)^3} \frac{V d^3\mathbf{P}_H}{(2\pi)^3}. \quad (5.13)$$

With the abbreviation $\Gamma := \bar{u}_+ \not{\epsilon}^*(P_Z)(g_V - g_A \gamma_5)u_-$, we find the spin and polarization sum

$$t_0 := \sum_{\text{pol. spins}} \sum_{\text{pol. spins}} |\Gamma|^2 = [\bar{u}_+ \not{\epsilon}^*(P_Z)(g_V - g_A \gamma_5)u_-] [\bar{u}_+ \not{\epsilon}^*(P_Z)(g_V - g_A \gamma_5)u_-]^\dagger \quad (5.14)$$

with

$$\begin{aligned} [\bar{u}_+ \not{\epsilon}^*(P_Z)(g_V - g_A \gamma_5)u_-]^\dagger &= u_-^\dagger (g_V - g_A \gamma_5) \not{\epsilon}^{\dagger}(P_Z) \bar{u}_+^\dagger \\ &= u_-^\dagger \gamma^0 \gamma^0 (g_V - g_A \gamma_5) \gamma^0 \gamma^0 \not{\epsilon}^{\dagger}(P_Z) \gamma^0 \gamma^0 \bar{u}_+^\dagger \\ &= \bar{u}_- (g_V - g_A \gamma^0 \gamma^5 \gamma^0) \not{\epsilon}(P_Z) u_+ \\ &= \bar{u}_- (g_V + g_A \gamma^5) \not{\epsilon}(P_Z) u_+. \end{aligned} \quad (5.15)$$

The evaluation of Eq. (5.14) is very crucial and similar summations will occur again in the following chapters. Therefore, it shall be carried out in detail here. We can write down the right-hand side of (5.14) component-by-component,

$$\begin{aligned} t_0 &= \sum_{\text{pol. spins}} \sum_{\text{pol. spins}} |\Gamma|^2 = \bar{u}_+ \not{\epsilon}^*(P_Z)(g_V - g_A \gamma_5)u_- \bar{u}_- (g_V + g_A \gamma^5) \not{\epsilon}(P_Z) u_+ \\ &= \sum_{\text{pol. spins}} \sum_{\text{pol. spins}} (\bar{u}_+)_\alpha (\not{\epsilon}^*(P_Z)(g_V - g_A \gamma_5))_{\alpha\beta} (u_-)_\beta (\bar{u}_-)_{\beta'} ((g_V + g_A \gamma^5) \not{\epsilon}(P_Z))_{\beta'\alpha'} (u_+)_{\alpha'}, \end{aligned} \quad (5.16)$$

and with Eqs. (A.4) and (A.5), we find

$$\begin{aligned} t_0 &= \sum_{\text{pol.}} \sum_{s_+} (\bar{u}_+)_\alpha \left(\not{\epsilon}^*(P_Z)(g_V - g_A \gamma_5) \right)_{\alpha\beta} (\not{p}_- - m)_{\beta\beta'} \left((g_V + g_A \gamma^5) \not{\epsilon}(P_Z) \right)_{\beta'\alpha'} (u_+)_{\alpha'} \\ &= \sum_{\text{pol.}} \sum_{s_+} (\bar{u}_+)_\alpha \left(\not{\epsilon}^*(P_Z)(g_V - g_A \gamma_5) \right)_{\alpha\beta} \left((\not{p}_- - m)(g_V + g_A \gamma^5) \not{\epsilon}(P_Z) \right)_{\beta\alpha'} (u_+)_{\alpha'} \\ &= \sum_{\text{pol.}} \sum_{s_+} \left(\not{\epsilon}^*(P_Z)(g_V - g_A \gamma_5) (\not{p}_- - m)(g_V + g_A \gamma^5) \not{\epsilon}(P_Z) \right)_{\alpha\alpha'} (\bar{u}_+)_\alpha (u_+)_{\alpha'} \\ &= \sum_{\text{pol.}} \left(\not{\epsilon}^*(P_Z)(g_V - g_A \gamma_5) (\not{p}_- - m)(g_V + g_A \gamma^5) \not{\epsilon}(P_Z) \right)_{\alpha\alpha'} (\not{p}_+ + m)_{\alpha'\alpha} \\ &= \sum_{\text{pol.}} \text{tr} \left(\not{\epsilon}^*(P_Z)(g_V - g_A \gamma_5) (\not{p}_- - m)(g_V + g_A \gamma^5) \not{\epsilon}(P_Z) (\not{p}_+ + m) \right) \\ &= \sum_{\text{pol.}} \text{tr} \left(\not{\epsilon}^*(P_Z)(g_V - g_A \gamma_5) \not{p}_- (g_V + g_A \gamma^5) \not{\epsilon}(P_Z) \not{p}_+ \right), \end{aligned} \quad (5.17)$$

where in the last step, we neglected all terms of order m and m^2 . Further, t_0

becomes

$$\begin{aligned}
t_0 &= \sum_{\text{pol.}} \left(g_V^2 \text{tr} \left(\not{\epsilon}^*(P_Z) \not{p}'_- \not{\epsilon}(P_Z) \not{p}'_+ \right) - g_A^2 \text{tr} \left(\not{\epsilon}^*(P_Z) \gamma^5 \not{p}'_- \gamma^5 \not{\epsilon}(P_Z) \not{p}'_+ \right) \right. \\
&\quad \left. - g_V g_A \text{tr} \left(\not{\epsilon}^*(P_Z) \gamma^5 \not{p}'_- \not{\epsilon}(P_Z) \not{p}'_+ \right) + g_V g_A \text{tr} \left(\not{\epsilon}^*(P_Z) \not{p}'_- \gamma^5 \not{\epsilon}(P_Z) \not{p}'_+ \right) \right) \\
&= \sum_{\text{pol.}} \left((g_V^2 + g_A^2) \text{tr} \left(\not{\epsilon}^*(P_Z) \not{p}'_- \not{\epsilon}(P_Z) \not{p}'_+ \right) - 2g_V g_A \text{tr} \left(\not{\epsilon}^*(P_Z) \gamma^5 \not{p}'_- \not{\epsilon}(P_Z) \not{p}'_+ \right) \right), \tag{5.18}
\end{aligned}$$

where the facts that γ^5 anti-commutes with the other γ -matrices and that $(\gamma^5)^2 = 1$ have been used (cf. Appx. B).

We now use Eq. (A.6) and the calculation rules for traces over γ -matrices from Appx. B and consider the polarization sum over the second trace in Eq. (5.18).

$$\begin{aligned}
\sum_{\text{pol.}} \text{tr} \left(\not{\epsilon}^*(P_Z) \gamma^5 \not{p}'_- \not{\epsilon}(P_Z) \not{p}'_+ \right) &= \sum_{\text{pol.}} \text{tr} \left(\gamma_5 \gamma_\mu \gamma_\nu \gamma_\sigma \gamma_\rho \right) p_-^\mu \epsilon^\nu(P_Z) p_+^\sigma \epsilon^{*\rho}(P_Z) \\
&= \sum_{\text{pol.}} \left(-4i \varepsilon_{\mu\nu\sigma\rho} p_-^\mu \epsilon^\nu(P_Z) p_+^\sigma \epsilon^{*\rho}(P_Z) \right) \\
&= -4i \varepsilon_{\mu\nu\sigma\rho} p_-^\mu p_+^\sigma \left(-g^{\nu\rho} + \frac{P_Z^\nu P_Z^\rho}{M_Z^2} \right) \\
&= -4i \varepsilon_{\mu\nu\sigma\rho} p_-^\mu p_+^\sigma \frac{P_Z^\nu P_Z^\rho}{M_Z^2} = 0 \tag{5.19}
\end{aligned}$$

due to the symmetry of $P_Z^\nu P_Z^\rho$ and the antisymmetry of $\varepsilon_{\mu\nu\sigma\rho}$. The polarization sum over the remaining trace in Eq. (5.18) yields

$$\begin{aligned}
t_0 &= \sum_{\text{pol.}} (g_V^2 + g_A^2) \text{tr} \left(\not{\epsilon}^*(P_Z) \not{p}'_- \not{\epsilon}(P_Z) \not{p}'_+ \right) \\
&= \sum_{\text{pol.}} (g_V^2 + g_A^2) \text{tr} \left(\gamma_\mu \gamma_\nu \gamma_\sigma \gamma_\rho \right) \epsilon^{\mu*}(P_Z) p_-^\nu \epsilon^\sigma(P_Z) p_+^\rho \\
&= -(g_V^2 + g_A^2) \text{tr} \left(\gamma_\mu \gamma_\nu \gamma_\mu \gamma_\rho \right) p_-^\nu p_+^\rho + \frac{(g_V^2 + g_A^2)}{M_Z^2} \text{tr} \left(\gamma_\mu \gamma_\nu \gamma_\mu \gamma_\rho \right) P_Z^\mu p_-^\nu P_Z^\sigma p_+^\rho \\
&= -(g_V^2 + g_A^2) \text{tr} \left(\not{\mu} \not{p}'_- \not{\mu} \not{p}'_+ \right) + \frac{(g_V^2 + g_A^2)}{M_Z^2} \text{tr} \left(\not{P}_Z \not{p}'_- \not{P}_Z \not{p}'_+ \right) \\
&= 8(g_V^2 + g_A^2)(p_+ p_-) + \frac{(g_V^2 + g_A^2)}{M_Z^2} \left(8(p_- P_Z)(p_+ P_Z) - 4M_Z^2(p_+ p_-) \right) \\
&= 4(g_V^2 + g_A^2) \left((p_+ p_-) + \frac{2}{M_Z^2} (p_+ P_Z)(p_- P_Z) \right). \tag{5.20}
\end{aligned}$$

Note that we employed the vectors $\mu = (\delta_{\mu 0}, \delta_{\mu 1}, \delta_{\mu 2}, \delta_{\mu 3})$ mentioned in Ch. 3. The

spin and polarization sum over the square of the transition amplitude then reads

$$\begin{aligned} \sum_{\text{pol. spins}} |\mathcal{S}|^2 &= \frac{(2\pi)^2 g^4 M_Z^2 t_0}{16V^4 E^2 \cos^4 \theta_W E_Z E_H (s - M_Z^2)^2} |(2\pi)^4 \delta(q_0 - P_Z - P_H)|^2 \\ &= \frac{(2\pi)^6 \tau g^4 M_Z^2 t_0 \delta(q_0 - P_Z - P_H)}{16V^3 E^2 \cos^4 \theta_W E_Z E_H (s - M_Z^2)^2} \end{aligned} \quad (5.21)$$

where we made use of [BD64]

$$|(2\pi)^4 \delta(x)|^2 = (2\pi)^4 \tau V \delta(x) \quad (5.22)$$

with the unit time τ . The incoming particle flux is [LL91]

$$|\mathbf{j}| = \frac{\sqrt{(p_+ p_-)^2 - m^4}}{V p_+^0 p_-^0} = \frac{\frac{1}{2}s}{VE^2}, \quad (5.23)$$

since we neglect $\mathcal{O}(m)$. Together with (5.21), we can insert this in Eq. (5.13) to calculate the differential cross section,

$$d^6\sigma = \frac{g^4 M_Z^2 t_0 \delta(q_0 - P_Z - P_H)}{32 \cos^4 \theta_W E_Z E_H s (s - M_Z^2)^2} d^3 \mathbf{P}_Z d^3 \mathbf{P}_H. \quad (5.24)$$

We now use the spatial components of the δ -function to integrate over the Z^0 boson's momentum and find

$$d^3\sigma = \frac{g^4 M_Z^2 t_0 \delta(2E - E_Z - E_H)}{32 \cos^4 \theta_W E_Z E_H s (s - M_Z^2)^2} d^3 \mathbf{P}_H \Big|_{\mathbf{P}_Z = -\mathbf{P}_H}. \quad (5.25)$$

We re-write the differential $d^3 \mathbf{P}_H = |P_H| E_H dE_H d\Omega_H$ with the solid angle Ω_H . Due to the condition $\mathbf{P}_Z = -\mathbf{P}_H$, the Z^0 boson's energy is dependent on the Higgs boson's energy, $E_Z = E_Z(E_H)$, and the argument of the remaining energy-conserving δ -function is a function of E_H , $g(E_H) = 2E - E_Z(E_H) - E_H$. Therefore, the integral over the Higgs boson's momentum follows the general rule [BD64]

$$\int dx f(x) \delta(g(x)) = \sum_{x_i=0} \frac{f(x_i)}{|g'(x_i)|} \quad (5.26)$$

where the x_i are the roots of the function $g(x)$ and the prime denotes the derivative with respect to the argument. Here, the argument is E_H and we have to calculate $dg(E_H)/dE_H$:

$$\begin{aligned} \frac{dg(E_H)}{dE_H} &= \frac{d}{dE_H} \left(2E - E_H - \sqrt{(|\mathbf{P}_H|^2 + M_Z^2)} \right) \\ &= \frac{d}{dE_H} \left(2E - E_H - \sqrt{(E_H^2 - M_H^2 + M_Z^2)} \right) \\ &= -\left(1 + \frac{E_H}{E_Z} \right) = -\frac{\sqrt{s}}{E_Z}. \end{aligned} \quad (5.27)$$

The root of the function $g(E_H)$ is at

$$E_H^0 = \frac{s + M_H^2 - M_Z^2}{2\sqrt{s}}. \quad (5.28)$$

Therefore, the differential cross section is

$$\begin{aligned} \frac{d\sigma}{d\Omega_H} &= \int dE_H \frac{g^4 M_Z^2 |\mathbf{P}_H| t_0 \delta(g(E_H))}{32 \cos^4 \theta_W E_Z s (s - M_Z^2)^2} \Big|_{\mathbf{P}_Z = -\mathbf{P}_H} \\ &= \frac{g^4 M_Z^2 |\mathbf{P}_H| t_0}{32 \cos^4 \theta_W s^{\frac{3}{2}} (s - M_Z^2)^2} \Big|_{\mathbf{P}_Z = -\mathbf{P}_H, E_H = E_H^0}. \end{aligned} \quad (5.29)$$

From (5.28) follows for the absolute value of the produced Z^0 boson's

$$|\mathbf{P}_Z| = |\mathbf{P}_H| = \sqrt{E_H^2 - M_H^2} = \frac{\sqrt{\lambda(s, M_Z^2, M_H^2)}}{2\sqrt{s}} \quad (5.30)$$

with

$$\lambda(s, M_Z^2, M_H^2) := s^2 + M_Z^4 + M_H^4 - 2sM_Z^2 - 2sM_H^2 - 2M_Z^2 M_H^2. \quad (5.31)$$

With this, we can revisit t_0 from Eq. (5.20). The four-product $(p_+ p_-)$ is $2E^2 = s/2$ and

$$(p_{\pm} P_Z) = EE_Z \pm EE_Z^3 = EE_Z \pm E|\mathbf{P}_Z| \cos \Theta_Z, \quad (5.32)$$

leading to

$$\begin{aligned} t_0 &= 4(g_V^2 + g_A^2) \left(4E^2 + \frac{2E^2 |\mathbf{P}_Z|^2}{M_Z^2} \sin^2 \Theta_Z \right) = 4s(g_V^2 + g_A^2) \left(1 + \frac{|\mathbf{P}_Z|^2}{2M_Z^2} \sin^2 \Theta_Z \right) \\ &= \frac{1}{2}(g_V^2 + g_A^2) \left(8sM_Z^2 + \lambda(s, M_Z^2) \right). \end{aligned} \quad (5.33)$$

Since $\mathbf{P}_Z = -\mathbf{P}_H$ and thus $\sin^2 \Theta_Z = \sin^2 \Theta_H$, we find

$$\frac{d\sigma}{d\Omega_H} = \frac{\alpha^2 (g_V^2 + g_A^2) \sqrt{\lambda(s, M_Z^2, M_H^2)}}{128 s^2 \sin^4 \theta_W \cos^4 \theta_W (s - M_Z^2)^2} \left(8sM_Z^2 + \lambda(s, M_Z^2, M_H^2) \sin^2 \Theta_H \right), \quad (5.34)$$

where we used $g^4 = e^4 / \sin^4 \theta_W = \alpha^2 / \sin^4 \theta_W$. From

$$\int d\Omega (a + b \sin^2 \theta) = 4\pi a + \frac{8\pi}{3} b \quad (5.35)$$

follows the total cross section for $e^+ e^- \rightarrow Z^0 H$

$$\sigma = \frac{\sqrt{\lambda(s, M_Z^2, M_H^2)}}{s} \frac{\pi \alpha^2 (g_V^2 + g_A^2)}{48 s \cos^4 \theta_W \sin^4 \theta_W} \frac{12sM_Z^2 + \lambda(s, M_Z^2, M_H^2)}{(s - M_Z^2)^2}. \quad (5.36)$$

The only restriction in deriving this expression is that the mass m of the colliding leptons must be small as compared to the leptons' collision energy. Since the c.m. energy must be in the order of a few hundred GeV to exceed the creation

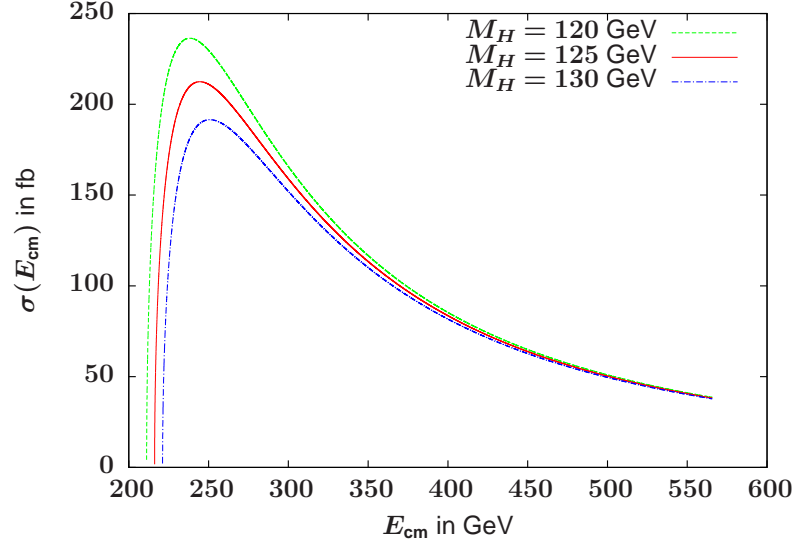


Figure 5.2: Field-free cross section as function of the c.m. energy $E_{\text{cm}} = \sqrt{s}$ for different Higgs boson masses: $M_H = 120$ GeV (green, dashed line), $M_H = 125$ GeV (red, solid line), and $M_H = 130$ GeV (blue, dashed-dotted line).

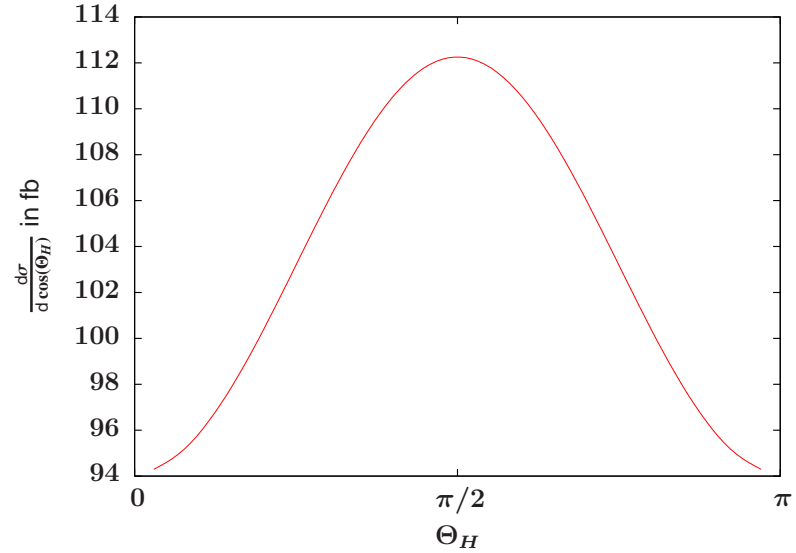


Figure 5.3: Differential cross section as function of the produced Higgs boson's polar angle for $M_H = 125$ GeV, $E = 122.3$ GeV. The total field-free cross section for this parameter set is maximal, i.e. $\sigma = 212$ fb.

threshold of the heavy bosons, this condition is also fulfilled by muons which have a rest mass of 105.6 MeV. Therefore, and because it does not depend on the lepton mass m , the total cross section (5.36) holds for muons as well as for electrons.

Fig. 5.2 shows the dependence of the total cross section (5.36) on the c.m. energy \sqrt{s} for different Higgs boson masses. Since the recent results of both the ATLAS and the CMS collaborations at CERN support a Higgs boson mass of $M_H \approx 125$ GeV [ATL12b; CMS12b], we will focus our further investigations on this value of M_H . It can be seen in Fig. 5.2 that there occurs a maximum of the total cross section at $\sqrt{s} \approx 244.5$ GeV and $\sigma(244.5 \text{ GeV}) \approx 212$ fb.

Fig 5.3 shows the dependence of the differential cross section $d\sigma/d\cos\Theta_H$ on the Higgs boson's polar angle Θ_H for $M_H = 125$ GeV. The free lepton energy $E = 122.3$ GeV is chosen such that the maximum cross section, $\sigma \approx 212$ fb, is reached. The angular distribution is symmetrical with a maximum at $\pi/2$ which corresponds to Higgs boson emission perpendicular to the collision axis. Due to the symmetry of the initial momenta, there is no preference for a certain azimuth angle Φ_H and the integration over $d\Phi_H$ yields a factor 2π .

Chapter 6

Higgs Boson Creation in a Circularly Polarized Laser Field

6.1 Analytical Calculation

In this Chapter, we study the process $\ell^+\ell^- \rightarrow HZ^0$ from Ch. 5 inside a plane laser wave of circular polarization (cf. Fig. 6.1). The four-potential of such a laser wave reads

$$A_c(kx) = a_1 \cos(kx) + a_2 \sin(kx) \quad (6.1)$$

with the space-time coordinate x , the wave vector $k = (\omega, 0, 0, \omega)$ for a laser with photon energy ω propagating in the z -direction, and

$$a_1 = (0, a, 0, 0) \quad \text{and} \quad a_2 = (0, 0, a, 0), \quad (6.2)$$

a being the amplitude of the laser field. The above relations lead to the four-products

$$\begin{aligned} A_c^2 &= a_1^2 = a_2^2 = -a^2, \\ (kA) &= (ka_1) = (ka_2) = (a_1a_2) = (kk) = 0. \end{aligned} \quad (6.3)$$

We will omit the index c and assume that, in this chapter, all quantities connected to the laser field refer to circular polarization.

As seen in Sec. 4, the lepton states must solve the Dirac equation (4.18), which is satisfied by the Volkov states (4.25). With the relations (6.3) and the abbreviation $\kappa = (kx)$, they read

$$\begin{aligned} \psi_{\pm}(x) &= \sqrt{\frac{1}{2Vq_{\pm}^0}} \left(1 \pm \frac{e \not{k} (\not{a}_1 \cos \kappa + \not{a}_2 \sin \kappa)}{2(kp_{\pm})} \right) u_{\pm} \\ &\quad \times \exp \left(i \left(\pm(q_{\pm}x) + \frac{e}{(kp_{\pm})} ((p_{\pm}a_1) \sin \kappa - (p_{\pm}a_2) \cos \kappa) \right) \right), \end{aligned} \quad (6.4)$$

where the spinors are as in the previous Chapter, i.e. $u_- = u(p_-, s_-)$ for leptons and $u_+ = v(p_+, s_+)$ for antileptons. Eq. (6.4) contains laser-dressed four-momenta

$$q_{\pm}^{\mu} = p_{\pm}^{\mu} + \xi^2 \frac{m^2}{2(kp_{\pm})} k^{\mu}, \quad (6.5)$$

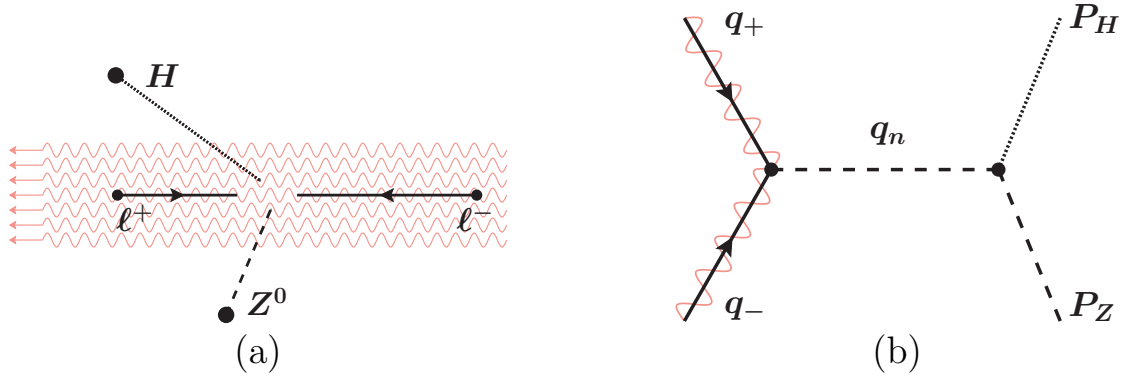


Figure 6.1: Schematic view of the considered process $\ell^+\ell^- \rightarrow HZ^0$ inside a laser field (a) and its Feynman diagram (b). The wiggled lines indicate that the leptons are described by laser-dressed states.

with the laser intensity parameter ξ as in Eq. (4.16). For a circularly polarized laser, it reads

$$\xi := \frac{ea}{m}. \quad (6.6)$$

Depending on the size of this parameter, the dressed momenta q_{\pm} can be much larger than the free momenta p_{\pm} which may vastly enhance the collision energy.

We can now write down the transition amplitude as in (5.9) but with the Volkov states ψ_{\pm} instead of the free Dirac spinors u_{\pm} :

$$\begin{aligned} \mathcal{S} = & \frac{-ig}{2\cos\theta_W} \iiint \bar{\psi}_+(x) \gamma_{\mu} (g_V - g_A \gamma_5) \psi_-(x) \\ & \cdot \frac{4\pi e^{iq(x-y)} - ig^{\mu\nu} + \frac{iq^{\mu}q^{\nu}}{M_Z^2}}{(2\pi)^4} \frac{1}{q^2 - M_Z^2} \\ & \cdot \frac{igM_Z g_{\nu\rho}}{\cos\theta_W} \frac{1}{2V\sqrt{E_Z E_H}} \epsilon_{\rho}^*(P_Z) e^{i(P_Z + P_H)y} d^4q d^4x d^4y, \end{aligned} \quad (6.7)$$

where, as before, the first integral contains the leptonic current J_{μ} , the second line is the propagator of the virtual Z^0 boson and the third line describes the outgoing particles. The expression for the transition amplitude is very similar to the one in the field-free case, the only difference being in the leptonic current since all other particles do not carry electric charge and thus do not interact with the laser field.

6.1.1 Expansion of the Leptonic Current

We now use the abbreviation $\Gamma_\mu = \gamma_\mu(g_V - g_A\gamma_5)$. Written out, the current J_μ is given by

$$\begin{aligned}
2V\sqrt{q_+^0 q_-^0} J_\mu &= \int d^4x \bar{\psi}_+ \Gamma_\mu \psi_- \\
&= \int d^4x \overline{\left(1 + \frac{e\not{A}}{2(kp_+)}\right) u_+ \Gamma_\mu \left(1 - \frac{e\not{A}}{2(kp_-)}\right) u_-} \\
&\quad \times \exp\left(-i\left((q_+x) + \frac{e}{(kp_+)}((p_+a_1)\sin\kappa - (p_+a_2)\cos\kappa)\right)\right) \\
&\quad \times \exp\left(i\left(-(q_-x) + \frac{e}{(kp_-)}((p_-a_1)\sin\kappa - (p_-a_2)\cos\kappa)\right)\right) \\
&= \int d^4x \bar{u}_+ \left(1 + \frac{e\not{A}}{2(kp_+)}\right) \Gamma_\mu \left(1 - \frac{e\not{A}}{2(kp_-)}\right) u_- \\
&\quad \times \exp(-i(q_+ + q_-)x) \times \exp(-i(\alpha_1 \sin\kappa - \alpha_2 \cos\kappa)) \\
&= \int d^4x \bar{u}_+ \left[\left(\not{\mu} - \frac{e^2 a^2 k_\mu}{2(kp_+)(kp_-)}\not{k}\right)(g_V - g_A\gamma_5) \right. \\
&\quad + \frac{e}{2} \left(\left(\frac{1}{(kp_+)}\not{q}_1 \Gamma_\mu - \frac{1}{(kp_-)}\Gamma_\mu \not{q}_1\right) \cos\kappa \right. \\
&\quad \left. \left. + \left(\frac{1}{(kp_+)}\not{q}_2 \Gamma_\mu - \frac{1}{(kp_-)}\Gamma_\mu \not{q}_2\right) \sin\kappa \right) \right] u_- \\
&\quad \times \exp(-i(q_+ + q_-)x) \times \exp(-i(\alpha_1 \sin\kappa - \alpha_2 \cos\kappa)) \quad (6.8)
\end{aligned}$$

with

$$\alpha_j = \frac{e(p_+a_j)}{(kp_+)} - \frac{e(p_-a_j)}{(kp_-)}. \quad (6.9)$$

Following standard QED procedure [Rit85], the functions $f(\kappa) = \exp(-i(\alpha_1 \sin\kappa - \alpha_2 \cos\kappa))$, $\sin\kappa f(\kappa)$, and $\cos\kappa f(\kappa)$ can be expanded in Fourier series of the form

$$\begin{aligned}
f(\kappa) &= \sum_{n=-\infty}^{\infty} b_n e^{-in\kappa}, \\
\cos(\kappa) f(\kappa) &= \sum_{n=-\infty}^{\infty} c_n e^{-in\kappa}, \\
\sin(\kappa) f(\kappa) &= \sum_{n=-\infty}^{\infty} d_n e^{-in\kappa} \quad (6.10)
\end{aligned}$$

with the coefficients

$$\begin{aligned}
b_n &= J_n(\bar{\alpha}) e^{in\kappa_0}, \\
c_n &= \frac{1}{2} \left(J_{n+1}(\bar{\alpha}) e^{i(n+1)\kappa_0} + J_{n-1}(\bar{\alpha}) e^{i(n-1)\kappa_0} \right), \\
d_n &= \frac{1}{2i} \left(J_{n+1}(\bar{\alpha}) e^{i(n+1)\kappa_0} - J_{n-1}(\bar{\alpha}) e^{i(n-1)\kappa_0} \right). \quad (6.11)
\end{aligned}$$

The summation index n corresponds to the number of laser photons that are absorbed ($n > 1$) or emitted ($n < 1$) at the lepton vertex. Large numbers n can further enhance the collision energy. The coefficients contain the regular cylindrical Bessel functions $J_n(\bar{\alpha})$ of integer order n [AS65]. The argument of the Bessel functions is

$$\bar{\alpha} = \sqrt{\alpha_1^2 + \alpha_2^2} \quad (6.12)$$

and the angle κ_0 is given by

$$\cos \kappa_0 = \frac{\alpha_1}{\bar{\alpha}}, \quad \sin \kappa_0 = \frac{\alpha_2}{\bar{\alpha}}. \quad (6.13)$$

Thus, we can introduce the dimensionless spinor-matrix product

$$\begin{aligned} \mathcal{M}_\mu^n &:= \bar{u}_+ \left((\not{\mu} - \frac{e^2 a^2 k_\mu}{2(kp_+)(kp_-)} \not{k})(g_V - g_A \gamma_5) \cdot b_n \right. \\ &\quad + \frac{e}{2} \left(\left[\frac{1}{(kp_+)} \not{q}_1 \not{k} \not{\mu} (g_V - g_A \gamma_5) - \frac{1}{(kp_-)} \not{\mu} (g_V - g_A \gamma_5) \not{k} \not{q}_1 \right] \cdot c_n \right. \\ &\quad \left. \left. + \left[\frac{1}{(kp_+)} \not{q}_2 \not{k} \not{\mu} (g_V - g_A \gamma_5) - \frac{1}{(kp_-)} \not{\mu} (g_V - g_A \gamma_5) \not{k} \not{q}_2 \right] \cdot d_n \right) \right) u_- \\ &=: \bar{u}_+ \Delta_\mu^n u_-, \end{aligned} \quad (6.14)$$

and the leptonic current becomes

$$J_\mu = \frac{1}{2V \sqrt{q_+^0 q_-^0}} \sum_{n=-\infty}^{\infty} \int d^4 x \mathcal{M}_\mu^n \cdot e^{-i(q_+ + q_-)x} \cdot e^{-in(kx)}. \quad (6.15)$$

With this, the transition amplitude (6.7) becomes

$$\begin{aligned} \mathcal{S} &= \sum_{n=-\infty}^{\infty} \iiint \frac{4\pi}{4(2\pi)^4 V^2 \sqrt{q_+^0 q_-^0} E_Z E_H} \frac{-ig}{2 \cos \theta_W} \mathcal{M}_\mu^n \frac{-ig^{\mu\nu} + \frac{iq_n^\mu q_n^\nu}{M_Z^2}}{q^2 - M_Z^2} \frac{ig M_Z g_{\nu\rho}}{\cos \theta_W} \epsilon_\rho^*(P_Z) \\ &\quad \times e^{i(q - q_+ - q_- - nk)x} e^{-i(q - P_H - P_Z)y} d^4 x d^4 y d^4 q \\ &= \sum_n \int d^4 q \frac{1}{4(2\pi)^3 V^2 \sqrt{q_+^0 q_-^0} E_Z E_H} \frac{g^2 M_Z}{\cos^2 \theta_W} \mathcal{M}_\mu^n \frac{-ig^{\mu\nu} + \frac{iq_n^\mu q_n^\nu}{M_Z^2}}{q^2 - M_Z^2} g_{\nu\rho} \epsilon_\rho^*(P_Z) \\ &\quad \times (2\pi)^4 \delta(q - q_+ - q_- - nk) (2\pi)^4 \delta(q - P_H - P_Z) \\ &= \sum_n \frac{(2\pi)^5}{4V^2 \sqrt{q_+^0 q_-^0} E_Z E_H} \frac{g^2 M_Z}{\cos^2 \theta_W} \mathcal{M}_\mu^n \frac{-ig^{\mu\nu} + \frac{iq_n^\mu q_n^\nu}{M_Z^2}}{q_n^2 - M_Z^2} g_{\nu\rho} \epsilon_\rho^*(P_Z) \delta(q_n - P_H - P_Z) \\ &=: \sum_n \mathcal{S}_n \end{aligned} \quad (6.16)$$

where we again made use of the relation (5.11) to combine the two δ -functions stemming from the integrations over the space-time coordinates x and y . The four-momentum of the virtual Z^0 boson, q_n , is given by $q_n = q_+ + q_- + nk$ and thus depends on the incoming particles' laser-dressed momenta q_\pm and the number of photons n absorbed from or emitted to the laser field.

6.1.2 The Differential Cross Section

The differential cross section is derived from the transition amplitude in the same way as in Ch. 5, i.e. by summing the square over the Z^0 boson's polarization states, averaging it over the initial spins, and division by a unit time τ and the incoming particle flux $|\mathbf{j}|$:

$$d^6\sigma = \frac{1}{4} \sum_{\text{pol. spins}} \frac{|\mathcal{S}|^2}{\tau |\mathbf{j}|} \frac{V d^3 \mathbf{P}_Z}{(2\pi)^3} \frac{V d^3 \mathbf{P}_H}{(2\pi)^3}. \quad (6.17)$$

This expression is similar to (5.13).

The Square of the Transition Amplitude

Due to the occurrence of the photon order n in the four-momentum conserving δ -function in Eq. (6.16), squaring the amplitude does not involve a double sum over two different summation indices,

$$\sum_n \sum_{n'} \delta(q_n - P_H - P_Z) \delta(q_{n'} - P_H - P_Z) = \sum_{n, n'} \delta_{nn'} \delta(q_n - P_H - P_Z), \quad (6.18)$$

and therefore $|\mathcal{S}|^2 = \sum_n |\mathcal{S}_n|^2$ with

$$\begin{aligned} |\mathcal{S}_n|^2 &= \frac{(2\pi)^2 g^4 M_Z^2}{16V^4 q_+^0 q_-^0 E_Z E_H \cos^4 \theta_W} \left| \mathcal{M}_\mu^n \frac{-ig^{\mu\rho} + \frac{iq_n^\mu q_n^\rho}{M_Z^2}}{q_n^2 - M_Z^2} \epsilon_\rho^*(P_Z) (2\pi)^4 \delta(q_n - P_Z - P_H) \right|^2 \\ &= \frac{(2\pi)^6 \tau g^4 M_Z^2 \delta(q_n - P_H - P_Z)}{16V^3 q_+^0 q_-^0 E_Z E_H \cos^4 \theta_W} \\ &\quad \times \left[\mathcal{M}_\mu^n \frac{-ig^{\mu\rho} + \frac{iq_n^\mu q_n^\rho}{M_Z^2}}{q_n^2 - M_Z^2} \epsilon_\rho^*(P_Z) \right] \left[\mathcal{M}_\nu^n \frac{-ig^{\nu\sigma} + \frac{iq_n^\nu q_n^\sigma}{M_Z^2}}{q_n^2 - M_Z^2} \epsilon_\sigma^*(P_Z) \right]^\dagger. \end{aligned} \quad (6.19)$$

Note that the square of the δ -function has been treated as in Eq. (5.22), yielding a unit time τ and a unit volume V .

The Spin and Polarization Sum over the Square of the Amplitude

We now define the abbreviation

$$\begin{aligned} T_n &:= \mathcal{M}_\mu^n (-g^{\mu\rho} + \frac{q_n^\mu q_n^\rho}{M_Z^2}) \epsilon_\rho^*(P_Z) \\ &= \bar{u}_+ \left[\frac{1}{M_Z^2} \Delta_\mu^n q_n^\mu q_n^\rho \epsilon_\rho^*(P_Z) - \Delta_\mu^n \epsilon^{*\mu}(P_Z) \right] u_- \end{aligned} \quad (6.20)$$

with the matrix Δ_μ^n as defined in Eq. (6.14), and write

$$|\mathcal{S}_n|^2 = \frac{(2\pi)^6}{16V^3 q_+^0 q_-^0 E_Z E_H \cos^4 \theta_W} \frac{g^4 M_Z^2}{(q_n^2 - M_Z^2)^2} \tau \delta(q_n - P_Z - P_H) T_n T_n^\dagger. \quad (6.21)$$

The adjoint is

$$\begin{aligned}
T_n^\dagger &= u_-^\dagger \gamma^0 \gamma^0 \left[\frac{1}{M_Z^2} \Delta_\nu^\dagger \gamma^0 \gamma^0 q_n^\nu q_n^\sigma \epsilon_\sigma \gamma^0 \gamma^0 - \Delta_\nu^\dagger \epsilon^\nu(P_Z) \gamma^0 \gamma^0 \right] \bar{u}_+^\dagger \\
&= \bar{u}_- \left[\frac{1}{M_Z^2} \bar{\Delta}_\nu^n q_n^\nu q_n^\sigma \epsilon_\sigma(P_Z) - \bar{\Delta}_\nu^n \epsilon^\nu(P_Z) \right] u_+ .
\end{aligned} \tag{6.22}$$

In the same manner as in the previous chapter, the spin and polarization sum over $T_n T_n^\dagger$ yields

$$\begin{aligned}
&\sum_{\text{pol.}} \sum_{\text{spins}} T_n T_n^\dagger \\
&= \sum_{\text{pol.}} \sum_{s_+} \sum_{s_-} \bar{u}_+ \left[\frac{1}{M_Z^2} \Delta_\mu^n q_n^\mu q_n^\rho \epsilon_\rho^*(P_Z) - \Delta_\mu^n \epsilon^{*\mu}(P_Z) \right] u_- \bar{u}_- \\
&\quad \times \left[\frac{1}{M_Z^2} \bar{\Delta}_\nu^n q_n^\nu q_n^\sigma \epsilon_\sigma(P_Z) - \bar{\Delta}_\nu^n \epsilon^\nu(P_Z) \right] u_+ \\
&= \sum_{\text{pol.}} \left(\frac{1}{M_Z^4} (q_n \epsilon(P_Z)) (q_n \epsilon^*(P_Z)) \text{tr} \left[\Delta_\mu^n q_n^\mu \not{p}_- \bar{\Delta}_\nu^n q_n^\nu \not{p}_+ \right] \right. \\
&\quad + \text{tr} \left[\Delta_\mu^n \epsilon_\mu^*(P_Z) \not{p}_- \bar{\Delta}_\nu^n \epsilon^\nu(P_Z) \not{p}_+ \right] \\
&\quad - \frac{1}{M_Z^2} (q_n \epsilon^*(P_Z)) \text{tr} \left[\Delta_\mu^n q_n^\mu \not{p}_- \bar{\Delta}_\nu^n \epsilon^\nu(P_Z) \not{p}_+ \right] \\
&\quad \left. - \frac{1}{M_Z^2} (q_n \epsilon(P_Z)) \text{tr} \left[\Delta_\mu^n \epsilon_\mu^*(P_Z) \not{p}_- \bar{\Delta}_\nu^n q_n^\nu \not{p}_+ \right] \right) \\
&= \frac{1}{M_Z^4} \left(\frac{(q_n P_Z)^2}{M_Z^2} - q_n^2 \right) \text{tr} \left[\Delta_\mu^n q_n^\mu \not{p}_- \bar{\Delta}_\nu^n q_n^\nu \not{p}_+ \right] , \\
&\quad + \frac{1}{M_Z^2} \text{tr} \left[\Delta_\mu^n P_Z^\mu \not{p}_- \bar{\Delta}_\nu^n P_Z^\nu \not{p}_+ \right] - \text{tr} \left[\Delta_\mu^n \not{p}_- \bar{\Delta}_\nu^n \not{p}_+ \right] , \\
&\quad + \frac{1}{M_Z^2} \text{tr} \left[\Delta_\mu^n q_n^\mu \not{p}_- \bar{\Delta}_\nu^n q_n^\nu \not{p}_+ \right] - \frac{1}{M_Z^4} (q_n P_Z) \text{tr} \left[\Delta_\mu^n q_n^\mu \not{p}_- \bar{\Delta}_\nu^n P_Z^\nu \not{p}_+ \right] , \\
&\quad + \frac{1}{M_Z^2} \text{tr} \left[\Delta_\mu^n q_n^\mu \not{p}_- \bar{\Delta}_\nu^n q_n^\nu \not{p}_+ \right] - \frac{1}{M_Z^4} (q_n P_Z) \text{tr} \left[\Delta_\mu^n P_Z^\mu \not{p}_- \bar{\Delta}_\nu^n q_n^\nu \not{p}_+ \right] \\
&= \frac{1}{M_Z^4} \left(\frac{(q_n P_Z)^2}{M_Z^2} - q_n^2 + 2M_Z^2 \right) \text{tr} \left[\Delta_\mu^n q_n^\mu \not{p}_- \bar{\Delta}_\nu^n q_n^\nu \not{p}_+ \right] \\
&\quad + \frac{1}{M_Z^2} \text{tr} \left[\Delta_\mu^n P_Z^\mu \not{p}_- \bar{\Delta}_\nu^n P_Z^\nu \not{p}_+ \right] - \text{tr} \left[\Delta_\mu^n \not{p}_- \bar{\Delta}_\nu^n \not{p}_+ \right] \\
&\quad - \frac{(q_n P_Z)}{M_Z^4} \text{tr} \left[\Delta_\mu^n q_n^\mu \not{p}_- \bar{\Delta}_\nu^n P_Z^\nu \not{p}_+ \right] - \frac{(q_n P_Z)}{M_Z^4} \text{tr} \left[\Delta_\mu^n P_Z^\mu \not{p}_- \bar{\Delta}_\nu^n q_n^\nu \not{p}_+ \right] \\
&=: t_n .
\end{aligned} \tag{6.23}$$

The evaluation of these traces using the relations of Appx. B is very lengthy and therefore omitted in this discussion. It has been included in the numerical calculation of the total cross section.

With the laser-dressed flux [LL91]

$$|\mathbf{j}| = \frac{\sqrt{(q_+ q_-)^2 - m_*^4}}{V q_+^0 q_-^0} \quad (6.24)$$

of the incoming particles containing their laser-dressed four-momenta q_\pm , we find

$$d^6\sigma = \sum_n \frac{g^4 M_Z^2}{64 E_Z E_H \cos^4 \theta_W \sqrt{(q_+ q_-)^2 - m_*^4}} \frac{t_n \delta(q_n - P_Z - P_H)}{(q_n^2 - M_Z^2)^2} d^3 \mathbf{P}_Z d^3 \mathbf{P}_H. \quad (6.25)$$

6.1.3 The Total Cross Section

The integration over the produced Z^0 boson's momentum $d^3 \mathbf{P}_Z$ can be performed eliminating the spatial components of the δ -function in (6.25),

$$d^3\sigma = \sum_n \frac{g^4 M_Z^2 t_n \delta(q_n^0 - E_Z - E_H)}{64 E_Z E_H \cos^4 \theta_W \sqrt{(q_+ q_-)^2 - m_*^4} (q_n^2 - M_Z^2)^2} d^3 \mathbf{P}_H \Big|_{\mathbf{P}_Z = \mathbf{q}_n - \mathbf{P}_H}, \quad (6.26)$$

and we remain with an energy-conserving δ -function. As before, we re-write the differential $d^3 \mathbf{P}_H = |\mathbf{P}_H| E_H dE_H d\Phi_H d\cos \Theta_H$. Since there is no dependence on the azimuth angle ϕ_H , the integration over $d\phi_H$ just gives a factor 2π . Unlike in the field-free case, the remaining δ -function is used for the integration over $d\cos \Theta_H$ now instead of dE_H because the argument of the δ -function depends on E_H in a nonlinear way. Defining

$$\begin{aligned} g(\cos \Theta_H) &= q_n^0 - E_Z - E_H \\ &= q_n^0 - E_H - \sqrt{|\mathbf{P}_Z|^2 + M_Z^2} \\ &= q_n^0 - E_H - \sqrt{|\mathbf{q}_n - \mathbf{P}_H|^2 + M_Z^2} \\ &= q_n^0 - E_H - \sqrt{|\mathbf{q}_n|^2 + |\mathbf{P}_H|^2 - 2|\mathbf{q}_n||\mathbf{P}_H|\cos \Theta_H + M_Z^2} \end{aligned} \quad (6.27)$$

with one root at

$$\cos \Theta_H^0 = \frac{M_Z^2 - M_H^2 - q_n^2 + 2q_n^0 E_H}{2|\mathbf{q}_n||\mathbf{P}_H|} \quad (6.28)$$

and the derivative

$$g'(\cos \Theta_H) = \frac{|\mathbf{P}_H||\mathbf{q}_n|}{E_Z}, \quad (6.29)$$

we can integrate over $d\cos \Theta_H$. The restriction that $|\cos \Theta_H| \leq 1$ leads to the integration limits

$$\begin{aligned} E_H^{\min} &= \frac{1}{2}(q_n^2 + M_H^2 - M_Z^2) \frac{q_n^0}{q_n^2} - \frac{|\mathbf{q}_n|}{2q_n^2} \sqrt{\lambda(q_n^2, M_Z^2, M_H^2)} \\ E_H^{\max} &= \frac{1}{2}(q_n^2 + M_H^2 - M_Z^2) \frac{q_n^0}{q_n^2} + \frac{|\mathbf{q}_n|}{2q_n^2} \sqrt{\lambda(q_n^2, M_Z^2, M_H^2)} \end{aligned} \quad (6.30)$$

for the integration over dE_H . The function $\lambda(q_n^2, M_Z^2, M_H^2)$ is defined as in (5.31) from the previous Chapter. With $g^4 = \alpha^2 / \sin^4 \theta_W$, the final expression for the total cross section reads

$$\begin{aligned} \sigma &= \sum_n \int_{E_H^{\min}}^{E_H^{\max}} dE_H \frac{2\pi\alpha^2 M_Z^2 t_n}{64 \cos^4 \theta_W \sin^4 \theta_W (q_n^2 - M_Z^2)^2 \sqrt{(q_+ q_-)^2 - m_*^4} |\mathbf{q}_n|} \bigg|_{\cos \Theta_H = \cos \Theta_H^0}^{P_Z = \mathbf{q}_n - P_H} \\ &=: \sum_n \sigma_n. \end{aligned} \quad (6.31)$$

Note that it can be written as a sum over *partial cross sections* σ_n of order n . The final integration has been performed numerically. Its results are presented in the following Sec. 6.2. Please also note that the field-free cross section (5.36) is reproduced in the limit of vanishing laser field, i.e. for $a \rightarrow 0$, as we would like to derive now.

6.1.4 Reproduction of the Field-Free Cross Section

In order to derive the field-free cross section (5.36), we first consider the matrix Δ_μ^n occurring in the spinor-matrix product (6.14):

$$\begin{aligned} \Delta_\mu^n &= (\not{\mu} - \frac{e^2 a^2 k_\mu}{2(kp_+)(kp_-)} \not{k})(g_V - g_A \gamma_5) \cdot b_n \\ &\quad + \frac{e}{2} \left[\frac{1}{(kp_+)} \not{q}_1 \not{k} \not{\mu} (g_V - g_A \gamma_5) - \frac{1}{(kp_-)} \not{\mu} (g_V - g_A \gamma_5) \not{k} \not{q}_1 \right] \cdot c_n \\ &\quad + \frac{e}{2} \left[\frac{1}{(kp_+)} \not{q}_2 \not{k} \not{\mu} (g_V - g_A \gamma_5) - \frac{1}{(kp_-)} \not{\mu} (g_V - g_A \gamma_5) \not{k} \not{q}_2 \right] \cdot d_n. \end{aligned} \quad (6.32)$$

Since, in the case without a laser field, the laser intensity parameter ξ vanishes, so does the product $ea = \xi/m$. Also, no photons are available for absorption and therefore $n = 0$. Thus, we only have

$$\Delta_\mu^{\text{ff}} = \not{\mu} (g_V - g_A \gamma_5) \cdot b_0 \quad (6.33)$$

and

$$\overline{\Delta}_\nu^{\text{ff}} = (g_V + g_A \gamma_5) \not{\nu} \cdot b_0^* \quad (6.34)$$

and the product

$$|b_0|^2 = 1. \quad (6.35)$$

With this, the trace product (6.23) becomes

$$\begin{aligned}
t_{\text{ff}} = & \frac{1}{M_Z^4} \left(\frac{(q_0 P_Z)^2}{M_Z^2} - q_0^2 \right) \text{tr} \left[\not{q}_0 (g_V - g_A \gamma_5) \not{p}_- (g_V + g_A \gamma_5) \not{q}_0 \not{p}_+ \right] \\
& + \frac{1}{M_Z^2} \text{tr} \left[\not{P}_Z (g_V - g_A \gamma_5) \not{p}_- (g_V + g_A \gamma_5) \not{P}_Z \not{p}_+ \right] \\
& \quad - \text{tr} \left[\not{\mu} (g_V - g_A \gamma_5) \not{p}_- (g_V + g_A \gamma_5) \not{\mu} \not{p}_+ \right] \\
& + \frac{1}{M_Z^2} \text{tr} \left[\not{q}_0 (g_V - g_A \gamma_5) \not{p}_- (g_V + g_A \gamma_5) \not{q}_0 \not{p}_+ \right] \\
& \quad - \frac{1}{M_Z^4} (q_0 P_Z) \text{tr} \left[\not{q}_0 (g_V - g_A \gamma_5) \not{p}_- (g_V + g_A \gamma_5) \not{P}_Z \not{p}_+ \right] \\
& + \frac{1}{M_Z^2} \text{tr} \left[\not{q}_0 (g_V - g_A \gamma_5) \not{p}_- (g_V + g_A \gamma_5) \not{q}_0 \not{p}_+ \right] \\
& \quad - \frac{1}{M_Z^4} (q_0 P_Z) \text{tr} \left[\not{P}_Z (g_V - g_A \gamma_5) \not{p}_- (g_V + g_A \gamma_5) \not{q}_0 \not{p}_+ \right] \\
= & \left(\frac{1}{M_Z^4} \left(\frac{(q_0 P_Z)^2}{M_Z^2} - q_0^2 \right) + \frac{2}{M_Z^2} \right) \text{tr} \left[\not{q}_0 (g_V - g_A \gamma_5) \not{p}_- (g_V + g_A \gamma_5) \not{q}_0 \not{p}_+ \right] \\
& - \frac{1}{M_Z^4} (q_0 P_Z) \left(\text{tr} \left[\not{q}_0 (g_V - g_A \gamma_5) \not{p}_- (g_V + g_A \gamma_5) \not{P}_Z \not{p}_+ \right] \right. \\
& \quad \left. + \text{tr} \left[\not{P}_Z (g_V - g_A \gamma_5) \not{p}_- (g_V + g_A \gamma_5) \not{q}_0 \not{p}_+ \right] \right) \\
& + \frac{1}{M_Z^2} \text{tr} \left[\not{P}_Z (g_V - g_A \gamma_5) \not{p}_- (g_V + g_A \gamma_5) \not{P}_Z \not{p}_+ \right] \\
& \quad - \text{tr} \left[\not{\mu} (g_V - g_A \gamma_5) \not{p}_- (g_V + g_A \gamma_5) \not{\mu} \not{p}_+ \right]. \tag{6.36}
\end{aligned}$$

Making use of the properties of the γ -matrices given in Appx. B, we find the trace in the first line of (6.36) to be

$$\begin{aligned}
& \text{tr} \left[\not{q}_0 (g_V - g_A \gamma_5) \not{p}_- (g_V + g_A \gamma_5) \not{q}_0 \not{p}_+ \right] \\
& = (g_V^2 + g_A^2) \text{tr} \left[\not{q}_0 \not{p}_- \not{q}_0 \not{p}_+ \right] + 2g_V g_A \underbrace{\text{tr} \left[\not{q}_0 \not{p}_- \gamma_5 \not{q}_0 \not{p}_+ \right]}_{=0} \\
& = 4(g_V^2 + g_A^2) \left[2(q_0 p_+) (q_0 p_-) - q_0^2 (p_+ p_-) \right] \\
& = 4(g_V^2 + g_A^2) \left[2 \cdot 2E^2 \cdot 2E^2 - 4E^2 \cdot 2E^2 \right] \\
& = 0. \tag{6.37}
\end{aligned}$$

The second and third traces become

$$\begin{aligned}
& \text{tr} \left[\not{q}_0 (g_V - g_A \gamma_5) \not{p}'_- (g_V + g_A \gamma_5) \not{P}_Z \not{p}'_+ \right] \\
&= (g_V^2 + g_A^2) \text{tr} \left[\not{q}_0 \not{p}'_- \not{P}_Z \not{p}'_+ \right] + 2g_V g_A \text{tr} \left[\not{q}_0 \not{p}'_- \gamma_5 \not{P}_Z \not{p}'_+ \right] \\
&\text{and} \\
& \text{tr} \left[\not{P}_Z (g_V - g_A \gamma_5) \not{p}'_- (g_V + g_A \gamma_5) \not{q}_0 \not{p}'_+ \right] \\
&= (g_V^2 + g_A^2) \text{tr} \left[\not{P}_Z \not{p}'_- \not{q}_0 \not{p}'_+ \right] - 2g_V g_A \text{tr} \left[\not{q}_0 \not{p}'_- \gamma_5 \not{P}_Z \not{p}'_+ \right]. \quad (6.38)
\end{aligned}$$

Therefore, the sum yields

$$\begin{aligned}
& 2(g_V^2 + g_A^2) \text{tr} \left[\not{q}_0 \not{p}'_- \not{P}_Z \not{p}'_+ \right] \\
&= 8(g_V^2 + g_A^2) \left[(q_0 p_-)(P_Z p_+) + (q_0 p_+)(P_Z p_-) - (q_0 P_Z)(p_+ p_-) \right] \\
&= 8(g_V^2 + g_A^2) \left[2E^2 \cdot (E_Z E + P_Z^3 E) + 2E^2 (E_Z E - P_Z^3 E) - 2E_Z E \cdot 2E^2 \right] \\
&= 0. \quad (6.39)
\end{aligned}$$

The next-to-last line in (6.36) yields

$$\begin{aligned}
& \frac{1}{M_Z^2} \text{tr} \left[\not{P}_Z (g_V - g_A \gamma_5) \not{p}'_- (g_V + g_A \gamma_5) \not{P}_Z \not{p}'_+ \right] \\
&= \frac{4}{M_Z^2} (g_V^2 + g_A^2) \left[2(P_Z p_+)(P_Z p_-) - P_Z^2 (p_+ p_-) \right] \quad (6.40)
\end{aligned}$$

and the last line is

$$-\text{tr} \left[\not{\mu} (g_V - g_A \gamma_5) \not{p}'_- (g_V + g_A \gamma_5) \not{\mu} \not{p}'_+ \right] = 8(g_V^2 + g_A^2)(p_+ p_-). \quad (6.41)$$

With this, the trace product is

$$\begin{aligned}
t_{\text{ff}} &= 4(g_V^2 + g_A^2) \left[(p_+ p_-) + \frac{2}{M_Z^2} (P_Z p_+)(P_Z p_-) \right] \\
&= \frac{1}{2} (g_V^2 + g_A^2) \left[8s + \frac{\lambda(s, M_Z^2, M_H^2) \sin^2 \Theta_Z}{M_Z^2} \right], \quad (6.42)
\end{aligned}$$

which has been derived as in (5.20).

We can now insert this trace product into Eq. (6.25) and obtain

$$\begin{aligned}
d^6 \sigma &= \frac{g^4 M_Z^2}{256(2\pi)^2 E_Z E_H \cos^4 \theta_W \sqrt{(p_+ p_-)^2 - m^4}} \frac{t_0 \delta(q_0 - P_Z - P_H)}{(q_0^2 - M_Z^2)^2} d^3 \mathbf{P}_Z d^3 \mathbf{P}_H \\
&= \frac{g^4 \cdot \frac{1}{2} (g_V^2 + g_A^2) (8s M_Z^2 + \lambda(s, M_Z^2, M_H^2) \sin^2 \Theta_Z) \delta(q_0 - P_Z - P_H)}{256(2\pi)^2 E_Z E_H \cos^4 \Theta_W \frac{1}{2} s (s - M_Z^2)^2} d^3 \mathbf{P}_Z d^3 \mathbf{P}_H. \quad (6.43)
\end{aligned}$$

As before, we integrate over $d^3\mathbf{P}_Z$ and eliminate the three momentum dimensions of the δ -function. Again with $d^3\mathbf{P}_H = |\mathbf{P}_H|E_H dE_H d\Phi_H d\cos\Theta_H$, this leads to

$$\frac{d\sigma}{d\Omega_H} = \int dE_H \frac{g^4(g_V^2 + g_A^2)(8sM_Z^2 + \lambda(s, M_Z^2, M_H^2) \sin^2 \Theta_H) \delta(2E - E_Z - E_H) |\mathbf{P}_H|}{256s(2\pi)^2 E_Z \cos^4 \Theta_W (s - M_Z^2)^2} \Big|_{\mathbf{P}_Z = -\mathbf{P}_H} \quad (6.44)$$

We can perform the integration like in Ch. 5 and obtain

$$\frac{d\sigma}{d\Omega} = \frac{\alpha^2(g_V^2 + g_A^2)(8sM_Z^2 + \lambda(s, M_Z^2, M_H^2) \sin^2 \Theta_H) \sqrt{\lambda(s, M_Z^2, M_H^2)}}{128s^2 \cos^4 \Theta_W \sin^4 \Theta_W (s - M_Z^2)^2} \Big|_{\mathbf{P}_Z = -\mathbf{P}_H, E_H = E_H^0} \quad (6.45)$$

which is Eq. (5.33) and of course leads to the total cross section in the field-free case (5.36):

$$\sigma_{\text{ff}} = \frac{\sqrt{\lambda(s, M_Z^2, M_H^2)}}{s} \frac{\pi\alpha^2(g_V^2 + g_A^2)}{48s \cos^4 \theta_W \sin^4 \theta_W} \frac{12sM_Z^2 + \lambda(s, M_Z^2, M_H^2)}{(s - M_Z^2)^2} \Big|_{\mathbf{P}_Z = -\mathbf{P}_H, E_H = E_H^0} \quad (6.46)$$

6.2 Numerical Results

6.2.1 Setup and Collision Momenta in the Laser Field

In this section, the results of the numerical calculation of the cross section (6.31) are presented for a setting where the leptons are moving along the propagation direction z of the laser beam and their free momenta p_{\pm} satisfy $p_+^3 = -p_-^3$ and therefore both particles have the same free energy $p^0 \equiv p_-^0 = p_+^0$. For this setup, we can find simple approximations for the laser-dressed energies q_{\pm}^0 from Eq. (6.5). Without loss of generality, we assume that the particle that co-propagates with the laser field is the lepton and the counterpropagating particle is the antilepton. Then, q_-^0 becomes

$$q_-^0 = p_-^0 + \frac{m^2 \xi^2 \omega}{2\omega(p_-^0 - p_-^3)} = p^0 + \frac{((p^0)^2 - (p_-^3)^2) \xi^2}{2(p^0 - p_-^3)} = p^0 + \frac{(p^0 + p_-^3) \xi^2}{2} \approx p^0(1 + \xi^2) \quad (6.47)$$

where we made use of $p_-^3 \approx p^0$ due to the highly relativistic free energy of the lepton. Hence, the co-moving lepton may experience a large energy shift, depending on the size of the laser intensity parameter ξ (6.6). For the energy of the counterpropagating antilepton, we find instead

$$q_+^0 = p^0 + \frac{m^2 \xi^2}{2(p^0 + p_-^3)} \approx p^0, \quad (6.48)$$

under the assumption that $\xi \ll p^0/m$ which is satisfied for all present-day and near-future lasers. The energy of the counterpropagating lepton is thus nearly unaffected by the laser field.

Since the lepton and antilepton are traveling along the laser propagation direction, the four-products $(p_{\pm}a_j)$ are 0 and thus the argument (6.9) of the Bessel functions in (6.11) is 0. Since all Bessel functions except $J_0(\bar{\alpha})$ have a root at $\bar{\alpha} = 0$ (cf. Appx. C) and Bessel functions of orders J_{n+1} , J_n and J_{n-1} occur in the expansion of the leptonic current, the only partial cross sections σ_n that contribute to the total cross section are those of photon order $n = -1, 0$, or 1 . This corresponds to the emission of one photon, zero emission or absorption, and the absorption of one photon from the laser field, respectively.

For reasons that will become clear in the following Sec. 6.3, we assume that in the following, the colliding leptons are a muon and an antimuon instead of electron and positron.

6.2.2 Maximum Cross Section

As mentioned in Ch. 5, the field-free cross section only depends on the total collision energy and, for the Higgs boson mass $M_H = 125$ GeV as found at CERN [CMS12b; ATL12b], is maximal for $E_{\text{cm}} \approx 244.5$ GeV. Without a laser field, this requires initial muon energies of $p^0 \approx 122$ GeV. Inside a laser field, however, the collision energy is determined by the laser-dressed momenta q_{\pm} (6.5) instead of the free momenta p_{\pm} . Assuming an intensity parameter of $\xi = 1$, Eqs. (6.47) and (6.48) imply that free muon energies of only $p^0 \approx 86.45$ GeV are required to obtain $E_{\text{cm}} = 244.5$ GeV. For $\xi = 3$, only $p^0 \approx 38.66$ GeV is needed. Assuming an optical laser with a wave length $\omega = 1$ eV, corresponding to a wavelength of $\lambda \approx 1.2$ μm , and muons as colliding particles, $\xi = 1$ would correspond to a laser intensity of $I \approx 7.6 \times 10^{22}$ W/cm², and $\xi = 3$ would mean $I \approx 6.8 \times 10^{23}$ W/cm².

Note that in the trace product t_n from Eq. (6.23), the wave vector k always appears both in the numerator and in the denominator. It is therefore independent of the photon energy ω . The only occurrence of the wave vector without it canceling out is in the argument of the Bessel functions. Since, in the kinematic constellation we are considering, this argument is $\bar{\alpha} = 0$, the cross section does not depend on the photon energy ω . It only plays a role in the determination of the laser intensity parameter ξ from the laser intensity I .

6.2.3 Produced Higgs Boson's Energy Distribution

As seen in Ch. 5, in the field-free case, the Higgs boson's energy is fixed by a δ -function. Due to the vast difference between the incoming muon's and antimuon's momenta q_{\pm} , the lab frame no longer corresponds to the c.m. system when the laser field is superimposed. In order to find the Higgs boson's energy in the new c.m. system, a Lorentz transformation is necessary. There, the momenta q'_{\pm} of the colliding leptons and, in particular, their z -components are opposite and equal:

$$\begin{aligned} q'^3_- &= -q'^3_+ \\ \Leftrightarrow \gamma_{\text{cm}}(q^3_- - \beta_{\text{cm}}q^0_-) &= -\gamma_{\text{cm}}(q^3_+ - \beta_{\text{cm}}q^0_+), \end{aligned} \tag{6.49}$$

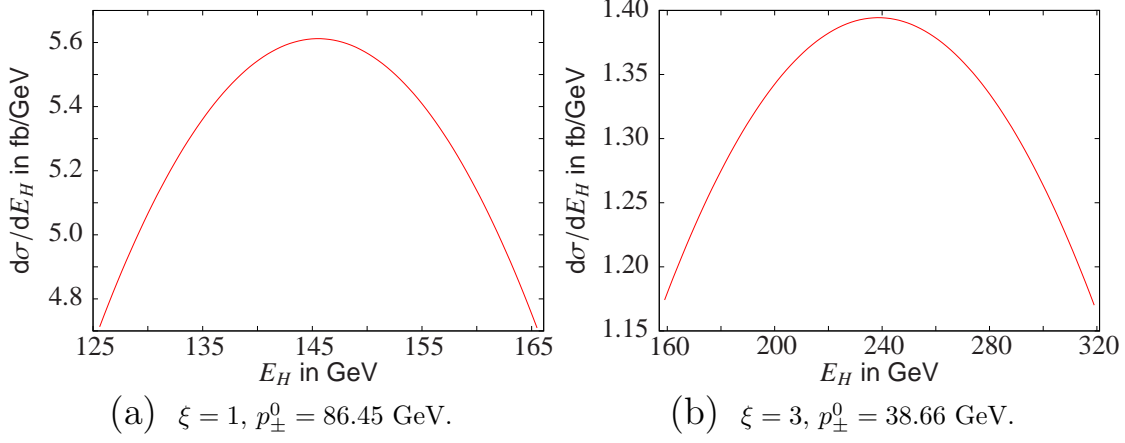


Figure 6.2: Differential cross sections $d\sigma/dE_H$ for different parameter sets. In both cases, the free muon momenta are such that $E_{\text{cm}} \approx 244.5$ GeV and the integration over the spectra yields the maximum cross section, $\sigma \approx 212$ fb.

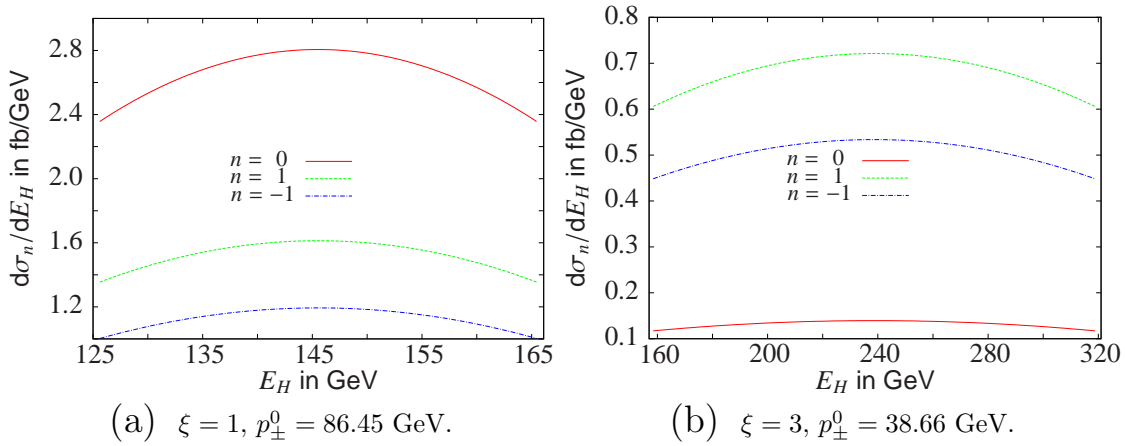


Figure 6.3: Partial differential cross sections $d\sigma_n/dE_H$ for the same parameter sets as in Fig. 6.2. In both cases, the red solid line represents $d\sigma_0$, the green dashed line is $d\sigma_1$, and the blue dashed-dotted line is $d\sigma_{-1}$.

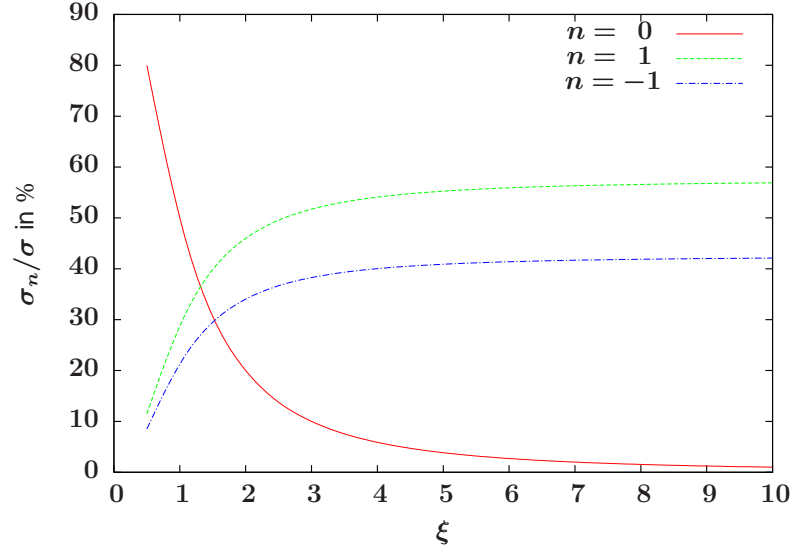


Figure 6.4: Ratio of partial and total cross sections σ_n/σ as a function of the laser intensity parameter ξ . The red solid line represents σ_0/σ , i.e. zero absorption or emission, the green dashed line is σ_1/σ , and the blue dashed-dotted line is σ_{-1}/σ . The contribution of the respective photon orders is independent of the collision energy but only depends on the laser intensity.

where γ_{cm} and β_{cm} are the Lorentz factor and the velocity of the c.m. system with respect to the lab frame. From (6.49) follows

$$\beta_{\text{cm}} = \frac{q_+^3 + q_-^3}{q_+^0 + q_-^0}. \quad (6.50)$$

The produced Higgs boson has a fixed energy E'_H in the c.m. system. From Eq. (5.28) in Ch. 5, we know that in the c.m. system, the Higgs boson's energy is

$$E'_H = \frac{s + M_H^2 - M_Z^2}{2\sqrt{s}}. \quad (6.51)$$

The momentum in z -direction has the maximum value

$$P_{\text{max}}'^3 = \sqrt{E_H'^2 - M_H^2}. \quad (6.52)$$

Performing the Lorentz transformation back into the lab system, we find that the Higgs boson's energy may vary between the values

$$\begin{aligned} E_H^{\text{min}} &= \gamma_{\text{cm}}(E'_H - \beta_{\text{cm}}P_{\text{max}}'^3) \quad \text{and} \\ E_H^{\text{max}} &= \gamma_{\text{cm}}(E'_H + \beta_{\text{cm}}P_{\text{max}}'^3). \end{aligned} \quad (6.53)$$

The width of the spectrum in the lab frame therefore is

$$\Delta E_H = 2\beta_{\text{cm}}P_{\text{max}}'^3. \quad (6.54)$$

Fig. 6.2 shows the differential cross section $d\sigma/dE_H$ as a function of the Higgs boson's energy E_H for different sets of parameters. In both cases, the photon

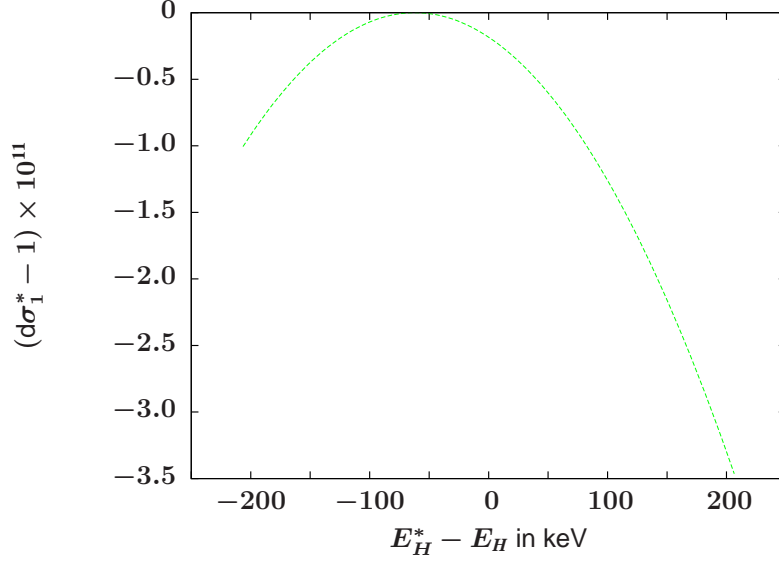


Figure 6.5: Partial differential cross section $d\sigma_1/dE_H$ for $\xi = 1$, $p_{\pm}^0 \approx 76.43386$ GeV, $\omega = 1$ eV. One photon is absorbed, the creation threshold is exceeded by 3.5 eV. The y -axis shows $d\sigma_1^* - 1$, $d\sigma_1^*$ being the ratio between $d\sigma_1(E_H)/dE_H$ and its maximum value ≈ 2.8 fb/GeV, and the x -axis shows the difference between E_H and the center of the allowed energy range $E_H^* \approx 132.58$ GeV.

energy $\omega = 1$ eV and the free momenta are chosen such that E_{cm} would yield the maximum cross section in the field-free case, i.e. $p_{\pm}^0 \approx 86.45$ GeV for $\xi = 1$ and $p_{\pm}^0 \approx 38.66$ GeV for $\xi = 3$. In both cases, the integral over the spectrum reproduces the field-free cross section $\sigma \approx 212$ fb. Both spectra are symmetrical and have a maximum at the center of the allowed energy range. The respective width of the spectrum, i.e. $\Delta E_H \approx 40$ GeV for $\xi = 1$ and $\Delta E_H \approx 160$ GeV for $\xi = 3$, agrees with Eq. (6.54).

Partial Differential Cross Sections

Fig. 6.3 shows the contribution of the respective photon orders to the differential cross section for the same parameter sets as in Fig. 6.2. The shape of the partial differential cross sections is the same as in Fig. 6.2, i.e. they are symmetric and have a maximum in the center of the allowed energy range. For $\xi = 1$, the main contribution stems from σ_0 , i.e. the term where no absorption or emission of laser photons takes place. This term yields 50 % of the total cross section. The absorption of one laser photon yields about 30 % of the total cross section, and the remaining 20 % come from the emission of one photon. The situation is different for $\xi = 3$. Here, the main contribution, yielding about 52 % of the total cross section, is the one from the absorption of one laser photon. σ_{-1} yields the second largest fraction, 38 %, and only 10 % of the total cross section stem from the zero-absorption or emission term σ_0 . It is found that the ratio of the partial and the total cross section is independent of the collision energy. It only depends on the laser parameter ξ and thus on the asymmetry of the colliding leptons' momenta (Fig. 6.4). For small laser intensity parameters ξ , the main contribution comes

from σ_0 which agrees with the fact that without the laser field, there is only σ_0 . Both the contribution of σ_1 and σ_{-1} increase with increasing laser intensity, while the contribution from σ_0 decreases.

6.2.4 Small Energy Excess

So far, we have shown differential cross sections for the collision energy exceeding the boson creation threshold by the amount that leads to the maximum cross section. This is surely the most interesting setting with regard to experimental realization. However, from a theoretical point of view, it is also interesting to look at a different energy excess. If more energy is available in the collision, i.e. if $E_{\text{cm}} > 244.5$ GeV, the main properties of the differential cross sections remain the same as above. However, if the creation threshold is exceeded by a small amount of energy only, the partial differential cross sections' dependences on the Higgs boson's energy change. Since in this case only a narrow range of Higgs boson energies are allowed, we define the center E_H^* of the allowed energy range,

$$E_H^* := \frac{E_H^{\text{max}} - E_H^{\text{min}}}{2} \quad (6.55)$$

with the limits E_H^{min} and E_H^{max} from Eq. (6.30). Additionally, the spectra are very flat. Therefore, we define the ratio $d\sigma_n^*$ as

$$d\sigma_n^* := \frac{d\sigma_n(E_H)}{dE_H} \left(\frac{d\sigma_n^{\text{max}}}{dE_H} \right)^{-1}, \quad (6.56)$$

i.e. the ratio between the differential cross section and its maximum value $d\sigma_n^{\text{max}}/dE_H$.

Fig. 6.5 shows the partial differential cross section $d\sigma_1/dE_H$ for $\xi = 1$, $\omega = 1$ eV, and $p_{\pm}^0 \approx 76.43$ GeV. With one absorbed laser photon, the creation threshold is exceeded by 3.5 eV. The width of the allowed energy range of the produced Higgs boson is only 413 keV. The x -axis therefore shows the difference to the center E_H^* of the allowed energy range. Here, $E_H^* \approx 132.58$ GeV. The difference between 1 and the ratio $d\sigma_1^*$ is shown on the y -axis. The maximum of the spectrum is not at the center, but at a smaller value of the Higgs boson's energy. Figs. 6.6a and 6.6b show the same distribution for zero absorption and the emission of one photon, respectively. In the former case, the creation threshold is exceeded by 2.5 eV and the width of the spectrum is 365 keV. In this case, the maximum of the spectrum lies at a larger value of the Higgs boson's energy. In the case where one laser photon is emitted, the energy excess is 1.5 eV, the width of the spectrum is 311 keV, and the maximum of the spectrum lies at a smaller Higgs boson energy. The center value $E_H^* \approx 132.58$ GeV is the same for all photon orders. However, the respective width of the allowed energy range is dependent on the available collision energy. When summed over all the photon orders, the maximum of the spectrum lies at the center of the allowed Higgs boson energy range. The total cross section $\sigma = \sum_n \sigma_n$ reproduces the field-free cross section¹ $\sigma_{\text{ff}} \approx 3.5 \times 10^{-3}$ fb.

¹For the calculation of the field-free cross section, $n = 0$ has been assumed.

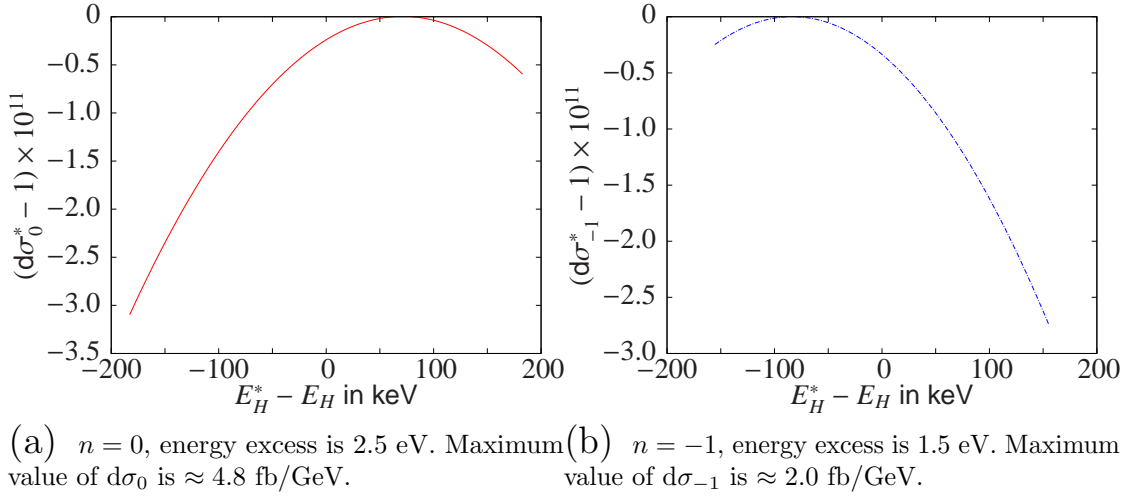


Figure 6.6: Same as Fig. 6.5 for zero absorption (a) and emission of one photon (b). For all photon orders, the center of the allowed energy range is $E_H^* \approx 132.58$ GeV.

6.2.5 Below-Threshold Creation

An interesting feature of collision experiments taking place inside a laser field is that the absorption of laser photons may add extra energy to the collision energy. In general, arbitrarily many laser photons can be absorbed at any electromagnetically interacting particles' vertex. In our case, since the created bosons do not interact with the laser field, photons can only be absorbed at the incoming muons' vertex. Also, since we are still considering perfectly collinear particle and photon directions, only one photon may be absorbed from the laser field (see the beginning of Sec. 6.2). If the energy of this single laser photon is large enough to exceed the energy threshold, the associated creation of a Higgs and a Z^0 boson is possible even if the energy of the colliding (laser-dressed) particles would not suffice, i.e. $\sqrt{(q_+ + q_-)^2} < M_Z + M_H$. In order to investigate this case, we assume a photon energy of $\omega = 10$ keV and choose p_\pm^0 in such a way that the creation threshold is exceeded by 10 eV (Fig. 6.7a) and 9.9 keV (Fig. 6.7b). For $\xi = 1$, this is the case for $p_\pm^0 \approx 76.433856$ GeV and $p_\pm^0 \approx 76.43386$ GeV, respectively. The difference between the two considered free energies is ≈ 3.5 keV. It leads to a three orders of magnitude larger energy excess and a 30 times wider energy spectrum in the latter case. In the case where the reaction threshold is exceeded by a small amount of energy, the maximum of the spectrum lies at a smaller value of the Higgs boson's energy, whereas for the larger excess, it is at the center of the allowed energy range. In both cases, the ratio of the cross section and the respective field-free cross section² is $\sigma_1/\sigma_{\text{ff}} \approx 30\%$. This ratio, as seen before, is only dependent on the laser intensity parameter ξ (cf. Fig. 6.4).

²The field-free cross section is calculated for the c.m. energy $\sqrt{(q_1)^2} = \sqrt{(q_+ + q_- + 1k)^2}$, i.e. where the laser-dressed muon momenta and the absorption of one laser photon is taken into account and equally distributed over two colliding free muons.

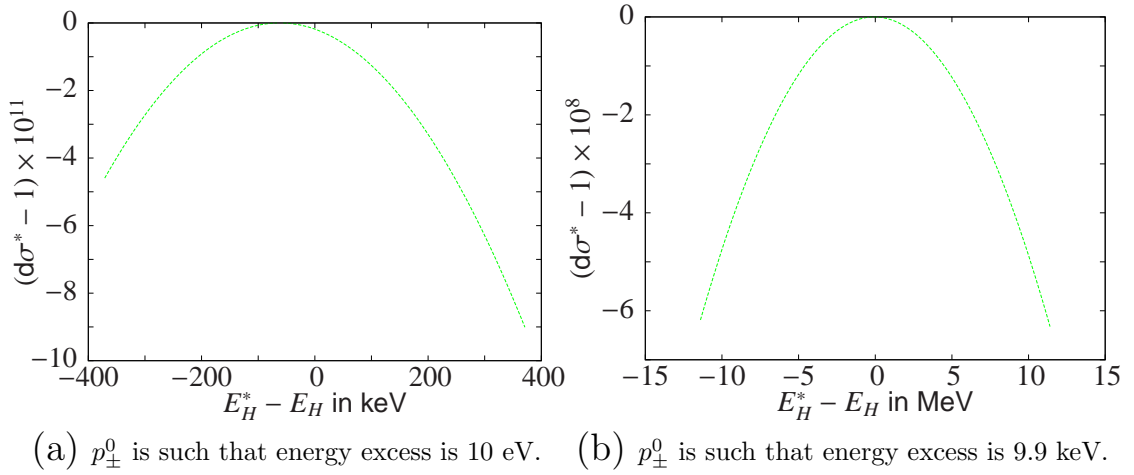


Figure 6.7: Differential cross section as function of Higgs boson's energy. Axes are as in Figs. 6.5 and 6.6. The maximum value of $d\sigma_1/dE_H$ is ≈ 2.8 fb/GeV in both cases and the center of the allowed energy range is $E_H^* \approx 132.58$ GeV.

6.3 Required Laser Parameters and other Experimental Demands

In this section, we perform some considerations regarding a possible experimental realization of the process considered above and show why we considered $\mu^+\mu^-$ instead of e^+e^- collisions.

In order to obtain a substantial effect on the c.m. energy in a real experiment, certain severe restrictions on the laser field as well as the lepton beams have to be met. First of all, the numerical calculations presented in the previous section strictly hold for perfect alignment of the muon and antimuon beams and the laser beam. This assumption is reasonable only if the angular spread in the particle beams is low, $\Delta\theta \ll 1/\gamma$ with the initial Lorentz factor γ . If $\Delta\theta > \xi/\gamma$, the fraction of substantially accelerated muons is very small. Typical beam divergences of muon beams are in the order of 1 mrad [AAA⁺03]. For a muon from the above example where $\xi = 1$ and the free muon energy is $p_{\pm}^0 = 86.45$ GeV, this angle with the laser propagation axis would yield to a quasi-energy of $q_{\pm} \approx 138$ GeV instead of the 173 GeV obtained for perfect alignment. Please note that the alignment and trapping of the lepton beams inside strong laser fields is not trivial. There are, however, schemes that use tailored pulse profiles and auxiliary fields that are aimed at overcoming this problem [CM99; SZ01; KMK⁺04; KP05].

Even if the alignment of the beams is perfect, the quasi-momentum q_{\pm} from Eq. (6.5) is a meaningful quantity only if the leptons remain inside the laser field for one whole oscillation cycle, which the counter-propagating antimuons from the above example surely will. The muons, however, already traveling with relativistic velocities before entering the laser wave, see a red-shifted laser photon frequency and thus a longer wavelength, leading to quite a large required pulse duration: the laser field must be extended over the whole longitudinal distance Δz the muons

with Lorentz factor $\gamma = p^0/m$ travel inside the laser field with intensity parameter ξ and wave length λ [Cha71],

$$\Delta z = 2\gamma^2(1 + \xi^2)\lambda. \quad (6.57)$$

In addition, in order to prevent the leptons from being kicked out of the laser field, its transversal extension must cover the whole muon trajectory, and thus the beam waist w_0 must be larger than

$$w_0 \geq \Delta x = \gamma\xi\lambda. \quad (6.58)$$

In a Gaussian beam, the beam waist w_0 and Rayleigh length z_R are connected via [Mes07]

$$z_R = \frac{\pi w_0^2}{\lambda}. \quad (6.59)$$

The confocal parameter $2z_R$ must be larger than Δz which leads to

$$w_0 \geq \gamma\lambda\sqrt{\frac{1 + \xi^2}{\pi}}. \quad (6.60)$$

The minimal laser beam waist is thus given by the maximum of Eqs. (6.58) and (6.60). For $\xi \gtrsim \sqrt{(\pi - 1)^{-1}} \approx 0.68$, the extension of the lepton trajectory in x -direction is larger than the limit in Eq. (6.60) and therefore we set $w_0 = \Delta x$. For smaller ξ , w_0 is given by (6.60). The Rayleigh length then follows from Eq. (6.59) and the pulse duration is $\tau = 2z_R/c$.

In Table 6.1, we give exemplary laser parameters corresponding to these findings: the first two columns give the laser dimensions for the examples considered in the previous Sec. 6.2. The third and fourth columns show the corresponding parameters if electrons were used instead of muons. The laser intensity I is related to the laser intensity parameter via

$$I = \varepsilon_0 \overline{\mathcal{E}^2} = \frac{a^2 \omega^2}{4\pi} = \frac{m^2 \omega^2 \xi^2}{4\pi e^2} = \frac{m^2 \omega^2 \xi^2}{4\pi \alpha} \quad (6.61)$$

with the electric field $\mathcal{E} = -\partial^0 \mathbf{A}$ of the laser field. Since it is proportional to m^2 , smaller values of I lead to substantial values of ξ for electrons. On the other hand, the smaller mass leads to a much larger Lorentz factor $\gamma = p^0/m$ and thus much larger spatiotemporal extensions of the laser beam (Eqs. (6.57) and (6.58)). Therefore, also pulse power (intensity \times area) and energy (power \times pulse duration) of the laser beams required for electron-positron acceleration are much larger than for muon-antimuon acceleration. While already the laser parameters given in column 1 of Tab. 6.1 vastly exceed current and near-future pulse energies, the parameters required for electron-positron acceleration are even further out of reach. This is one of the main arguments in favor of using muons instead of electrons.

Another advantage of $\mu^+ \mu^-$ instead of $e^+ e^-$ collisions lies in the mass dependence of radiation damping such as e.g. Compton scattering of the counterpropagating

	$\mu^+\mu^-$	$\mu^+\mu^-$	e^+e^-	e^+e^-
Intensity parameter ξ	1	3	1	3
Laser intensity I (W/cm ²)	7.6×10^{22}	6.8×10^{23}	1.8×10^{18}	1.6×10^{19}
Free lepton energy p_{\pm}^0 (GeV)	86.45	38.66	86.45	38.66
Lorentz factor γ	819	366	1.7×10^5	7.6×10^4
Beam waist w_0 (mm)	1	1.3	204	274
Pulse duration (ns)	16.8	29.5	7.3×10^5	1.3×10^6
Pulse power (W)	2.39×10^{21}	2.13×10^{22}	1.09×10^{33}	6.65×10^{34}
Pulse energy (J)	4.02×10^{13}	6.28×10^{14}	7.91×10^{29}	8.68×10^{31}

Table 6.1: Laser parameters required for the process $\ell^+\ell^- \rightarrow HZ^0$ considered in Sec. 6.2. The photon energy is $\omega = 1$ eV, corresponding to a laser wave length $\lambda = 1.2\mu\text{m}$. The pulse duration is $2z_R/c$ (6.57) and the radius of the beam is given by Eqs. (6.58) and (6.60).

antileptons or the emission of radiation by the vastly accelerated copropagating lepton. These processes are essentially governed by the parameter $R_{\pm} := \alpha\xi^2(kp_{\pm})/m^2$ [DP08]. For $\xi = 1$ and the corresponding free energy considered above, we find for muons

$$\begin{aligned} R_+^{\mu} &\approx 10^{-7} \\ R_-^{\mu} &\approx 4 \times 10^{-14}. \end{aligned} \quad (6.62)$$

For electrons, on the other hand, we find³

$$\begin{aligned} R_+^e &\approx 5 \times 10^{-3} \\ R_-^e &\approx 4 \times 10^{-14}. \end{aligned} \quad (6.63)$$

We see that for the counterpropagating positrons, the parameter is larger than for antimuons by four orders of magnitude, due to the smaller mass. For both lepton species, we find the parameter for the co-propagating particle to be very small, which means that radiation damping due to the acceleration is negligible. This also becomes clear when we consider the Larmor formula for the emitted power \mathcal{P} due to this effect [Jac75],

$$\mathcal{P} = \frac{2e^2}{3m^2} \left(\frac{dp_z}{dt} \right)^2 \quad (6.64)$$

with the time derivative dp_z/dt of the momentum p_z along the acceleration direction. It equals the force acting on the particle in z -direction and can also be expressed in the change of energy per unit distance, $\partial p^0/\partial z$ (cf. Sec. 14.2 in [Jac75]). We divide (6.64) by the energy provided by the external field $dp^0/dt = \partial p^0/\partial z \cdot dz/dt$ in order to obtain the radiated power per externally supplied power. Under the assumption that the velocity dz/dt is very close to the speed of light and therefore 1 in our units system, we find

$$\frac{\mathcal{P}}{dp^0/dt} = \frac{2e^2}{3m^2} \frac{\partial p^0}{\partial z}. \quad (6.65)$$

³At first sight, it may seem surprising that the values of R_- for co-propagating muons and electrons are the same. But since $(kp_-) = \omega(p^0 - p^3_-)$ and $m^2 = (p^0 - p^3_-)(p^0 + p^3_-)$, we can write $R_- = \alpha\xi^2\omega/2p^0$ which does not depend on the lepton mass.

If we now assume that the gain in energy $\Delta p^0 = q^0 - p^0$ is uniform over the whole interaction distance Δz (6.57), which is certainly not the case but still may serve to proof the point, we find that the ratio $\mathcal{P}/(dp^0/dt)$ is of substantial size only if the energy difference Δp^0 is of order m over a distance of $2e^2/(3m)$. For muons, this corresponds to an energy gain in the order of 105.6 MeV over a distance of 10^{-17} m, i.e. 10^{19} MeV/m, and for electrons, it corresponds to 3×10^{14} MeV/m. In the $\xi = 1$ example above, we have an energy gain of $\Delta p^0 \approx \xi^2 p^0 \approx 86.45$ GeV over a distance of $\Delta z \approx 3$ m for muons and $\Delta z \approx 140$ km for electrons, corresponding to 3×10^5 MeV/m and 0.6 MeV/m, respectively. In both cases, the values are significantly smaller than the ones required for a sizable ratio (6.65). Therefore, for the copropagating particles, the mass difference does not play a huge role.

For the counterpropagating particles, on the other hand, the mass dependence of the parameter R does impose an important difference between $\mu^+\mu^-$ and e^+e^- collisions. Let us consider their inelastic Compton scattering with the laser photons in the leptons' rest frame where the blue-shifted photon energy is given by $\omega' = \omega\sqrt{(1+\beta)(1-\beta)^{-1}}$ with the lepton velocity β . Let ω'_f and θ'_f denote the final energy and emission angle of the scattered photon, respectively. Then, in the lepton's rest frame, the differential Compton cross section is given by the Klein-Nishina formula [PS95]

$$\frac{d\sigma'_C}{d\cos\theta'_f} = \frac{\pi\alpha^2}{m^2} \left(\frac{\omega'_f}{\omega'}\right)^2 \left(\frac{\omega'_f}{\omega'} + \frac{\omega'}{\omega'_f} - \sin^2\theta'_f\right) \quad (6.66)$$

with the ratio of the final and initial photon energy

$$\frac{\omega'_f}{\omega'} = \frac{1}{1 + \frac{\omega'}{m(1-\cos\theta'_f)}}. \quad (6.67)$$

From the integrated cross section in the rest frame, a Compton scattering rate can be found by multiplying with the photon flux I/ω . The total number of events can be obtained by multiplying this rate by the pulse duration in the lepton's rest frame, τ/γ . For the constellation from the third column in Tab. 6.1, i.e. where positrons with the initial energy of $p^0 \approx 86.45$ GeV collide with a laser field with $\xi = 1$, we find that the number of Compton scattering events is two orders of magnitude larger than for the corresponding muons from the first column. Therefore, from this point of view, muon collisions seem much more promising.

We would like to mention that because the total cross section for the considered Higgs boson creation is quite small (but still of a typical order for weak interaction processes), there will occur a number of background processes. For instance, electron-positron pairs can be created in the lepton collision, $\ell^+\ell^- \rightarrow e^+e^-$. While this process will certainly be one of the most prominent production channels in the field-free case as well as inside the laser field, in the latter case there occur additional e^+e^- production channels: on the one hand, pairs can also be produced in the collision of the counterpropagating antileptons with the laser photons, $\ell^+ + n\omega \rightarrow \ell'^+ + e^+e^-$, which is the so-called (nonlinear) Bethe-Heitler process

	$\mu^+\mu^-$	e^+e^-
Intensity parameter ξ	0.5	0.5
Laser intensity I (W/cm ²)	1.9×10^{22}	1.8×10^{18}
Free lepton energy p_{\pm}^0 (GeV)	109	109
Lorentz factor γ	1035	2×10^5
Beam waist w_0 (mm)	0.78	162
Pulse duration (ns)	10.7	4.6×10^5
Pulse power (W)	3.66×10^{20}	1.49×10^{21}
Pulse energy (J)	3.9×10^{12}	6.7×10^{17}

Table 6.2: Laser parameters required for the process $\ell^+\ell^- \rightarrow HZ^0$ for $\xi = 0.5$. The photon energy is again $\omega = 1$ eV, corresponding to $\lambda = 1.2\mu\text{m}$.

[BH34]. On the other hand, a high-energetic γ -photon produced in the Compton scattering of one of the counterpropagating antileptons can in turn produce pairs via the so-called (nonlinear) Breit-Wheeler process [BW34] in the collision with a certain number of laser photons, $\gamma + n\omega \rightarrow e^+e^-$. We will consider an example for a linearly polarized laser field in the following chapter.

We have seen from Tab. 6.1 that the required laser parameters for $\mu^+\mu^-$ acceleration, while still less unrealistic than the ones for e^+e^- , vastly exceed presently achievable pulse powers (~ 500 TW [NIF]) and energies ($\sim 2 \times 10^{22}$ W/cm² [YCK⁺08]). In Tab. 6.2, we give the corresponding values for a smaller intensity parameter, $\xi = 0.5$. Here, the pulse powers and energies required are significantly smaller than for larger values of ξ . On the other hand, also the effect on the incident leptons' energies is much smaller. It is desirable to find a constellation where the boost of the free lepton energy is large and the pulse power and energy is not completely out of reach. This can be achieved, for instance, by increasing the photon energy. This would reduce the spatial extension of the lepton trajectory given by Eqs. (6.57) and (6.58) and thus the cross sectional area as well as pulse duration of the laser pulse could be reduced. However, for a fixed laser intensity parameter, larger photon frequencies require larger laser intensities. Another way of reducing the pulse power and energy would be to use a laser field of linear instead of circular polarization. There, the classical particle motion caused by the interaction with the electromagnetic field is restricted to the plane that is spanned by the directions of polarization and propagation of the laser wave and therefore, the spatial extension of the field in the perpendicular direction may be smaller (cf. Sec. 4.1). Thus, we may assume an elliptical shape of the laser field's cross sectional area instead of a circular shape as required by circular polarization which may vastly decrease the corresponding pulse power and energy. In the following chapter, we will therefore present the calculation and numerical results for the process $\mu^+\mu^- \rightarrow HZ^0$ in a laser field of linear polarization. For the reasons stated above, we will restrict our examinations to $\mu^+\mu^-$ collisions.

Chapter 7

Higgs Boson Creation in a Linearly Polarized Laser Field

7.1 Analytical Calculation

As seen in the previous section, an efficient boosting of the collision energy in $\mu^+\mu^-$ collisions via a circularly polarized laser requires very large beam diameters. A linearly polarized laser pulse may have an elliptically-shaped cross sectional area which decreases the required energy of the pulse. We therefore consider in this chapter the process of Fig. 6.1 inside a laser wave of linear polarization. The four-potential of such a laser field is given by

$$A_l(\kappa) := a_l \cos \kappa, \quad (7.1)$$

with

$$a_l = (0, a, 0, 0), \quad (7.2)$$

where a is again the amplitude of the laser field. We still consider propagation in z -direction, $k = (\omega, 0, 0, \omega)$, and thus the relations (6.3) are now

$$\begin{aligned} A_l^2 &= a_l^2 \cos^2 \kappa = -a^2 \cos^2 \kappa, \\ (kA_l) &= (ka_l) = (kk) = 0. \end{aligned} \quad (7.3)$$

The action needed in the Volkov states is

$$\begin{aligned} S^\pm &= \pm(p_\pm x) + \frac{e}{(kp_\pm)} \int^\kappa [p_\pm A_l(\tilde{\kappa}) + \frac{e}{2} A_l^2(\tilde{\kappa})] d\tilde{\kappa} \\ &= \pm(p_\pm x) + \frac{e}{(kp_\pm)} \left[\int^\kappa (a_l p_\pm) \cos \tilde{\kappa} d\tilde{\kappa} + \frac{e}{2} \int^\kappa a^2 \cos^2 \tilde{\kappa} d\tilde{\kappa} \right] \\ &= \pm(p_\pm x) + \frac{e(a_l p_\pm)}{(kp_\pm)} \sin \kappa - \frac{e^2 a^2}{8(kp_\pm)} \sin(2\kappa) - \frac{e^2 a^2 \kappa}{4(kp_\pm)} \\ &= \pm(q_\pm x) + \frac{e(a_l p_\pm)}{(kp_\pm)} \sin \kappa - \frac{e^2 a^2}{8(kp_\pm)} \sin(2\kappa). \end{aligned} \quad (7.4)$$

We again used the laser-dressed momenta

$$q_\pm^\mu = p_\pm^\mu + \frac{\xi^2 m^2}{2(kp_\pm)} k^\mu, \quad (7.5)$$

again with the laser intensity parameter ξ from Eq. (4.16). Since $\sqrt{-A_l^2} = a/\sqrt{2}$ for a linearly polarized field, it reads

$$\xi = \frac{ea}{\sqrt{2}m}. \quad (7.6)$$

The transition amplitude reads the same as in (6.7) but with the Volkov states for linear polarization,

$$\begin{aligned} \mathcal{S} = & \frac{-ig}{2\cos\theta_W} \iiint \bar{\psi}_+ \gamma_\mu (g_V - g_A \gamma_5) \psi_- \\ & \cdot \frac{e^{iq(x-y)} - i4\pi g^{\mu\nu} + \frac{i4\pi q^\mu q^\nu}{M_Z^2}}{(2\pi)^4} \frac{1}{q^2 - M_Z^2} \\ & \cdot \frac{igM_Z g_{\nu\rho}}{\cos\theta_W} \frac{1}{2V\sqrt{E_Z E_H}} \epsilon_\rho^*(P_Z) e^{i(P_Z + P_H)y} d^4 q d^4 x d^4 y. \end{aligned} \quad (7.7)$$

We now consider the leptonic current J_μ , as we did in (6.8):

$$\begin{aligned} 2V\sqrt{q_+^0 q_-^0} J_\mu = & \int d^4 x \bar{\psi}_+ \Gamma_\mu \psi_- \\ = & \int d^4 x \overline{\left(1 + \frac{e\not{k}\not{A}_l}{2(kp_+)}\right) u_+ \Gamma_\mu \left(1 - \frac{e\not{k}\not{A}_l}{2(kp_-)}\right) u_-} \\ & \times \exp\left(-i\left((q_+ x) + \frac{e(a_l p_+)}{(kp_+)} \sin\kappa + \frac{e^2 a^2}{8(kp_+)} \sin(2\kappa)\right)\right) \\ & \times \exp\left(i\left(-(q_- x) + \frac{e(a_l p_-)}{(kp_-)} \sin\kappa + \frac{e^2 a^2}{8(kp_-)} \sin(2\kappa)\right)\right) \\ = & \int d^4 x \bar{u}_+ \left(1 + \frac{e\not{A}_l\not{k}}{2(kp_+)}\right) \Gamma_\mu \left(1 - \frac{e\not{k}\not{A}_l}{2(kp_-)}\right) u_- \\ & \times \exp(-i(q_+ + q_-)x) \times \exp\left(-ie\left(\frac{(a_l p_+)}{(kp_+)} - \frac{(a_l p_-)}{(kp_-)}\right) \sin\kappa\right) \\ & \times \exp\left(-i\frac{e^2 a^2}{8}\left(\frac{1}{(kp_+)} + \frac{1}{(kp_-)}\right) \sin(2\kappa)\right) \\ = & \int d^4 x \bar{u}_+ \left(\Gamma^\mu + \frac{e}{2}\left(\frac{\not{q}_l\not{k}\Gamma^\mu}{(kp_+)} - \frac{\Gamma^\mu\not{k}\not{q}_l}{(kp_-)}\right) \cos\kappa - \frac{e^2\not{q}_l\not{k}\Gamma^\mu\not{k}\not{q}_l}{4(kp_+)(kp_-)} \cos^2\kappa\right) u_- \\ & \times \exp(-i(q_+ + q_-)x) \times \exp(-i(\alpha_1 \sin\kappa + \alpha_2 \sin(2\kappa))) , \end{aligned} \quad (7.8)$$

with the abbreviations

$$\begin{aligned} \tilde{\alpha}_1 &:= e\left(\frac{(a_l p_+)}{(kp_+)} - \frac{(a_l p_-)}{(kp_-)}\right) \quad \text{and} \\ \tilde{\alpha}_2 &:= \frac{e^2 a^2}{8}\left(\frac{1}{(kp_+)} + \frac{1}{(kp_-)}\right). \end{aligned} \quad (7.9)$$

Please note that the definition of $\tilde{\alpha}_j$ is different than the one of the α_j in the circularly polarized laser field (6.9).

Just like we did in (6.10), we now expand $\tilde{f}(\kappa) := \exp(-i(\tilde{\alpha}_1 \sin \kappa + \tilde{\alpha}_2 \sin(2\kappa)))$, $\cos \kappa \tilde{f}(\kappa)$, and $\cos^2 \kappa \tilde{f}(\kappa)$ in a Fourier series:

$$\begin{aligned}\tilde{f}(\kappa) &= \sum_{n=-\infty}^{\infty} \tilde{b}_n e^{-in\kappa}, \\ \cos(\kappa) \tilde{f}(\kappa) &= \sum_{n=-\infty}^{\infty} \tilde{c}_n e^{-in\kappa}, \\ \cos^2(\kappa) \tilde{f}(\kappa) &= \sum_{n=-\infty}^{\infty} \tilde{d}_n e^{-in\kappa}\end{aligned}\tag{7.10}$$

with the coefficients

$$\begin{aligned}\tilde{b}_n &= \tilde{J}_n(\tilde{\alpha}_1, \tilde{\alpha}_2), \\ \tilde{c}_n &= \frac{1}{2} \left(\tilde{J}_{n-1}(\tilde{\alpha}_1, \tilde{\alpha}_2) + \tilde{J}_{n+1}(\tilde{\alpha}_1, \tilde{\alpha}_2) \right) \\ \tilde{d}_n &= \frac{1}{4} \left(\tilde{J}_{n-2}(\tilde{\alpha}_1, \tilde{\alpha}_2) + 2\tilde{J}_n(\tilde{\alpha}_1, \tilde{\alpha}_2) + \tilde{J}_{n+2}(\tilde{\alpha}_1, \tilde{\alpha}_2) \right).\end{aligned}\tag{7.11}$$

Here we use the generalized Bessel functions (cf. Eq. (B2) in [Rei80])

$$\tilde{J}_n(\tilde{\alpha}_1, \tilde{\alpha}_2) := \sum_{\ell=-\infty}^{\infty} J_{n-2\ell}(\tilde{\alpha}_1) J_{\ell}(\tilde{\alpha}_2)\tag{7.12}$$

which are composed of products of regular cylindrical Bessel functions.

The further procedure is similar to the one for circular polarization. The only difference is in the spinor-matrix product

$$\begin{aligned}{}^l\mathcal{M}_{\mu}^n &:= \bar{u}_+ \left(\Gamma^{\mu} \tilde{b}_n + \frac{e}{2} \left(\frac{\not{q}_l \not{k} \Gamma^{\mu}}{(kp_+)} - \frac{\Gamma^{\mu} \not{k} \not{q}_l}{(kp_-)} \right) \tilde{c}_n - \frac{e^2 \not{q}_l \not{k} \Gamma^{\mu} \not{k} \not{q}_l}{4(kp_+)(kp_-)} \tilde{d}_n \right) u_- \\ &=: \bar{u}_+ {}^l\Delta_{\mu}^n u_-.\end{aligned}\tag{7.13}$$

The leptonic current becomes

$$J_{\mu} = \frac{1}{2V\sqrt{q_+^0 q_-^0}} \sum_{n=-\infty}^{\infty} \int d^4x {}^l\mathcal{M}_{\mu}^n e^{-i(q_++q_-)x} e^{-in(\kappa)},\tag{7.14}$$

which is similar to Eq. (6.15) and can be evaluated in the same manner. With

$$\begin{aligned}{}^lT_{\mu\rho}^n &:= {}^l\mathcal{M}_{\mu}^n (-g^{\mu\rho} + \frac{q_n^{\mu} q_n^{\rho}}{M_Z^2}) \epsilon_{\rho}^*(P_Z) \\ &= \bar{u}_+ \left(\frac{1}{M_Z^2} {}^l\Delta_{\mu}^n q_n^{\mu} q_n^{\rho} \epsilon_{\rho}^*(P_Z) - {}^l\Delta_{\mu}^n \epsilon_{\mu}^*(P_Z) \right) u_- \quad \text{and} \\ ({}^lT_{\nu\sigma}^n)^{\dagger} &= u_-^{\dagger} \gamma^0 \gamma^0 \left(\frac{1}{M_Z^2} {}^l\Delta_{\nu}^{n\dagger} \gamma^0 \gamma^0 q_n^{\nu} q_n^{\sigma} \epsilon_{\sigma} \gamma^0 \gamma^0 - {}^l\Delta_{\nu}^{n\dagger} \epsilon_{\nu}(P_Z) \gamma^0 \gamma^0 \right) \bar{u}_+^{\dagger} \\ &= \bar{u}_- \left[\frac{1}{M_Z^2} {}^l\bar{\Delta}_{\nu}^n q_n^{\nu} q_n^{\sigma} \epsilon_{\sigma}(P_Z) - {}^l\bar{\Delta}_{\nu}^n \epsilon_{\nu}(P_Z) \right] u_+,\end{aligned}\tag{7.15}$$

we find

$$\begin{aligned}
{}^l t_n &:= \sum_{\text{pol}} \sum_{\text{spins}} {}^l T_{\mu\rho}^n ({}^l T_{\nu\sigma}^n)^\dagger \\
&= \frac{1}{M_Z^4} \left(\frac{(q_n P_Z)^2}{M_Z^2} - q_n^2 + 2M_Z^2 \right) \text{tr} \left[{}^l \Delta_\mu^n q_n^\mu \not{\epsilon}_- {}^l \bar{\Delta}_\nu^n q_n^\nu \not{\epsilon}_+ \right] \\
&\quad + \frac{1}{M_Z^2} \text{tr} \left[{}^l \Delta_\mu^n P_Z^\mu \not{\epsilon}_- {}^l \bar{\Delta}_\nu^n P_Z^\nu \not{\epsilon}_+ \right] - \text{tr} \left[{}^l \Delta_\mu^n \not{\epsilon}_- {}^l \bar{\Delta}_\nu^n \not{\epsilon}_+ \right] \\
&\quad - \frac{(q_n P_Z)}{M_Z^4} \text{tr} \left[{}^l \Delta_\mu^n q_n^\mu \not{\epsilon}_- {}^l \bar{\Delta}_\nu^n P_Z^\nu \not{\epsilon}_+ \right] - \frac{(q_n P_Z)}{M_Z^4} \text{tr} \left[{}^l \Delta_\mu^n P_Z^\mu \not{\epsilon}_- {}^l \bar{\Delta}_\nu^n q_n^\nu \not{\epsilon}_+ \right], \quad (7.16)
\end{aligned}$$

which is again included in the numerical calculation of the total cross section

$$\begin{aligned}
\sigma &= \sum_n \int_{E_H^{\min}}^{E_H^{\max}} dE_H \frac{2\pi\alpha^2 M_Z^2 {}^l t_n}{64 \cos^4 \theta_W \sin^4 \theta_W (q_n^2 - M_Z^2)^2 \sqrt{(q_+ q_-)^2 - m_*^4} |\mathbf{q}_n|} \Bigg|_{\cos \Theta_H = \cos \Theta_H^0}^{\mathbf{P}_Z = \mathbf{q}_n - \mathbf{P}_H} \\
&= \sum_n \sigma_n. \quad (7.17)
\end{aligned}$$

The cosine of the Higgs boson's polar angle Θ_H^0 and the limits E_H^{\min} and E_H^{\max} for the integration over dE_H are obtained in the same way as in the previous chapter and are given by Eqs. (6.28) and (6.30), respectively. The only difference in the term for the cross section (7.17) and the one obtained for circular polarization, Eq. (6.31), is in the trace ${}^l t_n$ which contains

$$\begin{aligned}
{}^l \Delta_\mu^n &= \Gamma^\mu \tilde{b}_n + \frac{e}{2} \left(\frac{q_l \not{\epsilon} \Gamma^\mu}{(kp_+)} - \frac{\Gamma^\mu \not{\epsilon} q_l}{(kp_-)} \right) \tilde{c}_n - \frac{e^2 q_l \not{\epsilon} \Gamma^\mu \not{\epsilon} q_l}{4(kp_+)(kp_-)} \tilde{d}_n \quad \text{and} \\
{}^l \bar{\Delta}_\nu^n &= \bar{\Gamma}^\nu \tilde{b}_n + \frac{e}{2} \left(\frac{\bar{\Gamma}^\nu \not{\epsilon} q_l}{(kp_+)} - \frac{q_l \not{\epsilon} \bar{\Gamma}^\nu}{(kp_-)} \right) \tilde{c}_n - \frac{e^2 q_l \not{\epsilon} \bar{\Gamma}^\nu \not{\epsilon} q_l}{4(kp_+)(kp_-)} \tilde{d}_n. \quad (7.18)
\end{aligned}$$

Based on Eq. (7.17), we will show some numerical results in Sec. 7.2. Before, we briefly check that the field-free cross section (5.36) is reproduced, like we did in Sec. 6.1.4.

Considering the case of vanishing laser intensity, i.e. the limit of the field-free Higgs creation, we see that all terms in (7.18) except for

$$\begin{aligned}
{}^l \Delta_\mu^{\text{ff}} &= \not{\epsilon} (g_V - g_A \gamma_5) \tilde{b}_0 \quad \text{and} \\
{}^l \bar{\Delta}_\nu^{\text{ff}} &= (g_V + g_A \gamma_5) \not{\epsilon} \tilde{b}_0 \quad (7.19)
\end{aligned}$$

vanish. Since for $a = 0$, both arguments of the generalized Bessel functions are zero, $\tilde{\alpha}_j = 0$. Therefore, they become

$$\tilde{J}_0(\tilde{\alpha}_1, \tilde{\alpha}_2) = \sum_\ell J_{0-2\ell}(0) J_\ell(0) = J_0(0) J_0(0) = 1. \quad (7.20)$$

With this, (7.19) is the same as in (6.32), and the derivation of the field-free cross section is as in Sec. 6.1.4.

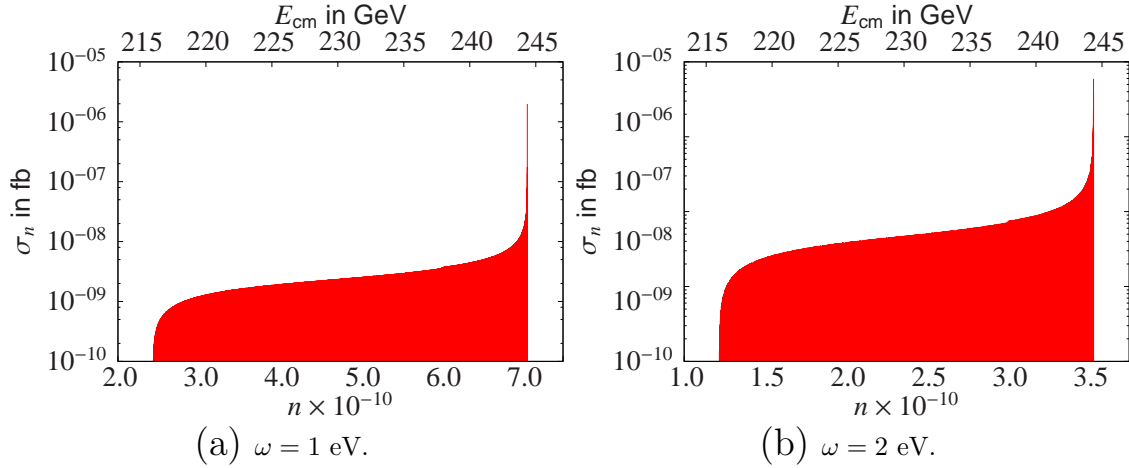


Figure 7.1: Partial cross sections σ_n as function of the photon order n (lower x -axis) on a logarithmic scale. On the upper x -axis, the corresponding c.m. energy $E_{\text{cm}}(n)$ is shown. The free muon energy is $p_{\pm}^0 = 70.59$ GeV, $\xi = 1$, photon energy is $\omega = 1$ eV (a) and $\omega = 2$ eV (b). Note that only every 10^6 -th photon order is depicted.

7.2 Numerical Results

We now discuss the results of the numerical calculation of the cross section (7.17) in the case where the muon beams and the laser field are perfectly collinear and the free momenta of the incoming muon and antimuon are $\mathbf{p}_+ = -\mathbf{p}_-$, i.e. the same scenario as in 6.2. Again, the four-products $(p_{\pm} a_j)$ are 0 and therefore the argument $\tilde{\alpha}_1 = 0$. Thus, the sum in the generalized Bessel functions (7.12) collapses and the inner summation index ℓ is fixed to $\ell = n/2$. Since the regular Bessel function $J_{\ell}(\tilde{\alpha}_2)$ must be of integer order, n must be even and thus only pairs of laser photons are absorbed or emitted at the muon vertex. The generalized Bessel functions become

$$\tilde{J}_n(0, \tilde{\alpha}_2) = J_{n/2}(\tilde{\alpha}_2) \quad (7.21)$$

and Eq. (7.17) reduces to

$$\sigma = \sum_{n \text{ even}} \sigma_n. \quad (7.22)$$

In contrast to the findings for circular polarization, the number n of absorbed or emitted laser photons may vary over a large range.

7.2.1 Partial Cross Sections

For large arguments, $\tilde{\alpha}_2 \gg 1$, the regular Bessel functions $J_{n/2}(\tilde{\alpha}_2)$ have maxima where the order $n/2$ is of the same order as the argument, i.e. at $n \approx 2\tilde{\alpha}_2$, and vanish for larger orders (cf. Appx. C). Since $p_+^3 = -p_-^3$ and therefore

$$\frac{1}{(kp_+)} + \frac{1}{(kp_-)} = \frac{1}{\omega} \left(\frac{1}{p^0 + p_-^3} + \frac{1}{p^0 - p_-^3} \right) = \frac{2p^0}{\omega m^2} \quad (7.23)$$

with $p^0 = p_+^0 = p_-^0$, the argument $\tilde{\alpha}_2$ from Eq. (7.9) can be re-written as

$$\tilde{\alpha}_2 = \frac{\xi^2 p^0}{2\omega}. \quad (7.24)$$

Fig. 7.1 shows the partial cross sections σ_n for $\xi = 1$ and different photon energies. It shows that σ_n is indeed maximal for $n_{\max} \approx \xi^2 p^0 / \omega$. With (7.23) and the laser-dressed muon and antimuon energies from Eqs. (6.47) and (6.48), respectively, the corresponding c.m. energy can be expressed as

$$\begin{aligned} E_{\text{cm}}(n_{\max}) &= \sqrt{(q_+ + q_- + n_{\max}k)^2} \\ &= \sqrt{(q_+^0 + q_-^0 + n_{\max}\omega)^2 - (q_+^3 + q_-^3 + n_{\max}\omega)^2} \\ &\approx \sqrt{(2p^0(1 + \xi^2))^2 - (2\xi^2 p^0)^2} \\ &= 2p^0 \sqrt{1 + 2\xi^2}. \end{aligned} \quad (7.25)$$

The difference to the c.m. energy in the case of circular polarization lies in the large number n_{\max} of maximally absorbed laser photons. Since, in the circularly polarized field, only one laser photon may be absorbed (in the considered setup with $\mathbf{p}_{\pm} \parallel \mathbf{k}$), the enhancement of the c.m. energy merely stems from the laser-dressed lepton energies. Here, a large amount of energy $n_{\max}\omega$ can additionally be absorbed from the laser field.

The free muon energy may be chosen such that this maximal c.m. energy would yield the maximum cross section in the field-free case, i.e. $E_{\text{cm}}(n_{\max}) \approx 244.5$ GeV. For $\xi = 1$, this is the case if $p^0 = 70.59$ GeV. Note that the expression for the maximal c.m. energy is independent of the photon energy ω .

Fig. 7.1a shows the partial cross section σ_n as a function of the photon order n for a photon energy of $\omega = 1$ eV. In this case, $n_{\max} = 7.059 \times 10^{10}$ and σ_n has its maximum for this value. There occurs a cut-off towards the left side of the distribution where the number of photons absorbed from the laser field does not suffice to exceed the reaction threshold. Note that only every 5×10^5 -th photon order is actually calculated because the computation time is very long due to the large Bessel orders (cf. Appx. C). The total cross section is then obtained from the sum of the calculated orders by multiplication with 2.5×10^5 (because only even photon orders contribute). This yields a total cross section of $\sigma \approx 38$ fb. Note that this cross section is sort of an average over all the contributing photon orders, each of which yields a different c.m. energy (see the upper x -axis in Fig. 7.1). Fig. 7.1b shows the partial cross section for a photon energy of $\omega = 2$ eV. Since the photon energy is doubled, the value of n_{\max} is only half of the value for $\omega = 1$ eV, i.e. $n_{\max} = 3.5295 \times 10^{10}$. Also, since the photon energy is twice as large, half as many photons need to be absorbed in order to exceed the reaction threshold. All in all, the range of contributing photon orders in Fig. 7.1b is half as wide as in Fig. 7.1a, while the respective values of σ_n are twice as large. Therefore, the sum over all photon orders still yields the same value of the total cross section, $\sigma = 38$ fb.

Our numerical calculations show that in the considered parameter range, i.e. for sufficiently small ω and sizable ξ so that $\tilde{\alpha}_2 \gg 1$, the cross section (7.17) does not

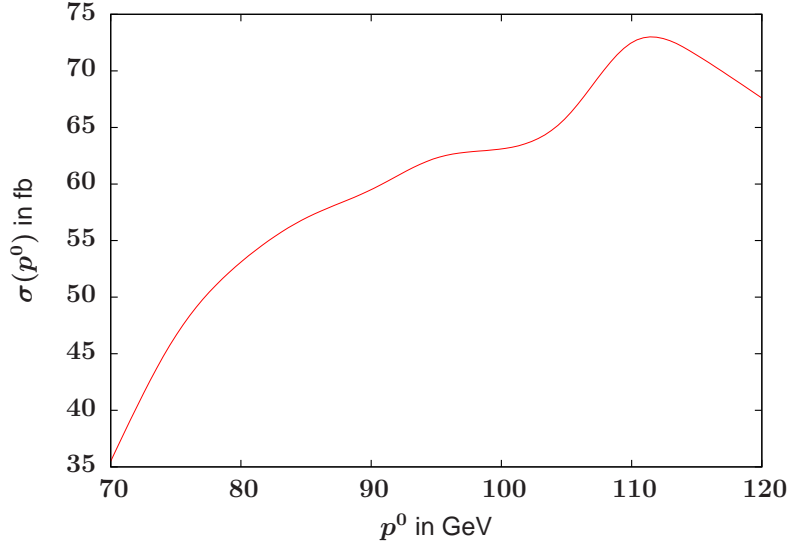


Figure 7.2: Total cross section σ as a function of the free lepton energy p^0 for fixed $\xi = 1$. Note that only 11 data points are calculated for the large photon energy of $\omega = 1$ MeV.

depend on the photon energy. It does, however, depend on the free muon energy p^0 . We have seen in Fig. 7.1 that there occurs a cut-off in the distribution of the partial cross section where the c.m. energy is too small to overcome the creation threshold. For larger free lepton energies, more photon orders are able to contribute to the total cross section. Model calculations with a large photon energy of 1 MeV indicate that for a fixed laser intensity parameter ξ , the total cross section as a function of p^0 reaches a maximum where the free lepton energies are large enough so that the *emission* of n_{\max} photon orders is energetically allowed, i.e. where

$$E_{\text{cm}}(-n_{\max}) = \sqrt{(q_+ + q_- - n_{\max}\omega)^2} \approx 2p^0 \gtrsim M_Z + M_H. \quad (7.26)$$

Fig. 7.2 shows the dependence of the total cross section on the free photon energy for $\xi = 1$ for $\omega = 1$ MeV. The inequality in Eq. (7.26) is fulfilled by $p^0 \gtrsim 108.1$ GeV which is where the distribution in Fig. 7.2 shows a steeper growth with increasing p^0 . In the field-free case, this energy would yield a cross section of $\sigma_{\text{ff}}(2p^0 \approx 216.2 \text{ fb}) \approx 1.7 \text{ fb}$ (cf. Fig. 5.2). In Fig. 7.2, the maximum of $\sigma \approx 73 \text{ fb}$ is reached at $p^0 \approx 110 \text{ GeV}$. For this free muon energy, the process $\mu^+\mu^- \rightarrow HZ^0$ would yield a field-free cross section of $\sigma_{\text{ff}}(2p^0 \approx 220 \text{ fb}) \approx 125 \text{ fb}$. In Sec. 6.2, we saw that the field-free cross section of $\sigma_{\text{ff}}(\sqrt{(q_+ + q_-)^2})$ is reproduced inside a circularly polarized laser wave. Here, $\sigma_{\text{ff}}(\sqrt{(q_+ + q_-)^2}) \approx 147 \text{ fb}$ for $p^0 \approx 110 \text{ GeV}$ which is roughly twice as large as the cross section obtained from the laser-dressed calculation inside the linearly polarized field. The reason for the difference in the total cross section lies in the fact that the cross section in the laser field is an average over a large range of collision energies corresponding to the contributing photon orders and can therefore not readily be related to a field-free cross section of a certain c.m. energy. The range of collision energies would cover a range of corresponding field-free cross sections varying between 1.7 fb and 212 fb.

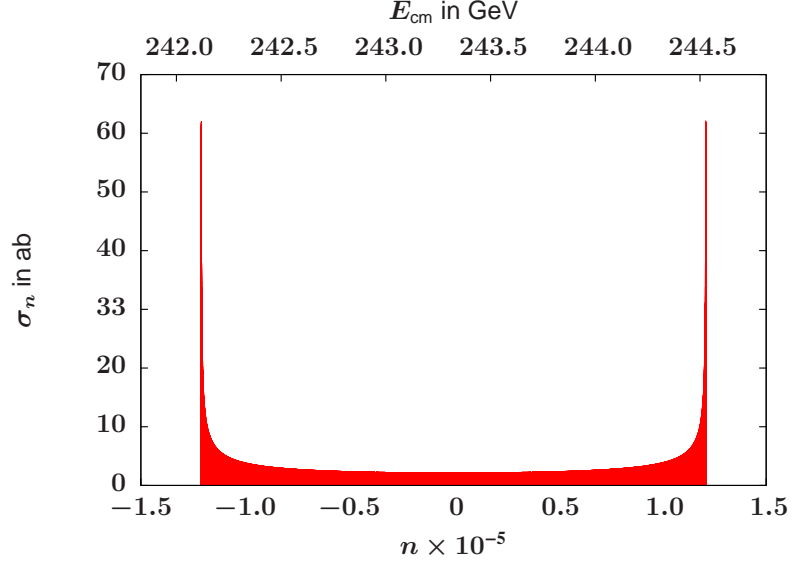


Figure 7.3: Partial cross sections σ_n as function of the photon order n (lower x -axis) for $\xi = 0.1$, $p^0 \approx 121.6$ GeV, and $\omega = 10$ keV. The upper x -axis shows the corresponding c.m. energy.

As an example for a scenario in which the free muon energy that leads to $E_{\text{cm}}(n_{\text{max}}) \approx 244.5$ GeV (cf. Eq. (7.25)) satisfies Eq. (7.26), we consider $\xi = 0.1$ and $p^0 \approx 121.6$ GeV. Here, the field-free energy would almost lead to the maximum cross section without a laser field. The collision energy is affected by the laser field mainly via the absorption of laser photons since for such a small laser intensity parameter, the laser-dressed energies of the leptons differ only marginally from their free energies. Fig. 7.3 shows the corresponding differential cross section for $\omega = 10$ keV. Since the emission of n_{max} photons is energetically allowed, there is no cutoff as for $\xi = 1$ above and there occurs a second maximum for $n = -n_{\text{max}}$. The summation over all photon orders leads to $\sigma \approx 210$ fb.

As mentioned above, the cross section $\sigma = \sum_n \sigma_n$, being a sum over a large number of different photon orders, represents an average over many different collision energies. Therefore, comparing it with a cross section obtained without a laser field with a fixed c.m. energy is not straightforward. However, a rate of Higgs creation events per unit time can be obtained by multiplying the cross section with the flux of the incoming particles $|\mathbf{j}|$ from Eq. (6.24). This rate has the usual meaning and can be accessed experimentally in the same way as in field-free experiments [ATL12b; CMS12b]. In our case where the free lepton momenta are opposite and equal, the particle flux becomes

$$|\mathbf{j}| = \frac{\sqrt{(q_+ q_-)^2 - m_*^4}}{V q_+^0 q_-^0} = \frac{|\beta_+ - \beta_-|}{V} \approx \frac{1}{V} \frac{2}{\frac{m^2 \xi^4}{4p_0^2(1+\xi^2)} + 1} \quad (7.27)$$

with the velocities $\beta_{\pm} = q_{\pm}^z / q_{\pm}^0$. Note that the penultimate step is valid for every constellation where $\mathbf{q}_+ \parallel \mathbf{q}_-$ [LL91].

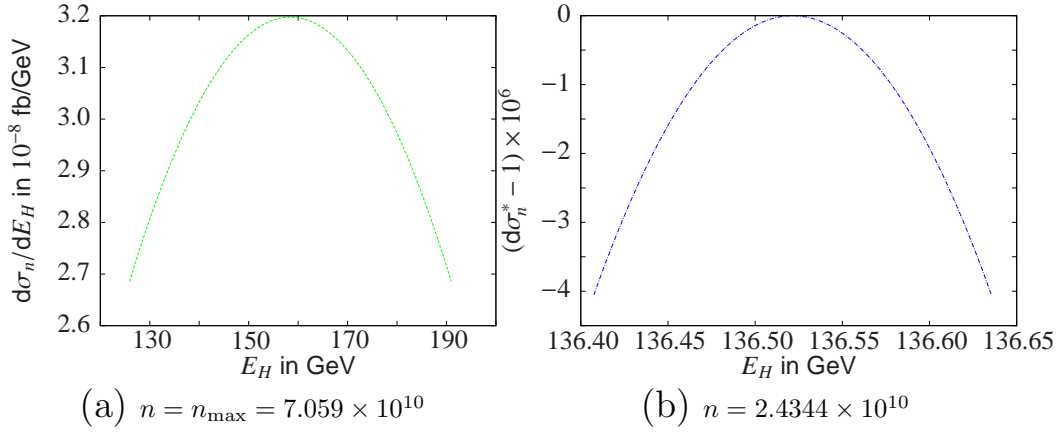


Figure 7.4: Partial differential cross sections $d\sigma_n/dE_H$ as function of Higgs boson's energy E_H for the maximum photon order n_{\max} (a) and a very small photon order (b). The laser intensity parameter is $\xi = 1$, the free muon energy is $p^0 = 70.59$ GeV, and the photon energy is $\omega = 1$ eV. Due to the very flat distribution in (b), the y -axis shows the difference between the ratio $d\sigma_n^*$ from (6.56) and 1.

7.2.2 Differential Cross Sections

Fig. 7.4 shows exemplary partial spectra $d\sigma_n/dE_H$ as functions of the produced Higgs boson's energy E_H for the parameters considered above, i.e. $\xi = 1$, $p^0 = 70.59$ GeV, and $\omega = 1$ eV. In Fig. 7.4a, the spectrum for the maximum photon order $n_{\max} = 7.059 \times 10^{10}$ is shown, and Fig. 7.2.2 shows the spectrum for $n = 2.4344 \times 10^{10}$ which is one of the smallest orders for which the reaction threshold is still exceeded. In both cases, the partial spectra are symmetric. As has already been seen in Sec. 6.2, the larger the amount of energy by which the reaction threshold is exceeded, i.e. the less symmetrical the distribution of the initial momenta, the wider is the allowed energy range: for the large photon order, the Higgs boson is produced with an energy between 126 GeV and 191 GeV, covering a range of about 65 GeV, while for the small amount of absorbed photons, the width of the allowed energy range is only about 230 MeV (cf. Eq. (6.54) in Sec. 6.2).

It is obvious from Fig. 7.4 that a wide range of different photon orders contributes to the total cross section where the energy of the Higgs boson is comparatively small, while large values of E_H can only be achieved via the absorption of a large number of laser photons. The number of photon orders that contribute for the parameter set considered above is very large ($\mathcal{O}(10^{10})$) and the numerical evaluation of Bessel functions of such large orders is very time-consuming. We saw in the previous discussion that the total cross section is independent of the photon energy ω , as long as $\tilde{a}_2 \gg 1$. Therefore, we performed the calculation of the total energy distribution in Fig. 7.5 for a higher photon energy, $\omega = 10$ keV, leading to $n_{\max} = 7.059 \times 10^6$ only. For each energy, every 1000-th photon order (i.e. every 500-th contributing order) has been calculated. As can be seen in the graph, small Higgs boson energies are favored in the total energy distribution. A mere Lorentz transformation of

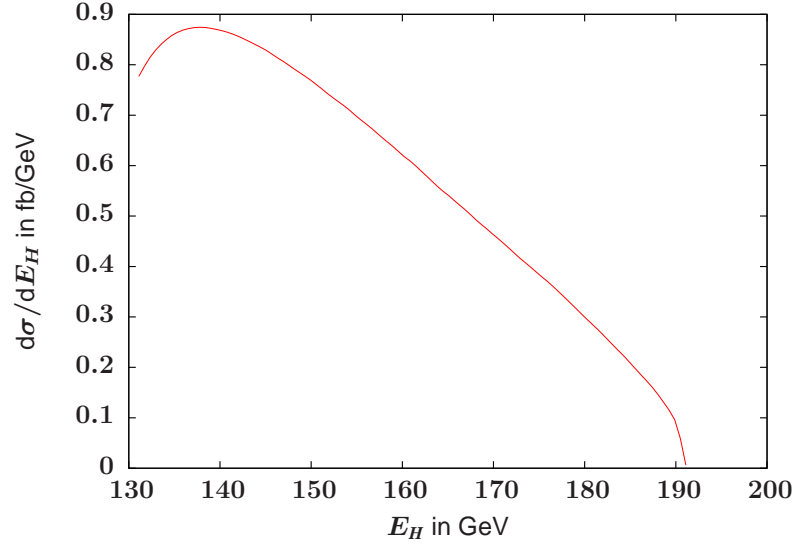


Figure 7.5: Differential cross section $d\sigma/dE_H$ as a function of the Higgs boson's energy E_H for $\xi = 1$, $p^0 = 70.59$ GeV, and $\omega = 10$ keV.

a corresponding field-free calculation would lead to a maximum at the center of the allowed energy range. Thus, the shift towards smaller Higgs boson energies is an effect of the laser field. It can be ascribed to the fact that more photon orders contribute for smaller values of E_H . Corresponding calculations indicate that the polar angle under which the Higgs boson is emitted is also smaller than in the field-free case with symmetrical initial energies. This is also due to the fact that for smaller photon orders, only small angles are allowed. This property of the laser-dressed process might lead to an advantage in the detection of the Higgs boson. In addition, the laser field will also affect the electrically charged decay products of the Higgs boson, e.g. by channeling them into small angular regions [LJK08].

Fig. 7.6 shows the corresponding differential cross section for $\xi = 0.1$ and $p^0 \approx 121.6$ GeV where the emission of n_{\max} laser photons is energetically allowed (cf. Fig. 7.3). Again, the spectrum does not depend on the photon energy ω and therefore, in order to save computation time, we show the spectrum for a larger photon energy of $\omega = 50$ keV. Here, all contributing photon orders have been taken into account in the numerical calculation. The maximum of the contribution is much sharper than for the example with $\xi = 1$. In a corresponding field-free scenario, the maximum of the spectrum would lie at $E_H \approx 137.6$ GeV. The maximum in Fig. 7.6 lies a few hundred MeV below this value. Thus, while the small laser intensity parameter leads to a rather small energy boost, it still affects the produced Higgs boson's energy distribution and thus emission angle which is governed by Eq. (6.28).

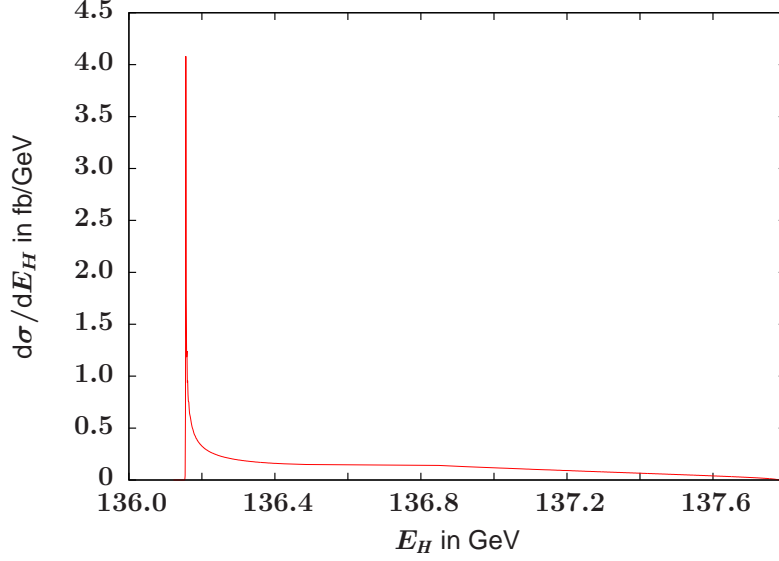


Figure 7.6: Differential cross section $d\sigma/dE_H$ as a function of the produced Higgs boson's energy E_H for $\xi = 0.1$, $p^0 \approx 121.6$ GeV, and $\omega = 50$ keV.

7.3 Required Laser Parameters and other Experimental Demands

As already discussed in Sec. 6.3, the laser beam must cover the whole lepton trajectory in order for the quasi-momenta q_{\pm} to be meaningful. This means, again, that the pulse length must exceed $\Delta z = 2\gamma^2(1 + \xi^2)\lambda$ and the transversal extent must be at least $\Delta x = \gamma\xi\lambda$ (cf. Eqs. (6.57) and (6.58)). Inside a circularly polarized field, the lepton motion describes a circle with radius Δx in the x - y plane. We have seen in Ch. 4 that inside a laser wave of linear polarization, the lepton trajectory is restricted to the x - z plane (if there is no initial momentum in y -direction). Therefore, we can assume that the extension of the laser pulse in y -direction is much smaller than in the polarization direction of the electric field of the laser wave. We thus assume an *elliptic Gaussian beam* according to Sec. 6.12 in [Yar89]. Such a beam features different beam waists w_x and w_y in x - and y -direction, respectively. It can be obtained from a cylindrical Gaussian beam by means of cylindrical focusing lenses. The corresponding Rayleigh lengths z_x and z_y derived from the respective beam waists via (6.59) have different values. For our purposes, we choose the beam waist w_x along the polarization direction such that the lepton trajectory is covered by the laser field. Like we saw in Sec. 6.3, this corresponds to a beam waist fulfilling both inequalities in Eqs. (6.58) and (6.60). In the perpendicular direction, we assume $w_y = \lambda \ll w_x$. The area of the focal spot is then $\pi w_x w_y$, leading to a much smaller required pulse power than for πw_x^2 . Please note, however, that due to the small Rayleigh length in y -direction, the beam divergence in the y - z plane is large. The requirement of high intensity over the whole required extension Δz for the substantial acceleration of the co-moving lepton thus requires advanced focusing of the laser beam in y -direction. Possible techniques that might become able to overcome this issue are e.g. waveguides

	$\mu^+\mu^-$	$\mu^+\mu^-$	$\mu^+\mu^-$	e^+e^-
Intensity parameter ξ	1	1	0.1	1
Photon frequency ω (eV)	1	10	1	1
Laser intensity I (W/cm ²)	7.6×10^{22}	7.6×10^{24}	7.6×10^{20}	1.8×10^{18}
Optimum p_{\pm}^0 (GeV)	70	70	122	70
Lorentz factor γ	670	670	1151	1.4×10^5
Beam waist w_x (mm)	0.8	0.08	0.8	170
Pulse duration (ns)	11.3	1.1	10.7	5×10^5
Pulse power (PW)	2.3×10^3	2.3×10^3	22.5	11
Pulse energy (GJ)	26	2.6	0.24	5.4×10^3

Table 7.1: Laser parameters required for the process $\ell^+\ell^- \rightarrow HZ^0$ considered in Sec. 7.2. The photon energy is $\omega = 1$ eV, leading to a laser wave length $\lambda = 1.2\mu\text{m}$. The pulse duration is $\Delta z/c$ and the radius of the beam is given by (see text or Sec. 6.3). An elliptically-shaped cross sectional area is assumed.

consisting of hollow capillaries [DMC⁺99] or plasma waveguides [SH00; BSH02].

With the intensity

$$I = \varepsilon_0 \overline{\mathcal{E}^2} = \frac{a^2 \omega^2 \sin^2 \kappa}{4\pi} = \frac{a^2 \omega^2}{8\pi} = \frac{m^2 \omega^2 \xi^2}{4\pi e^2} = \frac{m^2 \omega^2 \xi^2}{4\pi \alpha} \quad (7.28)$$

and the “optimum” free lepton energy p^0 such that Eq. (7.25) yields $E_{\text{cm}}(n_{\text{max}}) \approx 244.5$ GeV, we can now derive the required laser parameters like we did in Sec. 6.3.

Tab. 7.1 shows that, due to the different shapes of the laser beams, the (minimally) required pulse energies are indeed much smaller for a laser of linear polarization. For the sake of comparison, and in order to again underline the advantages of muon-antimuon instead of electron-positron collisions, we list an exemplary parameter set for an e^+e^- collision (column 4). We see again that for the latter, smaller values of the laser intensity lead to sizable values of ξ and thus substantial boosting of the electron energy. But, as already stated before, the larger Lorentz factor leads to greater spatiotemporal extensions of the beam and thus larger required pulse energies. For muons, we see that compared to the parameters needed for a circularly polarized laser wave, the required pulse energy for $\xi = 1$ is indeed much smaller (column 1).

The spatiotemporal dimensions of the laser beam we considered depend on the laser frequency ω . For a fixed intensity parameter ξ , the intensity scales as $\sim \omega^2$ and the area of the focal spot as considered above scales as $\sim \omega^{-2}$. Therefore, the pulse power is independent of the photon energy. However, the pulse duration is proportional to ω^{-1} and therefore the pulse energy may be reduced if larger laser frequencies, e.g. in an XUV pulse, are available. On the other hand, high intensities are harder to obtain for larger photon energies (column 2).

In column 3, we list the corresponding laser parameters for the laser intensity parameter $\xi = 0.1$ which we briefly considered in the previous section. We see that the extension in the polarization direction as well as the pulse duration of the laser

pulse are still in the same order of magnitude as for a larger intensity parameter. A reduction of these parameters can only be obtained by either increasing the photon energy and thus reducing the laser wave length or by assuming smaller free lepton energies and thus Lorentz factors. The latter would result in a smaller c.m. energy. Due to the smaller intensity required for $\xi = 1$, the required pulse power and energy are smaller than for a larger intensity parameter. The gain in the collision energy, on the other hand, is small as well.

As already mentioned in Sec. 6.3, the laser photons may inelastically scatter off the counter-propagating antimuons. From the integration of the Klein-Nishina formula (6.66), we find for the antimuons of the above example (column 1 in Tab. 7.1) a rest frame rate of $R'_C \approx 7.4 \times 10^{12} \text{ s}^{-1}$, resulting in a lab frame rate of $R_C \approx 10^{10} \text{ s}^{-1}$. Multiplied by the interaction time τ from Tab. 7.1, this results in approximately 125 total events per antimuon. In order to find an estimate for the energy loss due to this process, we consider the colliding antimuon in its rest frame. There, the final photon energy ω'_f is given by Eq. (6.67). Correspondingly, the antimuon gains the kinetic energy

$$\Delta E' = E'_f - E'_i = k - k' = \omega' \left(1 - \frac{1}{1 + \omega'/m(1 - \cos \theta'_f)} \right) \quad (7.29)$$

which becomes maximal for $\theta'_f = 180^\circ$, i.e. backscattering of the photon, yielding

$$\Delta E'_{\text{max}} = \frac{2(\omega')^2}{2\omega' + m}. \quad (7.30)$$

With the above parameters, we find for the initial photon energy in the antimuon's rest frame $\omega' \approx 1.3 \text{ keV}$ and thus a maximally possible energy shift of the antimuon of $\Delta E'_{\text{max}} \approx 34 \text{ meV}$. This corresponds to $p'_z \approx 2.7 \text{ meV}$ for the z -component of the antimuon's rest frame momentum. Transforming back into the lab frame via $q_f^z = \gamma p'_z + \beta \gamma E'_f$, we find that the maximum energy loss in the lab frame amounts to 1.7 MeV per event. Multiplied with the total number of events, this leads to a maximum energy loss of 213 MeV per antimuon which is small compared to the total collision energy.

We also mentioned in Sec. 6.3 that, in addition to the usual background processes, the collision of the counter-propagating antimuons with the laser photons can directly produce e^+e^- pairs via the so-called Bethe-Heitler process [BH34]. The laser intensity parameter ξ is proportional to the inverse particle mass. Therefore, for the produced electron and positron, we find $\xi_e = \xi m_\mu/m_e \approx 207\xi \gg 1$ with the electron mass m_e and the muon mass m_μ . In this limit, the rate of e^+e^- production in the rest frame of the colliding antimuon is (cf. Eq. (42) in [MMH⁺06])

$$R'_{e^+e^-} = \frac{\alpha^2}{\sqrt{2\pi}} m_e \left(\frac{\omega' \xi_e}{2\sqrt{3}m_e} \right)^3 \exp \left(-\frac{2\sqrt{3}m_e}{\omega' \xi_e} \right). \quad (7.31)$$

In our above example with $\xi = 1$ where the rest frame photon energy is again $\omega' \approx 1.3 \text{ keV}$, this leads to a rest frame rate of $R'_{e^+e^-} \approx 6 \times 10^{10} \text{ s}^{-1}$. Multiplied

with the pulse duration in the rest frame, τ/γ , this yields a total number of one created e^+e^- pair per antimuon. This is a much larger value than obtained for the incoherent production $\mu^+\mu^- \rightarrow e^+e^-$ which is the main e^+e^- pair production process in a (field-free) muon collider with a cross section of approximately 10 mb [Gin96]. The larger e^+e^- background will have to be considered in the detection of the experimental outcome of the collision. However, in the Bethe-Heitler process, most of the energy comes from the laser photons and therefore the effect on the antimuon is expected to be small. It can therefore still contribute to the process $\mu^+\mu^- \rightarrow HZ^0$. The laser beam, on the other hand, is very intense so we may neglect the intensity reduction due to the absorption of laser photons leading to Bethe-Heitler pair creation.

With the parameters from Tab. 7.1, we can revisit the cross section found in the previous Sec. 7.2. For $\xi = 1$, $p^0 \approx 70$ GeV, i.e. the parameters from the first column in Tab. 7.1, we found a total cross section of $\sigma \approx 38$ fb. The volume of the laser pulse is $V = \pi\lambda w_x \Delta z \approx 10^{-8}$ m³, and $|q_+^3/q_+^0 - q_-^3/q_-^0| \approx 2c$. With this, we find for the Higgs production rate $R = \sigma|\mathbf{j}| = \sigma|q_+^3/q_+^0 - q_-^3/q_-^0|/V \approx 2.3 \times 10^{-25}$ s⁻¹ and, multiplied with the pulse duration, we find a total probability \mathcal{P} for the creation of a Higgs and a Z^0 of $\mathcal{P} \approx 2.57 \times 10^{-33}$ per $\mu^+\mu^-$ collision.

For comparison, we estimate the corresponding probability obtained at the LHC. From [Tan13], we obtain the total cross section for Higgs boson production at the LHC to be $\sigma_{\text{LHC}} \approx 17.3$ pb, of which 335 fb stem from the associated production of a Z^0 and a Higgs boson as studied in this work. Assuming a peak luminosity of 10^{34} cm⁻²s⁻¹, a population of 10^{11} protons per bunch and a bunch spacing of 25 ns [Kei96], this yields a total probability for Higgs boson creation of $\mathcal{P} \approx 4.33 \times 10^{-31}$ per proton-proton collision. The probability for the associated production of a Higgs and a Z^0 boson is $\mathcal{P} \approx 8.38 \times 10^{-33}$ per proton-proton collision.

In a future linear electron-positron collider, peak luminosities of 2×10^{34} cm⁻²s⁻¹ are envisaged. With bunch populations of $\sim 2 \times 10^{10}$ electrons or positrons per bunch and 1000 bunches in a pulse of 1 ms duration [ILC07], the probability for the creation of a Higgs and a Z^0 boson is $\mathcal{P} \approx 1.06 \times 10^{-32}$.

We see that the probabilities for the Higgs boson creation with and without the laser field are of comparable size. Therefore, for comparable luminosities, one should also expect similar total yields. The laser field, however, reduces the luminosity as compared to a conventional collider due to several aspects. There are a number of proposals and design studies for muon colliders, e.g. [CAB⁺08; Ale12]; some of the given parameters vary strongly. The best match for our purpose is perhaps found in Tab. XIV of [AAA⁺03]. There, for a c.m. energy of 400 GeV, the number of muons per bunch and the bunch radius are given as 2×10^{12} and 26 μm , respectively. We now consider again the laser parameters from column 1 in 7.1. The large extension of the laser field in x -direction leads to a luminosity reduction of $26 \mu\text{m}/w_x \approx 3.3 \times 10^{-2}$. In addition, due to the small extension in y -direction, only a fraction of the initial muons is sufficiently accelerated. This decreases the luminosity by another factor of $w_y/26 \mu\text{m} \approx 3.8 \times 10^{-2}$. All in all, the luminosity loss due to the laser field is approximately three orders of magnitude. By increasing the beam waist in the y -direction, the number of efficiently accelerated muons can

be increased. If we set $w_y = 26 \mu\text{m}$, which would increase the power and energy of the laser pulse by a factor 22, the luminosity loss would only be the two orders of magnitude arising from the large beam extension in x -direction. Here, we did not take into account that the alignment of the muon and laser beams may lead to a reduction of the laser-dressed momentum; we expect variations in the muons' energy to be evened out by the broad range of absorbed photon numbers. An additional reduction of the luminosity may arise from the challenges regarding synchronizing of the laser and particle beams as well as reaching the muon collider's repetition rate of 15 Hz [AAA⁺03] with the considered high-energy laser; repetition rates in the Hz regime are envisaged at the ELI [ELIb].

Please note that a reduction of the spatiotemporal dimensions of the laser beam obtained by increasing the photon frequency reduces the required laser pulse energy and a corresponding decrease of the extension in x -direction has a positive effect on the collider luminosity. However, a reduction of the beam waist in y -direction further reduces the number of reacting muons. If sufficiently large laser pulse powers are available, it is conceivable to increase the beam waist in y -direction which would again increase the effective number of particles in the co-propagating beam and thus increase the collider luminosity.

Let us put the laser beam parameters from the first column in Tab. 7.1 into perspective. The most intense laser facility to date, the HERCULES laser in Michigan, has reached peak intensities of up to $2 \times 10^{22} \text{ W/cm}^2$ [YCK⁺08]. However, the pulse duration and focal radii, which are in the fs and μm order, respectively, are still substantially smaller than would be required in our example above. The most powerful and most energetic laser facility running today is the National Ignition Facility (NIF) at the Lawrence Livermore National Laboratory in Livermore, USA [NIF]. There, peak powers of up to 500 TW and energies of up to 2 MJ have been achieved in ultra-violet laser pulses of ~ 20 ns duration. More powerful laser facilities are under development. Efforts towards the 10 PW regime are currently being made [STF; CGC⁺09], bound to reach a few 100 PW within the future Extreme Light Infrastructure (ELI) [ELIa]. All in all, high-power laser technology already has and further will experience huge progress which offers prospect to reaching appropriate parameters.

Chapter 8

Conclusion of Part II

We have seen that, while an experimental realization is certainly very challenging in several aspects, the process $\ell^+\ell^- \rightarrow HZ^0$ may profit in several respects from the combination of conventional accelerator techniques with powerful high-energy laser sources. Most prominently, for sizable values of the laser intensity parameter ξ from Eq. (4.16), the quasi-energy of the leptons inside the laser field may be vastly enhanced as compared to the free energy with which they are injected in the laser field. In addition, the absorption of photons from the laser field may further enhance the collision energy. Therefore, the particle energies that have to be provided by the conventional lepton acceleration may be substantially reduced. Another advantage arises from the distributions of the produced Higgs bosons' energy and emission angle. Furthermore, while the produced bosons are neutral and therefore do not interact with the laser field, their decay products may be electrically charged. These charged particles are affected by the laser field and thus, for instance, are channeled into a smaller angular region than without the field.

We showed in Ch. 6 that inside a plane laser wave of circular polarization, the field-free cross section from Ch. 5 is found for comparable collision energies. In the idealized scheme we used, where the initial leptons are perfectly collinear with each other and the laser field and the free momenta are equal and opposite, only three different photon orders contribute to the total cross section which makes the numerical evaluation comparatively easy. Due to the large spatiotemporal extensions of the laser beam required in this setting, the beam power and energy that would be necessary for a substantial acceleration of the leptons are not coming into reach very soon. Therefore, we considered in Ch. 7 the lepton collision inside a plane laser wave of linear polarization. The advantage of this setup is that the laser pulse can be focused to a cross sectional area of elliptical shape. The theoretical analysis of the process inside a linearly polarized laser field is more involved than in the case of circular polarization; on the other hand, the required laser pulse power and energy are clearly more realistic. In fact, as we have discussed in Sec. 7.3, considering the ongoing advances in high-power laser technology, there is a good chance that appropriate parameters can be reached in experiments in the near or intermediate future.

Despite the shorter life time (which does not play a huge role for highly relativistic

muons), muon-antimuon collisions, as compared to electron-positron collisions, have several advantages regarding experimental realization, all of which are related to the smaller rest mass and thus larger Lorentz factor of the latter. First of all, radiation losses due to Compton scattering of the (anti)lepton beam counterpropagating with the laser beam, play a much larger role for electrons. In addition, while the necessary laser intensities are easier to obtain, the required laser pulse powers and energies are not.

Although it is still a long way down the road towards the combination of high-energy laser facilities and muon colliders, laser-assisted muon-antimuon collisions offer new opportunities in the physics of elementary particles, in particular with regard to the creation of Higgs bosons. A possible proof-of-principle experiment feasible with present-day technology might be the production of $\mu^+\mu^-$ pairs in laser-boosted e^+e^- collisions. It will be studied in the next part of this work.

Part III

Muon Pair Creation in Electron-Positron Collisions

As mentioned above, the collision energy required for the creation of Higgs and Z^0 bosons is very high. Therefore, further improvement of both laser and collider techniques is necessary to study the laser-assisted production process from the previous part in an actual experiment. However, the principle of laser acceleration we employed in our investigation of Higgs boson creation also works in QED processes, one of which – the creation of muon-antimuon pairs in a laser-boosted electron-positron collision – we study in this part. The required c.m. energy for the said process is three orders of magnitude smaller than for the creation of the heavy bosons. In addition, the expected cross section of such a QED process is typically much larger than typical weak interaction cross sections, and thus the numbers of produced pairs will be much larger, allowing to examine the effects of the laser field on the colliding as well as the produced particles in detail. Just like in the previous part, we first outline the analytical calculation of the well-known cross section for $e^+e^- \rightarrow \mu^+\mu^-$ without a laser field (Ch. 9) and then inside a laser field of circular (Ch. 10) and linear (Ch. 11) polarization. In Ch. 12, we specify the required laser parameters and other experimental demands, and we conclude this part in Ch. 13.

Chapter 9

Muon Pair Creation Without a Laser Field

The process $e^+e^- \rightarrow \mu^+\mu^-$ is a well-understood elementary QED process and serves as an introductory example in many field theory textbooks, e.g. in [PS95]. For future reference, we will now briefly outline the calculation of its cross section in the case without a laser field.

Like in Ch. 5, the lepton states in position space are given by the Fourier transformation of normalized free Dirac spinors (cf. Eq. (5.9)). The two important differences between the transition amplitude for the process $\ell^+\ell^- \rightarrow HZ^0$ and the one for the process $e^+e^- \rightarrow \mu^+\mu^-$ considered here is that the outgoing particles are leptons and as such carry charge and are also described by free Dirac spinors, and that the virtual particle propagating between the two vertices is a photon (see Fig. 9.1). The propagator of such a virtual photon reads

$$\mathcal{D}_{\mu\nu}(x-y) = \lim_{\epsilon \rightarrow +0} \int \frac{d^4q}{(2\pi)^4} \frac{4\pi e^{iq(x-y)} g^{\mu\nu}}{q^2 + i\epsilon}, \quad (9.1)$$

where q denotes the four-momentum of the virtual photon and ϵ is a small positive

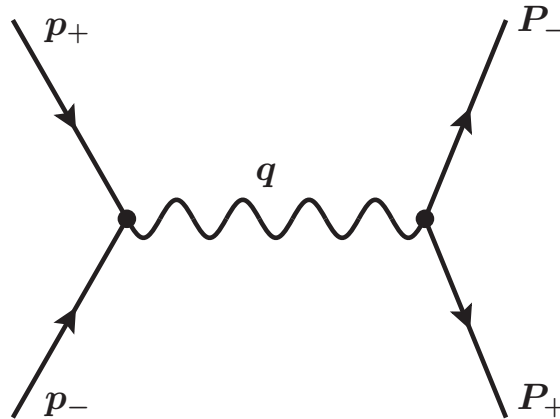


Figure 9.1: Feynman diagram for the considered process $e^+e^- \rightarrow \mu^+\mu^-$.

number which we will omit in the following. The transition amplitude then reads

$$\mathcal{S} = \frac{-4\pi\alpha i}{4(2\pi)^4 V^2 \sqrt{p_+^0 p_-^0 P_+^0 P_-^0}} \iiint \bar{u}_+ \gamma_\mu u_- e^{-i(p_+ + p_-)x} \cdot \frac{e^{iq(x-y)}}{q^2} \bar{U}_- \gamma^\mu U_+ e^{i(P_+ + P_-)y} d^4x d^4y d^4q. \quad (9.2)$$

Uppercase letters denote variables referring to muon and antimuon. The integrations over d^4x and d^4y can again be performed yielding δ -functions for the involved four-momenta,

$$\int d^4x e^{i(q - p_+ - p_-)x} \int d^4y e^{-i(q - P_+ - P_-)y} = (2\pi)^8 \delta(q - p_+ - p_-) \delta(p_+ + p_- - P_+ - P_-), \quad (9.3)$$

and the integration over d^4q fixes the value of the virtual photon's four-momentum to $q_0 = p_+ + p_-$. With this, the transition amplitude becomes

$$\mathcal{S} = \frac{-(2\pi)^5 \alpha i}{2V^2 \sqrt{p_+^0 p_-^0 P_+^0 P_-^0} (q_0)^2} \bar{u}_+ \gamma_\mu u_- \bar{U}_- \gamma^\mu U_+ \delta(q_- - P_+ - P_-). \quad (9.4)$$

The cross section is derived from the transition amplitude by averaging its square over the initial particles' spins and summing over the spins of the produced muon pair. The result has to be divided by a unit time as well as the flux of the incoming particles and finally integrated over the muon momenta,

$$d^6\sigma = \frac{1}{4} \sum_{\text{spins}} \frac{|\mathcal{S}|^2}{\tau |\mathbf{j}|} \frac{V d^3\mathbf{P}_+}{(2\pi)^3} \frac{V d^3\mathbf{P}_-}{(2\pi)^3}. \quad (9.5)$$

The spin sum over $|\bar{u}_+ \gamma_\mu u_- \bar{U}_- \gamma^\mu U_+|^2$ yields

$$\begin{aligned} \sum_{\text{spins}} |\bar{u}_+ \gamma_\mu u_- \bar{U}_- \gamma^\mu U_+|^2 &= \text{tr}[(\not{p}_+ + m) \not{\mu} (\not{p}_- - m) \not{\nu}] \text{tr}[(\not{P}_- - M) \not{\mu} (\not{P}_+ + M) \not{\nu}] \\ &= 32 [(p_+ P_+)(p_- P_-) + (p_+ P_-)(p_- P_+) + M^2(p_+ p_-) + m^2(P_+ P_-) + 2m^2 M^2] \\ &\approx 32 [(p_+ P_+)(p_- P_-) + (p_+ P_-)(p_- P_+) + M^2(p_+ p_-)] \\ &=: t_0, \end{aligned} \quad (9.6)$$

where we omitted terms of order $\mathcal{O}(m^2)$ due to the small electron mass.

We now consider the special case where $p_\pm = (\varepsilon, 0, 0, \mp\varepsilon)$, i.e. where the electron and positron have opposite and equal momenta. Then, the c.m. energy is $E_{\text{cm}} = 2\varepsilon = q_0^0$. Put in Eq. (9.5), this leads to

$$d^6\sigma = \frac{\alpha^2 t_0 \delta(q_0 - P_+ - P_-)}{32 E_{\text{cm}}^6 P_+^0 P_-^0} d^3\mathbf{P}_+ d^3\mathbf{P}_-. \quad (9.7)$$

The integration over the antimuon's momentum is carried out using the three momentum-conserving components of the δ -function, yielding $\mathbf{P}_+ = -\mathbf{P}_-$. The differential of the muon's momentum is re-written as $d\mathbf{P}_- = |\mathbf{P}_-| P_-^0 dP_-^0 d\Omega_-$ and

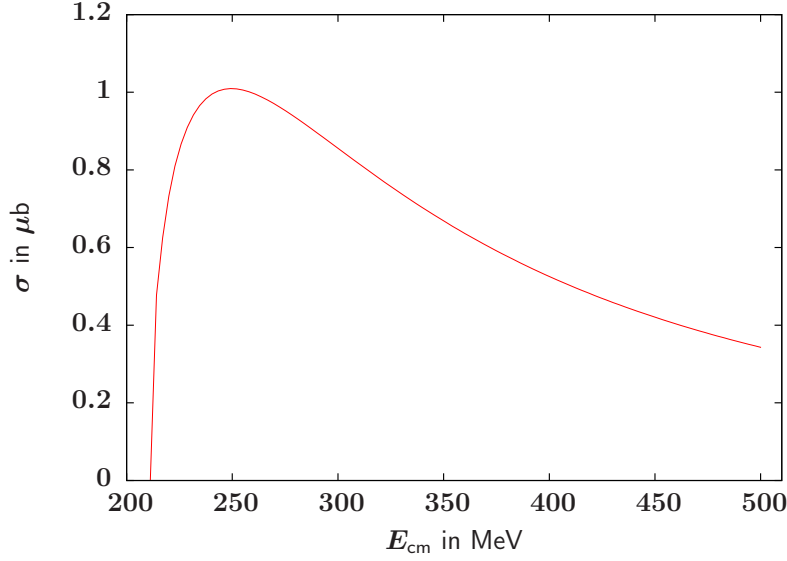


Figure 9.2: Cross section for the process $e^+e^- \rightarrow \mu^+\mu^-$ as function of the collision energy E_{cm} .

the integration over the muon's momentum yields a factor $1/2$ from the derivative of the δ -function's argument and fixes $P_-^0 = \varepsilon$. With this, we can revisit the trace product (9.6). We find

$$\begin{aligned} (p_\pm P_\pm) &= \varepsilon^2 - \varepsilon |\mathbf{P}_-| \cos \Theta_- , \\ (p_\pm P_\mp) &= \varepsilon^2 + \varepsilon |\mathbf{P}_-| \cos \Theta_- , \text{ and} \\ (p_+ p_-) &= 2\varepsilon^2 , \end{aligned} \tag{9.8}$$

and t_0 becomes

$$t_0 = 4E_{\text{cm}}^4 \left[1 + \frac{M^2}{\varepsilon^2} + \left(1 - \frac{M^2}{\varepsilon^2} \right) \cos^2 \Theta_- \right] . \tag{9.9}$$

The differential cross section is then

$$\frac{d\sigma}{d\Omega_-} = \frac{\alpha^2}{4E_{\text{cm}}^2} \sqrt{1 - \frac{M^2}{\varepsilon^2}} \left[1 + \frac{M^2}{\varepsilon^2} + \left(1 - \frac{M^2}{\varepsilon^2} \right) \cos \Theta_- \right] , \tag{9.10}$$

which, integrated over the muon's solid angle, leads to the total cross section

$$\sigma = \frac{4\pi\alpha^2}{3E_{\text{cm}}^2} \sqrt{1 - \frac{M^2}{\varepsilon^2}} \left(1 + \frac{M^2}{2\varepsilon^2} \right) , \tag{9.11}$$

in accordance with [PS95].

Fig. 9.2 shows the dependence of the total cross section (9.11) on the c.m. energy. There is a maximum of $\sigma_{\text{max}} \approx 1 \mu\text{b}$ for $E_{\text{cm}} \approx 250 \text{ MeV}$. For this collision energy, the differential cross section as a function of the produced muon's polar angle is shown in Fig. 9.3. The muon and antimuon are preferably emitted along the axis of the colliding particles' momenta.

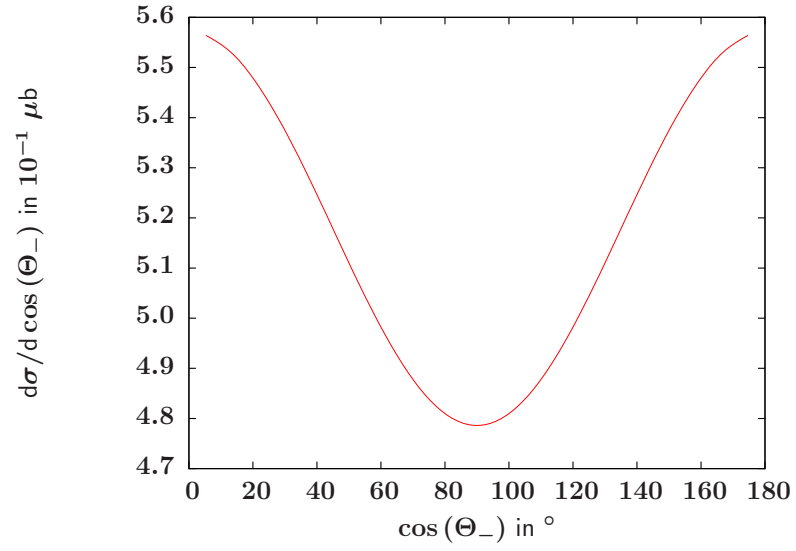


Figure 9.3: Differential cross section $d\sigma/d \cos \Theta_-$ as function of the produced muon's polar angle Θ_- .

Chapter 10

Muon Pair Creation in a Circularly Polarized Laser Field

10.1 Analytical Calculation

We now consider the creation of muon-antimuon pairs from Ch. 9 inside a laser wave of circular polarization. Fig. 10.1 shows the corresponding collision setup as well as the Feynman diagram for this process. The corresponding laser potential (6.1) is as in Ch. 6, leading to the same relations between the polarization and wave vectors of the laser as in (6.3). The Volkov states for the electron and positron are as in (6.4). Similar states describe the produced muon and antimuon; we will again denote their states and other properties by capital letters. The Volkov states for the muon and antimuon then read

$$\begin{aligned} \Psi_{\pm}(y) = & \sqrt{\frac{1}{2VQ_{\pm}^0}} \left(1 \pm \frac{e\not{k}(\not{\epsilon}_1 \cos \eta + \not{\epsilon}_2 \sin \eta)}{2(kP_{\pm})} \right) U_{\pm} \\ & \times e^{i\left(\pm(Q-y) + \frac{e}{(kP_{\pm})}((P_{\pm}a_1) \sin \eta - (P_{\pm}a_2) \cos \eta)\right)}, \end{aligned} \quad (10.1)$$

with $\eta = (ky)$. The effective four-momenta Q_{\pm} of the muon and antimuon are given by

$$Q_{\pm}^{\mu} = P_{\pm}^{\mu} + \Xi^2 \frac{M^2}{2(kP_{\pm})} k^{\mu} \quad (10.2)$$

with the muonic laser intensity parameter

$$\Xi = \frac{ea}{M} = \frac{m}{M} \xi. \quad (10.3)$$

With this, we find the transition amplitude

$$\mathcal{S} = -i\alpha \iint d^4x d^4y \bar{\psi}_{+}(x) \gamma_{\mu} \psi_{-}(x) \mathcal{D}_{\mu\nu}(x-y) \bar{\Psi}_{-}(y) \gamma_{\nu} \Psi_{+}(y) \quad (10.4)$$

with the photon propagator $\mathcal{D}_{\mu\nu}$ as given in (9.1).

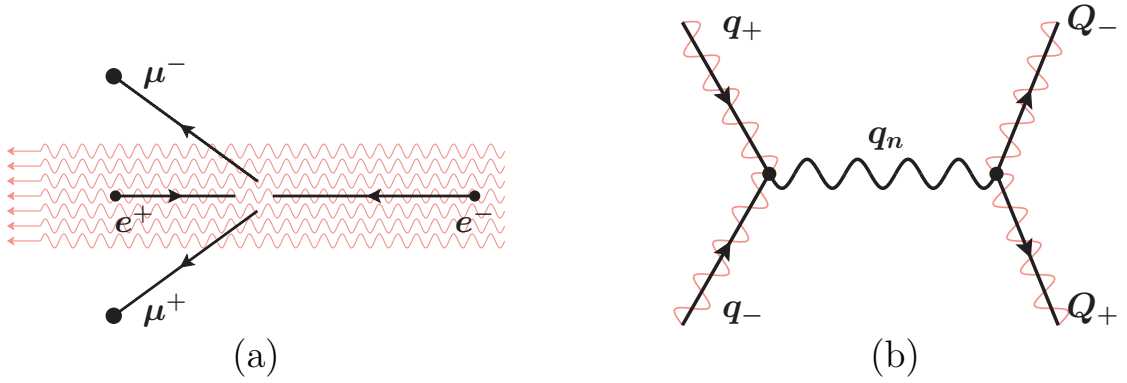


Figure 10.1: Schematic view of the considered process $e^+e^- \rightarrow \mu^+\mu^-$ inside a laser field (a) and its Feynman diagram (b). The wiggled lines indicate that the leptons are described by laser-dressed states.

The electron-positron and muon-antimuon currents, j_μ and J_ν , respectively, can be Fourier expanded as in Sec. 6.1.1. Again using the abbreviation $\kappa = (kx)$, we find for the electronic current

$$\begin{aligned}
 2V\sqrt{q_+^0 q_-^0} j_\mu &= \int d^4x \bar{\psi}_+ \gamma_\mu \psi_- \\
 &= \int d^4x \bar{u}_+ \left(1 + \frac{eA\not{k}}{2(kp_+)} \right) \gamma_\mu \left(1 - \frac{e\not{k}A}{2(kp_-)} \right) u_- \\
 &\quad \times e^{-i(q_++q_-)x} \times e^{-i(\alpha_1 \sin \kappa - \alpha_2 \cos \kappa)} \\
 &= \int d^4x \bar{u}_+ \left[\left(\not{\mu} - \frac{e^2 a^2 k_\mu}{2(kp_+)(kp_-)} \not{k} \right) \right. \\
 &\quad \left. + \frac{e}{2} \left(\left(\frac{q_1 \not{k} \not{\mu}}{(kp_+)} - \frac{\not{\mu} \not{k} q_1}{(kp_-)} \right) \cos \kappa + \left(\frac{q_2 \not{k} \not{\mu}}{(kp_+)} - \frac{\not{\mu} \not{k} q_2}{(kp_-)} \right) \sin \kappa \right) \right] u_- \\
 &\quad \times e^{-i(q_++q_-)x} \times e^{-i(\alpha_1 \sin \kappa - \alpha_2 \cos \kappa)} \quad (10.5)
 \end{aligned}$$

with the α_j as defined in (6.9). The functions $f(\kappa) = \exp(-i(\alpha_1 \sin \kappa - \alpha_2 \cos \kappa))$, $\sin \kappa f(\kappa)$ and $\cos \kappa f(\kappa)$ are again expanded in a Fourier series in the same manner as in (6.10) with the coefficients (6.11) and the argument (6.12) of the regular cylindrical Bessel functions of order n . The spinor-matrix product from Eq. (10.5) then becomes

$$\begin{aligned}
 {}^e \mathcal{M}_\mu^n &= \bar{u}_+ \left(\left(\not{\mu} - \frac{e^2 a^2 k_\mu}{2(kp_+)(kp_-)} \not{k} \right) \cdot b_n \right. \\
 &\quad \left. + \frac{e}{2} \left(\left[\frac{q_1 \not{k} \not{\mu}}{(kp_+)} - \frac{\not{\mu} \not{k} q_1}{(kp_-)} \right] \cdot c_n + \left[\frac{q_2 \not{k} \not{\mu}}{(kp_+)} - \frac{\not{\mu} \not{k} q_2}{(kp_-)} \right] \cdot d_n \right) \right) u_- \\
 &=: \bar{u}_+ \Delta_\mu^n u_- \quad (10.6)
 \end{aligned}$$

and the electronic current reads

$$j_\mu = \frac{1}{2V\sqrt{q_+^0 q_-^0}} \sum_{n=-\infty}^{\infty} \int d^4x {}^e \mathcal{M}_\mu^n \cdot e^{-i(q_++q_-)x} \cdot e^{-in(\kappa)}, \quad (10.7)$$

which is similar to the expression (6.15) found in Sec. 6.1.1.

For the muonic current, the expansion is very similar. We find

$$\begin{aligned}
2V\sqrt{Q_+^0 Q_-^0} J^\nu &= \int d^4 y \bar{\Psi}_- \gamma^\nu \Psi_+ \\
&= \int d^4 y \bar{U}_- \left[\left(\not{y} - \frac{e^2 a^2 k^\nu}{2(kP_+)(kP_-)} \not{k} \right) \right. \\
&\quad \left. + \frac{e}{2} \left(\left(\frac{\not{y} \not{k} \not{q}_1}{(kP_+)} - \frac{\not{q}_1 \not{k} \not{y}}{(kP_-)} \right) \cos \eta + \left(\frac{\not{y} \not{k} \not{q}_2}{(kP_+)} - \frac{\not{q}_2 \not{k} \not{y}}{(kP_-)} \right) \sin \eta \right) \right] U_+ \\
&\quad \times e^{i(Q_+ + Q_-)y} \times e^{-i(\beta_1 \sin \eta - \beta_2 \cos \eta)}
\end{aligned} \tag{10.8}$$

with

$$\beta_j = \frac{(a_j P_-)}{(kP_-)} - \frac{(a_j P_+)}{(kP_+)} . \tag{10.9}$$

Note that the sign is different from the corresponding definition (6.9). We now expand $F(\eta) := \exp(-i(\beta_1 \sin \eta - \beta_2 \cos \eta))$, $\sin \eta F(\eta)$, and $\cos \eta F(\eta)$ like before and find

$$\begin{aligned}
F(\eta) &= \sum_{N=-\infty}^{\infty} B_N e^{-iN\eta} , \\
\cos(\eta) F(\eta) &= \sum_{N=-\infty}^{\infty} C_N e^{-iN\eta} , \\
\sin(\eta) F(\eta) &= \sum_{N=-\infty}^{\infty} D_N e^{-iN\eta}
\end{aligned} \tag{10.10}$$

with the coefficients

$$\begin{aligned}
B_N &= J_N(\bar{\beta}) e^{iN\eta_0} , \\
C_N &= \frac{1}{2} \left(J_{N+1}(\bar{\beta}) e^{i(N+1)\eta_0} + J_{N-1}(\bar{\beta}) e^{i(N-1)\eta_0} \right) , \\
D_N &= \frac{1}{2i} \left(J_{N+1}(\bar{\beta}) e^{i(N+1)\eta_0} - J_{N-1}(\bar{\beta}) e^{i(N-1)\eta_0} \right) .
\end{aligned} \tag{10.11}$$

The argument of the Bessel functions is

$$\bar{\beta} = \sqrt{\beta_1^2 + \beta_2^2} \tag{10.12}$$

and the angle η_0 is given by

$$\cos \eta_0 = \frac{\beta_1}{\bar{\beta}} , \quad \sin \eta_0 = \frac{\beta_2}{\bar{\beta}} . \tag{10.13}$$

With this, we write for the muonic spinor-matrix product

$$\begin{aligned} {}^\mu \mathcal{M}_N^\nu &= \bar{U}_- \left((\not{v} - \frac{e^2 a^2 k^\nu}{2(kP_+)(kP_-)} \not{k}) \cdot B_N \right. \\ &\quad \left. + \frac{e}{2} \left(\left[\frac{\not{v} \not{k} \not{q}_1}{(kP_+)} - \frac{\not{q}_1 \not{k} \not{v}}{(kP_-)} \right] \cdot C_N + \left[\frac{\not{v} \not{k} \not{q}_2}{(kP_+)} - \frac{\not{q}_2 \not{k} \not{v}}{(kP_-)} \right] \cdot D_N \right) \right) U_+ \\ &=: \bar{U}_- \Gamma_N^\nu U_+ \end{aligned} \quad (10.14)$$

and the muonic current becomes

$$J^\nu = \frac{1}{2V \sqrt{Q_+^0 Q_-^0}} \sum_{N=-\infty}^{\infty} \int d^4 y {}^\mu \mathcal{M}_N^\nu \cdot e^{i(Q_+ + Q_-)y} \cdot e^{-iN(\eta)}. \quad (10.15)$$

In contrast to the bosons that are created in the process considered in Part II of this work, the produced muons are electrically charged and thus interact with the laser field. Therefore, the absorption or emission of laser photons is possible not only at the electronic vertex, but also at the muonic one. The numbers of absorbed or emitted photons at the electron and muon vertex are n and N , respectively.

Inserted in Eq. (10.4), the expressions found for the electronic and muonic current lead to

$$\begin{aligned} \mathcal{S} &= \frac{-i\alpha 4\pi}{4(2\pi)^4 V^2 \sqrt{q_+^0 q_-^0 Q_+^0 Q_-^0}} \sum_{n,N} \iiint d^4 x d^4 y d^4 q \frac{{}^\mu \mathcal{M}_N^\nu {}^e \mathcal{M}_\nu^n}{q^2} \\ &\quad \cdot e^{-i(q - Q_+ - Q_- + Nk)y} e^{i(q - q_+ - q_- - nk)x} \\ &= \frac{-i\alpha (2\pi)^5}{2V^2 \sqrt{q_+^0 q_-^0 Q_+^0 Q_-^0}} \sum_{r,n} {}^\mu \mathcal{M}_{r-n}^\nu {}^e \mathcal{M}_\nu^n \frac{\delta(q_+ + q_- + rk - Q_+ - Q_-)}{(q_+ + q_- + nk)^2}, \end{aligned} \quad (10.16)$$

where we introduced the total number of absorbed or emitted photons, $r = n + N$. The momentum of the virtual photon is $(q_+ + q_- + nk)$, i.e. it is composed of the initial particles' momenta and the momenta of the photons that are absorbed at their vertex. Because of the conservation of energy and momentum, it must equal the four-momentum at the muon vertex, $(Q_+ + Q_- - Nk)$. This means that the sum of the produced muon and antimuon's four-momenta $Q_+ + Q_-$ equals the sum of the absorbed laser photons' four-momenta Nk and the four-momentum of the virtual photon $q_+ + q_- + nk$. In the following, we will use the abbreviation

$$q_r = q_+ + q_- + rk, \quad (10.17)$$

which is now *not* the virtual photon's momentum but the total four-momentum involved in the process. It determines the c.m. energy, $\sqrt{s} = \sqrt{(q_r)^2}$.

The differential cross section is obtained from the transition amplitude in the same way as before, only now there is a double sum over the number of photons absorbed in total and at the electron vertex. Due to the δ -function, there occurs no double

summation over the total photon number r and $|\mathcal{S}|^2 = \sum_r |\mathcal{S}_r|^2$. The square of the partial transition amplitudes \mathcal{S}_r reads

$$\begin{aligned} |\mathcal{S}_r|^2 &= \frac{\alpha^2 (2\pi)^6 \tau \delta(q_r - Q_+ - Q_-)}{4V^3 q_+^0 q_-^0 Q_+^0 Q_-^0} \left| \sum_n \frac{{}^\mu \mathcal{M}_{r-n}^\nu {}^e \mathcal{M}_\nu^n}{(q_+ + q_- + nk)^2} \right|^2 \\ &= \frac{\alpha^2 (2\pi)^6 \tau \delta(q_r - Q_+ - Q_-)}{4V^3 q_+^0 q_-^0 Q_+^0 Q_-^0} \sum_{n,n'} \frac{({}^e \mathcal{M}_\mu^{n'})^\dagger ({}^\mu \mathcal{M}_{r-n'}^\mu)^\dagger {}^\mu \mathcal{M}_{r-n}^\nu {}^e \mathcal{M}_\nu^n}{(q_+ + q_- + nk)^2 (q_+ + q_- + n'k)^2}. \end{aligned} \quad (10.18)$$

Summation over the initial and outgoing particles' spins yields

$$\begin{aligned} T_{nn'}^r &:= \sum_{\text{spins}} ({}^e \mathcal{M}_\mu^{n'})^\dagger ({}^\mu \mathcal{M}_{r-n'}^\mu)^\dagger {}^\mu \mathcal{M}_{r-n}^\nu {}^e \mathcal{M}_\nu^n \\ &= \bar{u}_- \bar{\Delta}_\mu^{n'} u_+ \bar{U}_+ \bar{\Gamma}_{r-n'}^\mu U_- \bar{U}_- \Gamma_{r-n}^\nu U_+ \bar{u}_+ \Delta_\nu^n u_- \\ &= \text{tr} \left((\not{p}_+ + M) \bar{\Gamma}_{r-n'}^\mu (\not{p}_- - M) \Gamma_{r-n}^\nu \right) \text{tr} \left((\not{p}'_- - m) \bar{\Delta}_\mu^{n'} (\not{p}'_+ + m) \Delta_\nu^n \right) \end{aligned} \quad (10.19)$$

with the matrices Δ_μ^n and Γ_{r-n}^μ from Eqs. (10.6) and (10.14), respectively.

With this, we find for the differential of the partial cross section σ_r :

$$\begin{aligned} d^6 \sigma_r &= \frac{1}{4} \sum_{\text{spins}} \frac{|\mathcal{S}_r|^2}{\tau |\mathbf{j}|} \frac{V d^3 \mathbf{Q}_+}{(2\pi)^3} \frac{V d^3 \mathbf{Q}_-}{(2\pi)^3} \\ &= \frac{\alpha^2 T_{nn'}^r \delta(q_r - Q_+ - Q_-)}{16 Q_+^0 Q_-^0 \sqrt{(q_+ q_-)^2 - m_*^4} (q_+ + q_- + nk)^2 (q_+ + q_- + n'k)^2} d^3 \mathbf{Q}_+ d^3 \mathbf{Q}_-. \end{aligned} \quad (10.20)$$

Integration over the antimuon's momentum yields

$$d^3 \sigma_r = \frac{\alpha^2 T_{nn'}^r \delta(q_r^0 - Q_+^0 - Q_-^0)}{16 Q_+^0 Q_-^0 \sqrt{(q_+ q_-)^2 - m_*^4} (q_+ + q_- + nk)^2 (q_+ + q_- + n'k)^2} d^3 \mathbf{Q}_- \Big|_{\mathbf{Q}_+ = \mathbf{q}_r - \mathbf{Q}_-}. \quad (10.21)$$

With the differential $d^3 \mathbf{Q}_- = |\mathbf{Q}_-| Q_-^0 dQ_-^0 d\Omega_-$, we can again use the integration over $d \cos \Theta_-$ to eliminate the remaining energy-conserving δ -function like we did in Chs. 6 and 7. The root of the function $g(\cos \Theta_-) = q_r^0 - Q_+^0(\cos \Theta_-) - Q_-^0$ is at

$$\cos \Theta_-^0 = \frac{2q_r^0 Q_-^0 - (q_r)^2}{2|\mathbf{q}_r||\mathbf{Q}_-|} \quad (10.22)$$

and the derivative is

$$g'(\cos \Theta_-) = \frac{|\mathbf{q}_r||\mathbf{Q}_-|}{Q_+^0}. \quad (10.23)$$

From $|\cos \Theta_-^0| \leq 1$ follow the limits for the integration over the muon's energy Q_-^0 :

$$\begin{aligned} E_-^{\min} &:= \frac{q_r^0}{2} - \frac{|\mathbf{q}_r|}{2} \sqrt{1 - \frac{4M_*^2}{(q_r)^2}} \quad \text{and} \\ E_-^{\max} &:= \frac{q_r^0}{2} + \frac{|\mathbf{q}_r|}{2} \sqrt{1 - \frac{4M_*^2}{(q_r)^2}}. \end{aligned} \quad (10.24)$$

The integration over $d\Phi_-$ gives a factor 2π , and thus we find for the partial cross section

$$\sigma_r = \int_{E_-^{\min}}^{E_-^{\max}} \sum_{nn'} \frac{\pi \alpha^2 T_{nn'}^r}{8 \sqrt{(q_+ q_-)^2 - m_*^4} (q_+ + q_- + nk)^2 (q_+ + q_- + nk)^2 |\mathbf{q}_r|} dQ_-^0 \quad (10.25)$$

and the total cross section is

$$\sigma = \sum_r \sigma_r. \quad (10.26)$$

10.1.1 Reproduction of the Field-Free Cross Section

In order to derive the field-free cross section from the previous chapter, we consider the trace product from Eq. (10.19). Since $a = 0$, the arguments of all the Bessel functions vanish, and no photons can be absorbed or emitted, $r = n = n' = 0$. The only remaining terms in the matrices Δ_μ^n and Γ_{r-n}^μ are

$$\Delta_{\text{ff}}^\mu = \not{\mu} b_0 \quad (10.27)$$

and

$$\Gamma_{\text{ff}}^\mu = \not{\mu} B_0. \quad (10.28)$$

Therefore, the trace product becomes

$$T_{\text{ff}} = \text{tr} \left((\not{P}_+ + M) \not{\mu} (\not{P}_- - M) \not{\nu} \right) \text{tr} \left((\not{p}_- - m) \not{\mu} (\not{p}_+ + m) \not{\nu} \right) |b_0|^2 |B_0|^2 \quad (10.29)$$

with $|b_0|^2 = |B_0|^2 = 1$. This equals t_0 from Eq. (9.6). We now again assume to be in the reference frame with $p_\pm = (\varepsilon, 0, 0, \mp\varepsilon)$. With $Q_\pm = P_\pm$ and $q_\pm = p_\pm$ and after the integration over $d^3\mathbf{P}_+$, we obtain

$$\begin{aligned} d^3\sigma_{\text{ff}} &= \frac{\alpha^2 T_{\text{ff}} \delta(2\varepsilon - P_+^0 - P_-^0)}{16 P_+^0 P_-^0 2\varepsilon^2 (p_+ + p_-)^4} d^3\mathbf{P}_- \Big|_{\mathbf{P}_+ = -\mathbf{P}_-} \\ &= \frac{\alpha^2 T_{\text{ff}} \delta(2\varepsilon - 2P_-^0)}{8 P_-^0 E_{\text{cm}}^6} dP_-^0 d\Omega_- \end{aligned} \quad (10.30)$$

and

$$\frac{d\sigma_{\text{ff}}}{d\Omega_-} = \frac{\alpha^2}{4E_{\text{cm}}^2} \sqrt{1 - \frac{M^2}{\varepsilon^2}} \left[1 + \frac{M^2}{\varepsilon^2} + \left(1 - \frac{M^2}{\varepsilon^2} \right) \cos \Theta_- \right] \quad (10.31)$$

which is the same as (9.10) and leads to the same total cross section (9.11).

10.2 Numerical Results

We again consider the setup with opposite and equal initial momenta, $p_\pm = (\varepsilon, 0, 0, \mp\varepsilon)$. Like we saw in Sec. 6.2, the laser-dressed energy of the electron that co-propagates with the laser field is then $q_-^0 \approx (1 + \xi^2)\varepsilon$, while the energy of the counterpropagating positron is nearly unaffected, $q_+^0 \approx \varepsilon$. The collision energy is composed of the initial particles' laser-dressed momenta as well as the total

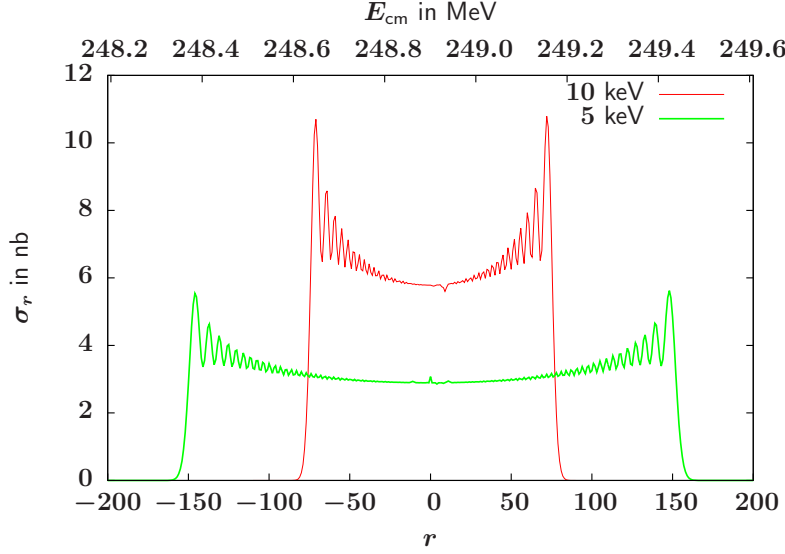


Figure 10.2: Partial cross section σ_r as a function of the total number r of absorbed laser photons (lower x -axis). On the upper x -axis, the corresponding collision energy is shown. The laser intensity parameter is $\xi = 1$ and the free lepton energy is $\varepsilon = 88$ MeV. The thin red line shows the distribution for $\omega = 10$ keV, the thick green one for $\omega = 5$ keV. The total cross section in both cases is $\sigma = \sum_r \sigma_r \approx 1 \mu\text{b}$.

number of laser photons absorbed at both vertices, $E_{\text{cm}} = \sqrt{(q_+ + q_- + rk)^2}$. The argument of the electronic Bessel functions is $\bar{\alpha} = 0$, and therefore, n and n' must be in $\{-1, 0, 1\}$, i.e. the maximum number of absorbed or emitted photons at the electron vertex is 1 (cf. Sec. 10.2). For the number of absorbed photons at the muon vertex, this means $N, N' \in \{r-1, r, r+1\}$.

10.2.1 Partial Cross Sections

We saw in the previous chapter that the field-free cross section has a maximum for $E_{\text{cm}} \approx 250$ MeV. For a laser intensity parameter of $\xi = 1$, this energy is obtained for $\varepsilon \approx 88$ MeV without the absorption or emission of laser photons. We find that, independently of the photon energy ω , the value of the field-free cross section is obtained when summed over all contributing photon orders. Fig. 10.2 shows the dependence of the partial cross section σ_r on the total number r of absorbed or emitted laser photons for this parameter set with a photon energy of $\omega = 10$ keV (thin red line) and $\omega = 5$ keV (thick green line). Since, unlike in the Higgs creation process considered in Ch. 6, photons can be absorbed at both vertices of the Feynman diagram in Fig. 10.1b, the numerical evaluation of the cross section (10.26) is very involved; therefore, the computation for smaller photon energy which leads to large numbers of contributing photon orders is very time-consuming. On the other hand, the numerical calculations for different ω show that there is no dependence of the total cross section on the photon energy; its only effect is on the number of contributing photon orders. Therefore, we may assume that the calculation for, e.g., $\omega = 1$ eV would yield the same outcome as for $\omega = 10$ keV

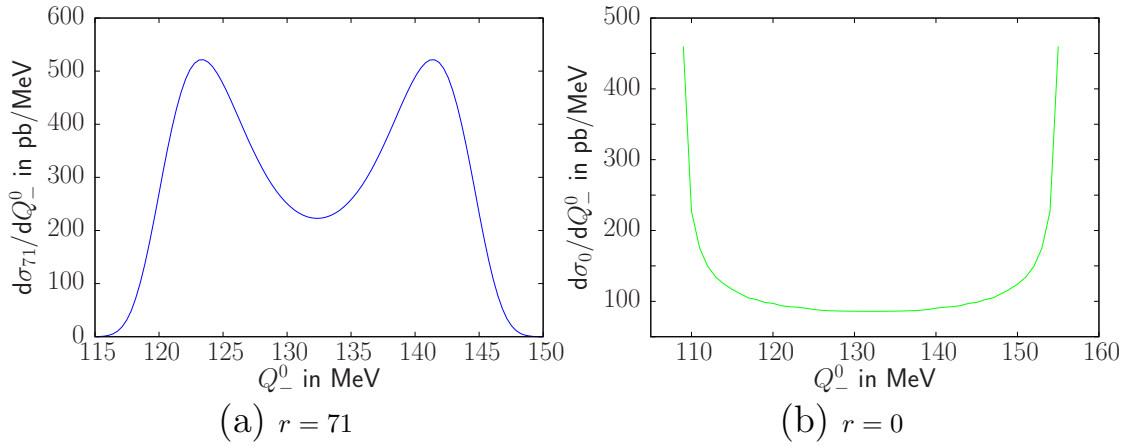


Figure 10.3: Partial differential cross sections $d\sigma_r/dQ_-^0$ for $r = 71$ (a) and $r = 0$ (b). The laser intensity parameter is $\xi = 1$, the free electron energy is $\varepsilon = 88$ MeV, and the photon energy is $\omega = 10$ keV.

but with the contribution of $\sim 10^6$ photon orders.

10.2.2 Differential Cross Sections

We now consider the energy distribution of the produced muon. We have seen in Sec. 6.2.3 that the asymmetry of the colliding leptons' momenta leads to a certain width of the spectrum; the energy-conserving δ -function in Eq. (10.21) does not fix the muon's energy but rather its polar angle. In the (primed) c.m. system, the muon and antimuon's momenta are opposite and equal, $\mathbf{Q}'_+ = -\mathbf{Q}'_-$. In particular, the z -components are

$$Q'^3_- = \gamma_{\text{cm}}(Q_-^3 - \beta_{\text{cm}}Q_-^0) = -Q'^3_+ = -\gamma_{\text{cm}}(Q_+^3 - \beta_{\text{cm}}Q_+^0), \quad (10.32)$$

from which follows the velocity of the c.m. system with respect to the lab frame

$$\beta_{\text{cm}} = \frac{Q_+^3 + Q_-^3}{Q_+^0 + Q_-^0}. \quad (10.33)$$

In the c.m. system, both the muon and antimuon have the energy $Q'^0_+ = Q'^0_- = \varepsilon'$, where ε' is the initial (laser-dressed) energy of the colliding electron and positron. It is given by

$$\varepsilon' = \frac{\sqrt{s}}{2} = \frac{\sqrt{(q_+ + q_- + rk)^2}}{2}. \quad (10.34)$$

The largest possible muon momentum in z -direction is $Q'^3_{-, \text{max}} = \sqrt{\varepsilon'^2 - M_*^2}$. The width ΔQ_-^0 of the energy distribution in the lab system is then obtained from the Lorentz transformation back into this system. Similarly to Eq. (6.54), it reads

$$\Delta Q_-^0 = 2\beta_{\text{cm}}Q'^3_{-, \text{max}}. \quad (10.35)$$

Fig. 10.3 shows exemplary partial cross sections $d\sigma_r/dQ_-^0$ as function of the produced muon's energy for $\xi = 1$, $\varepsilon = 88$ MeV, and $\omega = 10$ keV. There occur two

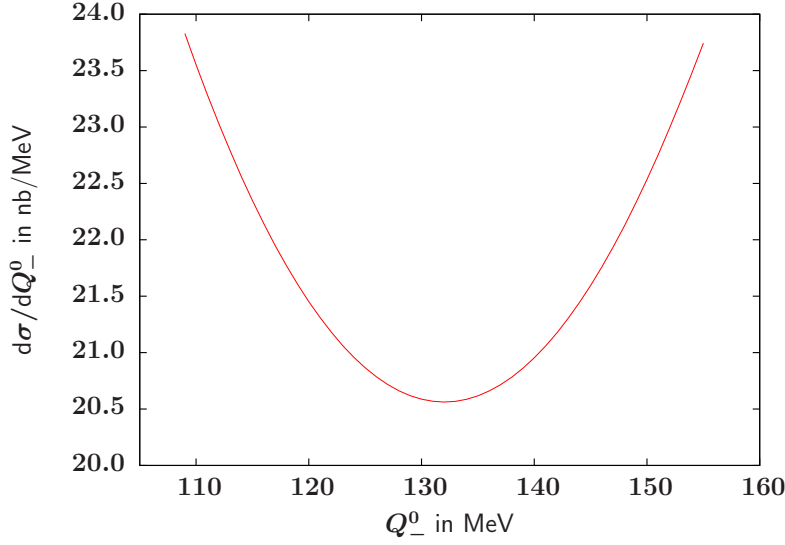


Figure 10.4: Total differential cross section $d\sigma/dQ_-^0$ for $\xi = 1$, $\varepsilon = 88$ MeV, and $\omega = 10$ keV.

maxima; the larger the amount of absorbed or emitted photons, the closer to each other are these maxima. Without the (total) absorption or emission of laser photons, the maxima are at the edges of the distribution. Note that for each order r , the summation over n, n' has been performed. Since $n, n' \in \{-1, 0, 1\}$, the effect of the absorption or emission at the electronic vertex on the width of the energy distribution is negligible. The summation over all photon orders r yields the total differential cross section $d\sigma/dQ_-^0$ shown in Fig. 10.4. The total energy spectrum has maxima at the minimum and maximum muon energy.

We now consider the corresponding energy distributions for the produced antimuon. Its momentum is fixed by the δ -function in the transition amplitude and reads $\mathbf{Q}_+ = \mathbf{q}_r - \mathbf{Q}_-$. For its energy $Q_+^0 = \sqrt{|\mathbf{Q}_+|^2 + M_*^2}$ we therefore find

$$\begin{aligned}
 Q_+^0 &= \sqrt{|\mathbf{q}_r - \mathbf{Q}_-|^2 + M_*^2} \\
 &= \sqrt{(Q_-^0)^2 + |\mathbf{q}_r|^2 - 2|\mathbf{q}_r||\mathbf{Q}_-|\cos\Theta_-} \\
 &= q_r^0 - Q_-^0
 \end{aligned} \tag{10.36}$$

with muon's polar angle as fixed by (10.22). The lower and upper limits of the allowed energy range for the antimuon, E_+^{\min} and E_+^{\max} , respectively, are therefore determined from the limits (10.24) via

$$\begin{aligned}
 E_+^{\min} &= q_r^0 - E_-^{\max} = E_-^{\min} \quad \text{and} \\
 E_+^{\max} &= q_r^0 - E_-^{\min} = E_-^{\max}.
 \end{aligned} \tag{10.37}$$

Since the partial spectra for the muon are symmetric with respect to $q_r^0/2$, so are the antimuon's partial spectra and their respective shapes are identical. If, for instance, the muon is produced with an energy corresponding to the left-hand side maximum of Fig. 10.3a, the antimuon has the energy of the right-hand maximum and vice

versa. Since the total spectrum in Fig. 10.4 is the sum over all contributing partial cross sections and those are identical for the muon and antimuon, the antimuon's total cross section is also the same as the one for the muon. Here, again, a muon energy that is smaller by a certain amount than the center of the energy range corresponds to an antimuon energy larger than the center value by the same amount. The fact that the total differential cross section has its maxima at the edges of the allowed energy range means that a kinematic scenario is preferred where either the muon or antimuon is produced with the maximum possible energy, while the other particle is equipped with the minimally possible one.

Chapter 11

Muon Pair Creation in a Linearly Polarized Laser Field

11.1 Analytical Calculation

We have seen in the previous chapter that, like we found for the associated production of Higgs and Z^0 bosons studied in Pt. II, the total cross section of the reaction inside a laser field of circular polarization is the same as without a laser field. The situation is different inside a linearly polarized laser field, see Ch. 7. There, the summation over all photon orders does not necessarily lead to the field-free Higgs creation cross section. Because the laser parameters required in the case of linear polarization are more likely to come into reach than for circular polarization, and the examination of the process $e^+e^- \rightarrow \mu^+\mu^-$ in this part of the work is meant to serve as a proof-of-principle investigation, we now study the latter process inside a laser field of linear polarization. The laser potential (7.1) and its intensity parameter (7.6), as well as the corresponding electronic Volkov states, are as in Ch. 7. Similarly, the muonic Volkov states read

$$\begin{aligned} \Psi_{\pm} = & \sqrt{\frac{1}{2VQ_{\pm}}} \left(1 \pm \frac{e\not{k}\not{q}_l \cos \eta}{2(kP_{\pm})} \right) U_{\pm} \\ & \times \exp \left(i \left(\pm(Q_{\pm}y) + \frac{e(a_l P_{\pm})}{(kP_{\pm})} \sin \eta - \frac{e^2 a^2}{8(kP_{\pm})} \sin(2\eta) \right) \right) \end{aligned} \quad (11.1)$$

with the laser-dressed momenta as defined in (10.2) but with the laser intensity parameter for the linearly polarized laser field

$$\Xi_l = \frac{ea}{\sqrt{2}M} = \frac{m}{M} \xi_l. \quad (11.2)$$

In the following, we will again omit the index l in the laser intensity parameter.

The electronic current j_μ is given by

$$\begin{aligned}
2V\sqrt{q_+^0 q_-^0} j_\mu &= \int d^4x \bar{\psi}_+ \gamma_\mu \psi_- \\
&= \int d^4x \overline{\left(1 + \frac{e \not{k} \not{A}_l}{2(kp_+)}\right)} u_+ \Gamma_\mu \left(1 - \frac{e \not{k} \not{A}_l}{2(kp_-)}\right) u_- \\
&\quad \times \exp\left(-i\left((q_+x) + \frac{e(a_l p_+)}{(kp_+)} \sin \kappa + \frac{e^2 a^2}{8(kp_+)} \sin(2\kappa)\right)\right) \\
&\quad \times \exp\left(i\left(-(q_-x) + \frac{e(a_l p_-)}{(kp_-)} \sin \kappa + \frac{e^2 a^2}{8(kp_-)} \sin(2\kappa)\right)\right) \\
&= \int d^4x \bar{u}_+ \left(\not{\mu} + \frac{e}{2}\left(\frac{\not{q}_l \not{k} \not{\mu}}{(kp_+)} - \frac{\not{\mu} \not{k} \not{q}_l}{(kp_-)}\right) \cos \kappa - \frac{e^2 \not{q}_l \not{k} \not{\mu} \not{k} \not{q}_l}{4(kp_+)(kp_-)} \cos^2 \kappa\right) u_- \\
&\quad \times \exp(-i(q_+ + q_-)x) \times \exp(-i(\tilde{\alpha}_1 \sin \kappa + \tilde{\alpha}_2 \sin(2\kappa))) , \quad (11.3)
\end{aligned}$$

just like in Ch. 7, and is expanded in a Fourier series in the same way (cf. Eqs. (7.9)-(7.12)). The spinor-matrix product occurring in (11.3) is written as

$$\begin{aligned}
{}^e \mathcal{M}_\mu^n &:= \bar{u}_+ \left(\not{\mu} \tilde{b}_n + \frac{e}{2}\left(\frac{\not{q}_l \not{k} \not{\mu}}{(kp_+)} - \frac{\not{\mu} \not{k} \not{q}_l}{(kp_-)}\right) \tilde{c}_n - \frac{e^2 \not{q}_l \not{k} \not{\mu} \not{k} \not{q}_l}{4(kp_+)(kp_-)} \tilde{d}_n\right) u_- \\
&=: \bar{u}_+ {}^l \Delta_\mu^n u_- \quad (11.4)
\end{aligned}$$

with the coefficients \tilde{b}_n , \tilde{c}_n and \tilde{d}_n from (7.11), and the electronic current becomes

$$j_\mu = \frac{1}{2V\sqrt{q_+^0 q_-^0}} \sum_{n=-\infty}^{\infty} \int d^4x {}^l \Delta_\mu^n e^{-i(q_+ + q_- + nk)x} . \quad (11.5)$$

The muonic current J^ν is given by

$$\begin{aligned}
2V\sqrt{Q_+^0 Q_-^0} J^\nu &= \int d^4y \bar{\Psi}_- \gamma^\nu \Psi_+ \\
&= \int d^4y \overline{\left(1 - \frac{e \not{k} \not{A}_l}{2(kP_-)}\right)} U_- \not{\nu} \left(1 + \frac{e \not{k} \not{A}_l}{2(kP_+)}\right) U_+ \\
&\quad \times \exp\left(i\left((Q_-y) + \frac{e(a_l P_-)}{(kP_-)} \sin \eta + \frac{e^2 a^2}{8(kP_-)} \sin(2\eta)\right)\right) \\
&\quad \times \exp\left(i\left((Q_+y) + \frac{e(a_l P_+)}{(kP_+)} \sin \eta + \frac{e^2 a^2}{8(kP_+)} \sin(2\eta)\right)\right) \\
&= \int d^4y \bar{U}_- \left(\not{\nu} + \frac{e}{2}\left(\frac{\not{\nu} \not{k} \not{q}_l}{(kP_+)} - \frac{\not{q}_l \not{k} \not{\nu}}{(kP_-)}\right) \cos \eta - \frac{e^2 \not{q}_l \not{k} \not{\nu} \not{k} \not{q}_l}{4(kP_+)(kP_-)} \cos^2 \eta\right) U_+ \\
&\quad \times \exp(i(Q_+ + Q_-)y) \times \exp(-i(\tilde{\beta}_1 \sin \eta + \tilde{\beta}_2 \sin(2\eta))) , \quad (11.6)
\end{aligned}$$

with

$$\begin{aligned}
\tilde{\beta}_1 &= e \left(\frac{(a_l P_-)}{(kP_-)} - \frac{(a_l P_+)}{(kP_+)}\right) \\
\tilde{\beta}_2 &= -\frac{e^2 a^2}{8} \left(\frac{1}{(kP_+)} + \frac{1}{(kP_-)}\right) . \quad (11.7)
\end{aligned}$$

Please note again the difference between the definition here and the one in the previous chapter, as well as the minus sign as compared to the corresponding definition for the electrons (7.9). The functions $\tilde{F}(\eta) := \exp(-i(\tilde{\beta}_1 \sin \eta + \tilde{\beta}_2 \sin(2\eta)))$, $\cos \eta \tilde{F}(\eta)$, and $\cos^2 \eta \tilde{F}(\eta)$ are again expanded in a Fourier series, yielding

$$\begin{aligned}\tilde{F}(\eta) &= \sum_{N=-\infty}^{\infty} \tilde{B}_N e^{-iN\eta}, \\ \cos \eta \tilde{F}(\eta) &= \sum_{N=-\infty}^{\infty} \tilde{C}_N e^{-iN\eta}, \\ \cos^2 \eta \tilde{F}(\eta) &= \sum_{N=-\infty}^{\infty} \tilde{D}_N e^{-iN\eta}\end{aligned}\quad (11.8)$$

with the coefficients

$$\begin{aligned}\tilde{B}_N &= \tilde{J}_N(\tilde{\beta}_1, \tilde{\beta}_2), \\ \tilde{C}_N &= \frac{1}{2} \left(\tilde{J}_{N-1}(\tilde{\beta}_1, \tilde{\beta}_2) + \tilde{J}_{N+1}(\tilde{\beta}_1, \tilde{\beta}_2) \right), \\ \tilde{D}_N &= \frac{1}{4} \left(\tilde{J}_{N-2}(\tilde{\beta}_1, \tilde{\beta}_2) + 2\tilde{J}_N(\tilde{\beta}_1, \tilde{\beta}_2) + \tilde{J}_{N+2}(\tilde{\beta}_1, \tilde{\beta}_2) \right).\end{aligned}\quad (11.9)$$

The generalized Bessel functions are the same as in Eq. (7.12), i.e. $\tilde{J}_N(\tilde{\beta}_1, \tilde{\beta}_2) = \sum_{\ell} J_{N-2\ell}(\tilde{\beta}_1) J_{\ell}(\tilde{\beta}_2)$. With this, we again write the spinor-matrix product

$$\begin{aligned}{}^{\mu}\mathcal{M}_N^{\nu} &:= \bar{U}_- \left(\not{v} \tilde{B}_N + \frac{e}{2} \left(\frac{\not{v} \not{q}_l}{(kP_+)} - \frac{\not{q}_l \not{v}}{(kP_-)} \right) \tilde{C}_N - \frac{e^2 \not{q}_l \not{v} \not{q}_l}{4(kP_+)(kP_-)} \tilde{D}_N \right) U_+ \\ &=: \bar{U}_- {}^l\Gamma_N^{\nu} U_+\end{aligned}\quad (11.10)$$

and the muonic current reads

$$J^{\nu} = \frac{1}{2V \sqrt{Q_+^0 Q_-^0}} \sum_{N=-\infty}^{\infty} \int d^4 y {}^{\mu}\mathcal{M}_N^{\nu} e^{i(Q_+ + Q_- - Nk)y}. \quad (11.11)$$

We can now write down the transition amplitude like in the previous chapter:

$$\begin{aligned}\mathcal{S} &= -i\alpha \iint d^4 x d^4 y \bar{\psi}_+(x) \gamma_{\mu} \psi_-(x) \mathcal{D}_{\mu\nu}(x-y) \bar{\Psi}_-(y) \gamma_{\nu} \Psi_+(y) \\ &= \frac{-i\alpha(2\pi)^5}{2V^2 \sqrt{q_+^0 q_-^0 Q_+^0 Q_-^0}} \sum_{r,n} {}^{\mu}\mathcal{M}_{r-n}^{\nu} {}^e\mathcal{M}_{\nu}^n \frac{\delta(q_+ + q_- + rk - Q_+ - Q_-)}{(q_+ + q_- + nk)^2},\end{aligned}\quad (11.12)$$

again with the total number $r = n + N$ of absorbed laser photons. This expression is similar to the one obtained for circular polarization, Eq. (10.16), with the only difference being in the spinor-matrix products ${}^{\mu}\mathcal{M}_N^{\nu}$ and ${}^e\mathcal{M}_{\mu}^n$. In particular, there is no double sum over r necessary due to the δ -function, and the square of the transition amplitude can be written as a sum over squared partial amplitudes,

$|\mathcal{S}|^2 = \sum_r |\mathcal{S}_r|$. With the spin sum over the square of the spinor-matrix products

$$\begin{aligned} {}^l T_{nn'}^r &= \sum_{\text{spins}} ({}^e \mathcal{M}_\mu^{n'})^\dagger ({}^\mu \mathcal{M}_{r-n'}^\mu)^\dagger {}^\mu \mathcal{M}_{r-n}^\nu {}^e \mathcal{M}_\nu^n \\ &= \bar{u}_- {}^l \bar{\Delta}_\mu^{n'} u_+ \bar{U}_+ {}^l \bar{\Gamma}_{r-n'}^\mu U_- \bar{U}_- {}^l \Gamma_{r-n}^\nu U_+ \bar{u}_+ {}^l \Delta_\nu^n u_- \\ &= \text{tr} \left((\not{P}_+ + M) {}^l \bar{\Gamma}_{r-n'}^\mu (\not{P}_- - M) {}^l \Gamma_{r-n}^\nu \right) \text{tr} \left((\not{p}_- - m) {}^l \bar{\Delta}_\mu^{n'} (\not{p}_+ + m) {}^l \Delta_\nu^n \right), \end{aligned} \quad (11.13)$$

containing the matrices ${}^l \Delta_\mu^n$ and ${}^l \Gamma_N^\mu$ from Eqs. (11.4) and (11.10), respectively, we find for the differential $d^6\sigma_r$ of the partial cross section

$$d^6\sigma_r = \frac{\alpha^2 {}^l T_{nn'}^r \delta(q_r - Q_+ - Q_-)}{16 Q_+^0 Q_-^0 \sqrt{(q_+ q_-)^2 - m_*^4} (q_+ + q_- + nk)^2 (q_+ + q_- + n'k)^2} d^3\mathbf{Q}_+ d^3\mathbf{Q}_-. \quad (11.14)$$

The integration over the produced muon and antimuon momenta is performed in the same way as in Ch. 10. The integration over the muon's polar angle is again performed by making use of the remaining energy-conserving δ -function, leading to the same expression for $\cos \Theta_-$ as in (10.22) and thus to the same integration limits for the integral over the muon's energy (10.24). The integration over the azimuth angle of the produced muon must be performed numerically since, unlike for the symmetrical circular polarization, the polarization direction of the laser field is favored. Therefore, the final expression for the partial cross section is

$$\sigma_r = \int_0^{2\pi} \int_{E_-^{\min}}^{E_-^{\max}} \sum_{nn'} \frac{\pi \alpha^2 {}^l T_{nn'}^r}{8 \sqrt{(q_+ q_-)^2 - m_*^4} (q_+ + q_- + nk)^2 (q_+ + q_- + n'k)^2 |\mathbf{q}_r|} dQ_-^0 d\Phi_- \quad (11.15)$$

and the total cross section is again given by the sum over all photon orders,

$$\sigma = \sum_r \sigma_r. \quad (11.16)$$

As can be seen from Eqs. (11.4) and (11.10), the field-free cross section is reproduced in the same way as in 10.1.1 for vanishing laser intensity.

11.2 Numerical Results

Like before, we performed the numerical evaluation of the cross section (11.16) in the reference frame with $p_\pm = (\varepsilon, 0, 0, \mp\varepsilon)$. Like in the previous chapter, the collision energy is given by $E_{\text{cm}} = \sqrt{q_r^2}$. Since – like in the Higgs production process inside a linearly polarized laser field considered in 7.2 – the first argument of the electronic Bessel functions is $\tilde{\alpha}_1 = 0$ for the considered setup, only even numbers n of laser photons can be absorbed or emitted at the electron vertex. However, there is no further general restriction to n like there was in the case of circular polarization.

Due to the large muon mass, the impact of the laser field on the muons is much smaller than on the electrons which emanates in the much smaller laser intensity

parameter $\Xi = \xi m/M$. Therefore, we expect that the number of absorbed or emitted laser photons at the electron vertex n is much larger than N . In fact, the numerical evaluation of the cross section shows that photon absorption or emission at the muon vertex is negligible for $\xi = 1$. With $N = N' = 0$ follows $n = n' = r$ and there is no double summation. We can thus write for the partial cross section (11.15)

$$\sigma_r \approx \int_0^{2\pi} \int_{E_-^{\min}}^{E_-^{\max}} \frac{\pi \alpha^2 T_{rr}^r}{8 \sqrt{(q_+ q_-)^2 - m_*^4 (q_+ + q_- + rk)^2 (q_+ + q_- + rk)^2} |\mathbf{q}_r|} dQ_-^0 d\Phi_- . \quad (11.17)$$

The muonic part of the trace product ${}^l T_{rr}^r$ reduces to the term containing \tilde{B}_0 since the other summands are of order Ξ or Ξ^2 . We now consider the electronic Bessel functions. As already mentioned, for $p_{\pm} = (\varepsilon, 0, 0, \mp\varepsilon)$, the first Bessel argument vanishes, $\tilde{\alpha}_1 = 0$. The second Bessel argument $\tilde{\alpha}_2$ can be written as

$$\tilde{\alpha}_2 = \frac{e^2 a^2}{8} \left(\frac{1}{(kp_+)} + \frac{1}{(kp_-)} \right) = \frac{\xi^2 \varepsilon}{2\omega} . \quad (11.18)$$

As we have seen in Sec. 7.2 and according to Appx. C, the Bessel function

$$\tilde{J}_r(0, \tilde{\alpha}_2) = J_{r/2}(\tilde{\alpha}_2) \quad (11.19)$$

has a maximum for $r/2 = \tilde{\alpha}_2$ (for sufficiently large arguments $\tilde{\alpha}_2$). We may therefore, like we did in 7.2, consider a constellation where the absorption of $r_{\max} = \xi^2 \varepsilon / \omega$ laser photons leads to the c.m. energy for which the field-free cross section has its maximum,

$$E_{\text{cm}}(r_{\max}) = \sqrt{(q_+ + q_- + r_{\max} \omega)^2} = 2\varepsilon \sqrt{1 + 2\xi^2} \approx 250 \text{ MeV} . \quad (11.20)$$

Note that, unlike in the Higgs boson case, there is an additional factor $\tilde{J}_0(\tilde{\beta}_1, \tilde{\beta}_2)$ in the trace product, due to the factor \tilde{B}_0 . Therefore, $\sigma_{r_{\max}}$ is not necessarily the maximum partial cross section.

11.2.1 Partial Cross Sections

We find that for $\xi = 1$, Eq. (11.20) requires a free electron energy of $\varepsilon = 72.3 \text{ MeV}$. Fig. 11.1 shows the partial cross section as a function of the photon order r for $\xi = 1$, $\varepsilon = 72.3 \text{ MeV}$. The photon energy is $\omega = 10 \text{ keV}$ (a) and $\omega = 1 \text{ eV}$ (b). In the latter case, only every 2000-th photon order has been actually calculated and the result has been multiplied by 1000 (cf. Sec. 11.2). In both cases, the sum over all contributing photon orders yields $\sigma = \sum_r \sigma_r \approx 210 \text{ nb}$; like in the different scenarios considered above, the photon energy only plays a role for the number of contributing photon orders and has no influence on the total cross section. The cutoff to the left of the distribution is where the number of absorbed laser photons is not large enough to exceed the reaction threshold (see the upper x -axis of the plots).

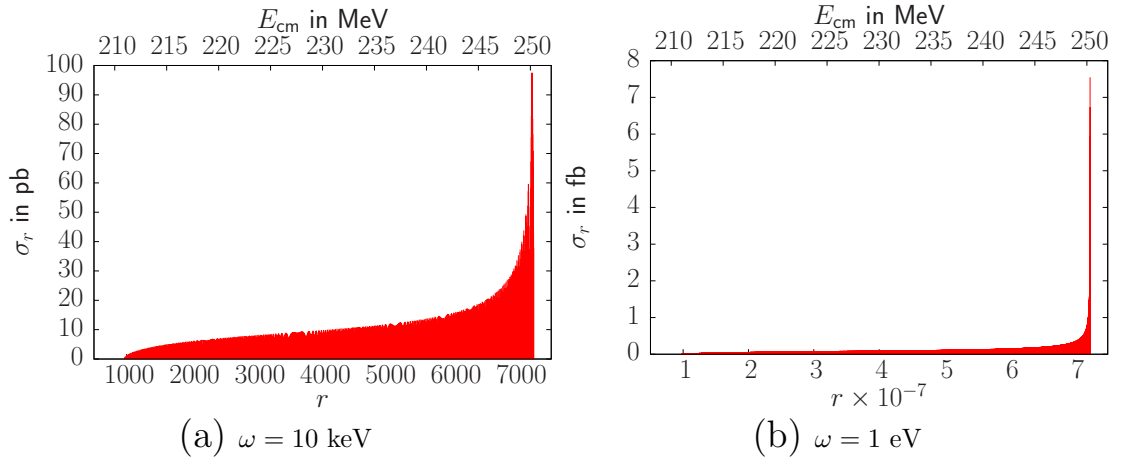


Figure 11.1: Partial cross section σ_r as function of the total number r of absorbed laser photons (lower x -axis). The upper x -axis shows the corresponding collision energy E_{cm} . In both cases, the laser parameter is $\xi = 1$ and free electron energy is $\varepsilon = 72.3$ MeV; in (a), the photon energy is set to $\omega = 10$ keV, in (b) it is $\omega = 1$ eV.

11.2.2 Differential Cross Sections

Fig. 11.2 shows the dependence of the partial differential cross section $d\sigma_r/dQ_-^0$ on the muon's energy for the parameter set from Fig. 11.1b for different photon orders r . For small photon orders (Fig. 11.2a), the range of allowed muon energies is much smaller than for larger orders (Fig. 11.2b) which is in agreement with the considerations in the previous chapter (cf. Eq. (10.35)). In all cases, the distribution is symmetric with maxima at the edges of the allowed energy range. When summed over all photon orders, however, the fact that large muon energies require a large amount of absorbed laser photons leads to an asymmetry and a preference of smaller muon energy. This can be seen in Fig. 11.3 where the total differential cross section $d\sigma/dQ_-^0$ is shown for $\omega = 10$ keV.

Since, like in Sec. 10.2, the partial differential cross sections for the antimuon are the same as for the muon, the total cross section is also the same. For each single photon order, a scenario is preferred where either the muon energy is maximal and the antimuon energy is minimal or vice versa. In total, both particles are preferably produced with a low energy.

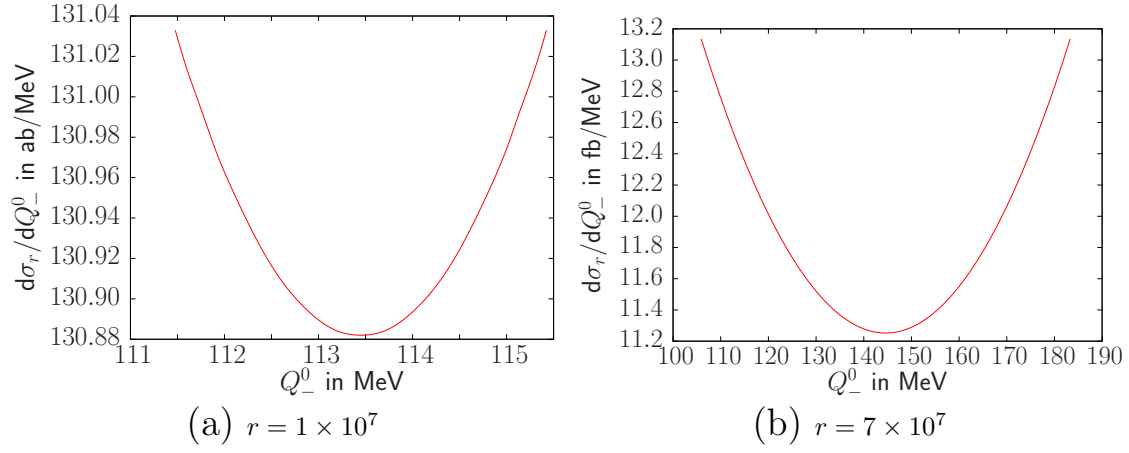


Figure 11.2: Partial differential cross section $d\sigma_r/dQ_-^0$ for two different values of r as function of the produced muon's energy for $\xi = 1$, $\varepsilon = 72.3$ MeV and $\omega = 1$ eV.

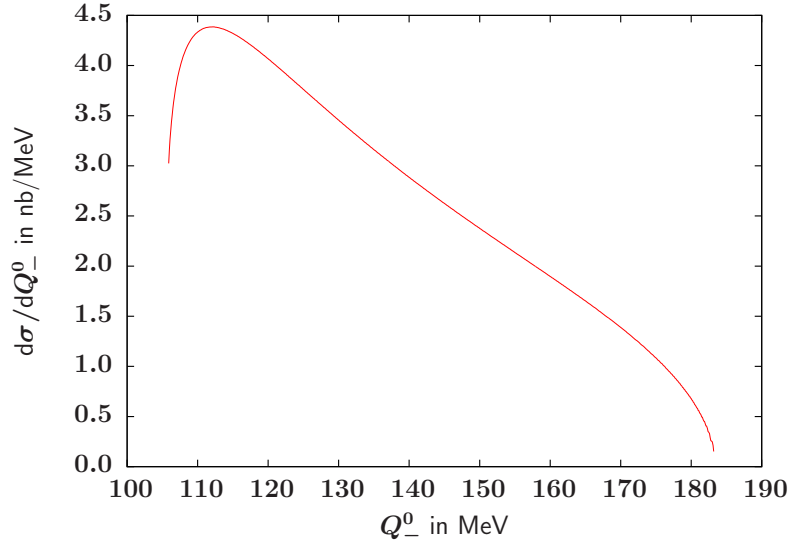


Figure 11.3: Total differential cross section $d\sigma/dQ_-^0$ as function of the produced muon's energy for $\xi = 1$, $\varepsilon = 72.3$ MeV and $\omega = 10$ keV.

Chapter 12

Required Laser Parameters and Other Experimental Demands

We now study the laser parameters that are required for the muon pair production processes considered in Chs. 10 and 11. As seen in Secs. 6.3 and 7.3, the condition that the laser beam must cover the whole electron and positron trajectories determines its minimally required spatiotemporal dimensions and thus its power and energy. The values corresponding to the parameter sets used in Secs. 10.2 and 11.2 are given in Tab. 12.1. Column 1 shows the parameters with which the results from Sec. 10.2 have been obtained. The comparatively large photon energy leads to a very high laser intensity for $\xi = 1$. For such a high laser intensity, several new aspects like vacuum polarization effects are already becoming important [DPMHK12]. However, the total cross section is independent of the photon energy ω and therefore, the same result is achieved with $\omega = 1$ eV, for which the required laser parameters are given in the second column of Tab. 12.1. Due to the smaller photon energy and thus larger wave length, the pulse duration and beam radius (which are both proportional to the laser wave length λ) are larger than for $\omega = 10$ keV, but the intensity that leads to $\xi = 1$ is smaller. We have seen already in Part II that using a linearly polarized laser wave with an elliptically-shaped cross

	Circular Polarization		Linear Polarization	
Intensity parameter ξ	1	1	1	1
Photon energy ω (eV)	10^4	1	1	1
Laser intensity I (W/cm ²)	1.8×10^{26}	1.8×10^{18}	1.8×10^{18}	1.8×10^{18}
Free electron energy ε (MeV)	88	88	88	72
Lorentz factor γ	172	172	172	141
Beam radius Δx (μm)	2×10^{-2}	206	206	169
Pulse duration (ps)	7.43×10^{-2}	743	743	599
Pulse power (TW)	2.4×10^3	2.4×10^3	14	11
Pulse energy (kJ)	0.18	1.8×10^3	10.4	5.7
Total cross section (μb)	1	1	0.3	0.2

Table 12.1: Laser parameters required for the process $e^+e^- \rightarrow \mu^+\mu^-$ for the parameter sets considered in 10.2 (first two columns) and 11.2 (last two columns).

sectional area may vastly reduce the required pulse power and energy. For the same set of ξ , ε and ω as in column 2, we find that employing a linearly polarized laser wave whose focus perpendicular to the polarization direction is λ reduces the required power and energy of the pulse by approximately two orders of magnitude. In the last column, the parameters used in Sec. 11.2 are listed. As compared to the case with the larger free electron energy, the total cross section is smaller, but so are also the required power and energy of the laser pulse due to the smaller Lorentz factor.

The required pulse powers and energies are much smaller than for the Higgs creation process considered in Part II. In principle, they can be reached by present-day or near-future facilities such as the NIF or HERCULES lasers or the future ELI [NIF; YCK⁺08; ELIa] (cf. Sec. 7.3).

The Compton scattering rate for the parameters of column 4 is $R_C \approx 5 \times 10^{10} \text{ s}^{-1}$. Multiplied with the duration of the laser pulse, this results in approximately 32 Compton scattering events per positron and thus a maximum energy loss of 2.4 MeV (cf. Secs. 6.3 and 7.3). This is again rather small compared to the total collision energy which is in the order of 250 MeV.

With the parameters in column 4 of Tab. 12.1, we can estimate the number of muon-antimuon pairs that are produced in each electron-positron collision. We saw in Ch. 7 that the flux of the incoming particles can be written as $|\mathbf{j}| \approx 2c/V$. The interaction volume V is given by the volume of the laser pulse. For the parameters from the fourth column of Tab. 12.1, it is $V \approx 10^{-10} \text{ m}^3$. With this, the muon pair production rate is $R \approx 10^{-16} \text{ s}^{-1}$, leading to a total $\mu^+\mu^-$ production probability of approximately 6.3×10^{-26} per e^+e^- collision.

Chapter 13

Conclusion of Part III

The examination of the process $e^+e^- \rightarrow \mu^+\mu^-$ carried out in this part has shown that, like already seen in the previous Part II, the c.m. energy of an electron-positron collision may be significantly enhanced by superimposing an intense laser field. In contrast to the Higgs boson creation process studied above, the produced particles considered in this part carry electric charge and therefore, like the colliding electron and positron, interact with the laser field which emanates in the possibility of absorption or emission of laser photons at the vertex of the final particles. This particularly affects the process taking place inside a laser field of circular polarization studied in Ch. 10. In the idealized setup where the initial particles' momenta are perfectly (anti)parallel to the laser wave vector, only one photon may be absorbed or emitted at the vertex of the initial electron and positron. The total photon number, however, may be large due to the possible absorption or emission at the muonic vertex. Summation over all photon orders yields the field-free cross section from Ch. 9, like it was the case for the Higgs boson creation process in a circularly polarized field studied in Ch. 6. We saw in Ch. 11 that, like we found for the Higgs boson creation process in Ch. 7, this is not necessarily the case inside a linearly polarized laser field. There, the absorption of large amounts of photons is possible at the electron vertex. Thus, since we considered lasers with an intensity parameter $\xi = 1$ for electrons and the corresponding parameter $\Xi = m/M\xi \approx 1/207$ for muons is very small, photon absorption or emission at the muon vertex may be neglected in this case. Like for the Higgs boson creation process, the energy spectrum of the produced particles is shifted by the laser field and smaller (anti)muon energies are preferred.

Part IV

Summary and Outlook

Summary

The studies presented in this thesis are motivated by the desire to find a collider scheme in which a detailed investigation of the fundamental properties of the recently discovered Higgs boson is possible at a reasonably-sized lepton collider. This might be achieved by the combination of conventional particle accelerators with strong laser fields.

In Part II, the associated production of Higgs and Z^0 bosons was studied in detail. In the analytical expression for the transition amplitude, the impact of the laser field on the colliding leptons was accounted for by describing the latter by Volkov states. The current of these leptons was expanded in a Fourier series involving n -th order regular cylindrical Bessel functions in the case of a circularly polarized laser field and generalized Bessel functions for linear polarization. The order n corresponds to the number of absorbed (if $n > 0$) or emitted (if $n < 0$) laser photons. The total cross section then consists of a sum over *partial cross sections* corresponding to single photon orders.

For the numerical evaluation, an idealized setup was assumed where the initial lepton momenta are opposite and equal and are perfectly (anti)parallel to the propagation direction of the laser field. For sizable values of the laser intensity parameter, the laser-dressed particle momenta may be substantially larger than the initial free momenta which vastly enhances the collision energy. The obtained total cross sections are independent of the laser frequency for all combinations of laser intensity parameters and free lepton energies that were investigated. For circular polarization, the field-free cross section of corresponding collision energy was obtained. Here, maximally one laser photon may be absorbed or emitted in the considered kinematical setup. For linear polarization, the number of absorbed laser photons may become very large and thus supply an additional energy gain. Each photon order thus corresponds to a certain collision energy. The total cross section then constitutes a kind of average over a vast range of collision energies and thus cannot be correlated to a certain field-free cross section like in the circularly polarized laser field. The total energy spectrum of the Higgs boson was found to have a distinct tendency towards smaller Higgs boson energies, the reason being that for a large Higgs boson energy, the absorption of many laser photons is required, and therefore, more orders contribute for smaller energy. This effect also leads to a preference of smaller emission angles of the Higgs boson, which might be an advantage with regard to their detection in a real experiment.

For different lepton species, the required laser parameters were specified. For electrons, smaller laser intensities lead to sizable laser intensity parameters than

for muons. However, their large Lorentz factor leads to very huge spatiotemporal dimensions of the laser pulse. This arises from the restriction that the laser pulse must cover the whole lepton trajectory. Thus, very high pulse power and energy are necessary. While the required intensity for effective muon acceleration is larger by two orders of magnitude due to their larger rest mass, the required power and energy of the laser pulse are smaller by several orders of magnitude compared to those needed for electrons. This, together with other advantages like smaller radiation damping effects, renders laser-boosted muon-antimuon collisions preferable over electron-positron collisions.

For circular polarization, the required laser pulse parameters for substantial muon acceleration still are found to lie several orders of magnitude above those of present-day and near-future facilities. Due to the specific geometry of the lepton trajectory inside a linearly polarized laser field, it is possible to consider an elliptically-shaped laser pulse instead of a circular one like required for circular polarization. Depending on the focus size in the direction perpendicular to the polarization direction, this may vastly reduce the required pulse power and energy. The laser pulse parameters thus obtained for muon-antimuon collisions are likely to come into reach in the medium term.

For a fixed laser intensity parameter and free lepton energy, a higher photon energy reduces the required focal area and pulse duration of the laser pulse and thus its power and energy. On the other hand, for a fixed laser intensity parameter, a larger photon energy corresponds to a larger intensity of the laser field. A reduction of the focal size perpendicular to the polarization direction leads to a smaller number of effectively accelerated muons and thus in an additional loss in collider luminosity. Thus, a balance between the energy gain and luminosity loss has to be found in order to optimize the benefits from a possible combination of a muon collider and a strong laser.

Part III was dedicated to the investigation of the process $e^+e^- \rightarrow \mu^+\mu^-$. The most prominent differences to the high-energy process considered in the previous part are due to the fact that the produced muon and antimuon carry electric charge. They therefore, like the colliding electron and positron, interact with the laser field and have to be described by laser-dressed states. For each lepton species, a separate laser intensity parameter occurs due to their different rest masses.

In the analytical evaluation of this process taking place inside laser waves of circular and linear polarization, the expansion of the initial particles' current are similar to the ones obtained in the previous part. In addition, the muon-antimuon current is expanded in a similar way, and absorption or emission of laser photons at their vertex is possible. Thus, there occur different photon numbers for the photons absorbed or emitted at the electron-positron and muon-antimuon vertices, respectively, and the partial cross sections are related to the *total* number of absorbed or emitted laser photons.

In the numerical evaluation of the considered process, again in the kinematical setup described above, the total cross section was found to be independent of the photon energy in the investigated parameter regime like it was the case for the Higgs boson creation considered above. Here, due to the possible photon absorption

or emission at the muon-antimuon vertex, the total photon order may become large not only for linear, but also for circular polarization. In the latter case, the summation over all photon orders leads again to the field-free cross section obtained for a corresponding collision energy. A total energy distribution of the produced muon and antimuon was found where the muon (antimuon) is preferably produced with the maximum (minimum) allowed energy or vice versa. For a linear polarized laser field, the distribution of the partial cross sections as well as the energy distribution of the produced particles resemble those found for the Higgs boson creation. Here, too, small energies of the produced particles are preferred due to the vast range of contributing photon orders.

The required parameters of the laser pulse for the process investigated in this part are in principle achievable with present-day technology and therefore, the experimental implementation of the considered muon pair creation process might serve to study the specific features, e.g. the shape of the produced particles' energy spectra, we found for the laser-boosted muon pair as well as Higgs boson creation.

Outlook

We saw that a particle collider may benefit from the combination of conventional accelerator techniques with strong (linearly polarized) laser pulses in several respects. Most prominently, the collision energy in such a collider may be enhanced without increasing the size of the accelerating facility. In addition, the specific distributions of the produced particles' energies and emission angles might to some extent render their detection easier. A natural continuation of this work might be the investigation of the Higgs boson's decay products. Since the decay of the Higgs boson occurs on a very short time scale and we deal with very long laser pulses, the electrically charged decay products will still experience interactions with the laser field and have to be described by laser-dressed states.

As already mentioned in the introduction, the Higgs boson can be created at a muon collider via a direct s -channel production. The examination of this process inside the considered laser field would be an interesting complement to this work. Despite the challenges that would have to be met by such a collider scheme, we found promising prospects of possible advantages compared to conventional particle accelerators.

Part V

Appendices

Appendix A

Feynman Rules and S-Matrix Formalism

We now list the Feynman rules and fundamental properties of elementary particles that were used in this thesis according to [Nac86].

Free Dirac Spinors

For a free negatively-charged spin-1/2 particle with mass m , momentum p_- and spin quantum number s_- , we define a free spinor $u(p_-, s_-)$ and, correspondingly, $v(p_+, s_+)$ for a positively-charged antiparticle with momentum p_+ and spin projection s_+ . These spinors must satisfy the free Dirac equation

$$\begin{aligned}(\not{p}_- - m)u(p_-, s_-) &= 0 \\ (\not{p}_+ + m)v(p_+, s_+) &= 0.\end{aligned}\tag{A.1}$$

The adjoint spinors $\bar{u}(p_-, s_-) = u^\dagger(p_-, s_-)\gamma^0$ and $\bar{v}(p_+, s_+) = v^\dagger(p_+, s_+)\gamma^0$ satisfy the corresponding equations

$$\bar{u}(p_-, s_-)(\not{p}_- - m) = 0\tag{A.2}$$

$$\bar{v}(p_+, s_+)(\not{p}_+ + m) = 0.\tag{A.3}$$

We normalize the free Dirac spinors according to Appx. A in [Nac86],

$$\begin{aligned}\bar{u}(p_-, s_-)u(p_-, s'_-) &= 2m\delta_{s_-s'_-} \\ \bar{v}(p_+, s_+)v(p_+, s'_+) &= -2m\delta_{s_+s'_+}\end{aligned}$$

and the completeness condition is

$$\sum_{s_-=-1/2}^{1/2} u(p_-, s_-)\bar{u}(p_-, s_-) = (\not{p}_- - m)\tag{A.4}$$

$$\sum_{s_+=-1/2}^{1/2} v(p_+, s_+)\bar{v}(p_+, s_+) = (\not{p}_+ + m).\tag{A.5}$$






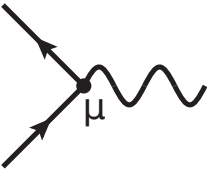
Spin-1 particles

Free massive spin-1 particles with mass M and four-momentum k are described by polarization states $\epsilon(k)$ for which $\epsilon_{i\mu}^*(k)\epsilon_j^\mu(k) = \delta_{ij}$ (see Appx. G in [Nac86]). The polarizations sum occurring in Pt. II yields

$$\sum_{\text{pol.}} \epsilon_\mu(k)\epsilon_\nu^*(k) = -g_{\mu\nu} + \frac{k_\mu k_\nu}{M^2}. \quad (\text{A.6})$$

Feynman Rules of QED


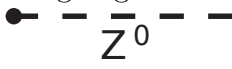
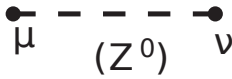
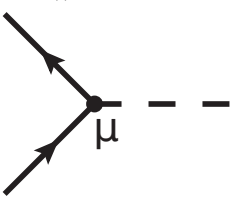
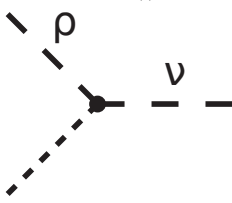
The relations between physical conditions and their corresponding Feynman diagram parts and analytical descriptions in position space for QED processes (without a laser field) are listed in Appx. B in [Nac86]. In our units system, they read

Lepton in initial state	Lepton in final state
$u(p_-, s_-)$ Incoming lepton line  ℓ^-	$\bar{u}(p_-, s_-)$ Outgoing lepton line  ℓ^-
Antilepton in initial state	Antilepton in final state
$\bar{v}(p_+, s_+)$ Outgoing lepton line  ℓ^+	$v(p_+, s_+)$ Incoming lepton line  ℓ^+
Virtual photon	Elementary process
$\frac{-ig^{\mu\nu}}{q^2 + i\epsilon}$ Inner photon line 	$ie\gamma^\mu$ Vertex 

With the free Dirac spinors from above, the virtual photon momentum q , and the Dirac matrices γ^μ . The corresponding expressions in position space are obtained by Fourier transformation.

Feynman Rules of QFD

The Feynman rules of quantum flavordynamics (QFD) are listed in Appx. G in [Nac86]. The ones used in our investigation of the process $\ell^+\ell^- \rightarrow HZ^0$ are

Higgs boson in final state	Z^0 boson in final state
<p>1</p> <p>Outgoing H line</p> 	<p>$\epsilon^*(P_Z)$</p> <p>Outgoing Z^0 line</p> 
Virtual Z^0 boson	
<p>Propagator</p> $\frac{4\pi i(-g^{\mu\nu} + \frac{P_Z^\mu P_Z^\nu}{M_Z^2})}{P_Z^2 - M_Z^2 + i\Gamma M_Z}$	<p>Inner Z^0 line</p> 
Vertex involving leptons	Vertex involving bosons
$\frac{-ig}{2\cos\theta_W}(g_V - g_A\gamma^5)\gamma^\mu$ 	$\frac{igM_Z g^{\nu\rho}}{\cos\theta_W}$ 

with the Z^0 boson's polarization state $\epsilon(k)$ as described above. In the denominator of the virtual Z^0 boson's propagator, there occurs the decay width Γ . Throughout this thesis, we considered the total collision energy large enough so that we may neglect the finite width. The description of the vertices contains the Weinberg angle θ_W for which

$$\begin{aligned}\sin^2\theta_W &\approx 0.23 \\ \cos^2\theta_W &= 1 - \sin^2\theta_W.\end{aligned}$$

The weak coupling constant is given by $g = e/\sin\theta_W$. The weak neutral coupling constants g_V and g_A are

$$\begin{aligned}g_V &= 2\sin^2\theta_W - 0.5 \\ g_A &= -0.5\end{aligned}$$

for both electrons and muons.

S -Matrix Formalism

A detailed introduction to the S -matrix formalism employed in this thesis can be found e.g. in [PS95; Nac86]. The scattering matrix, the so-called S matrix, is composed of all initial and final as well as virtual particles involved in a physical process and the corresponding vertices according to the Feynman rules stated above. It describes the amplitude for the transition from the initial to the final state. Its

square corresponds to a probability, from which a cross section is obtained by averaging over the initial particles' spins and summation over the final particles' spins (for fermions) or polarization states (for vector bosons), division by a unit time and the flux of the incoming particles, as well as integration over the final particles' momenta.

Appendix B

Properties of the γ -matrices

We now list some of the important properties of the Dirac matrices (3.1) and (3.2) that have been used throughout this thesis. They can also be found in Appx. A of [Nac86].

The following important rules apply for products of γ -matrices:

$$\{\gamma^\mu, \gamma^\nu\} = 2g^{\mu\nu} \cdot 1 \quad (\text{B.1})$$

$$\{\gamma^\mu, \gamma^5\} = 0 \quad (\text{B.2})$$

$$\gamma^\mu \gamma^\mu = 4 \cdot 1 \quad (\text{B.3})$$

$$\gamma^5 \gamma^5 = 1 \quad (\text{B.4})$$

$$\gamma^\mu \gamma^\nu = 2g^{\mu\nu} \cdot 1 - \gamma^\nu \gamma^\mu \quad (\text{B.5})$$

$$\gamma^\mu \gamma^\nu \gamma^\mu = -2\gamma^\nu \quad (\text{B.6})$$

$$\gamma^\mu \gamma^\nu \gamma^\rho \gamma^\sigma \gamma_\mu = -2\gamma^\sigma \gamma^\rho \gamma^\nu \quad (\text{B.7})$$

$$\gamma^0 \gamma^{\mu\dagger} \gamma^0 = \gamma^\mu \quad (\text{B.8})$$

with the 4x4 unity matrix 1. From these rules follows for products of γ -matrices and four-component vectors

$$\not{a}\not{b} = 2(ab) - \not{b}\not{a} \quad (\text{B.9})$$

$$\gamma^\mu \not{a} \gamma_\mu = -2\not{a} \quad (\text{B.10})$$

$$\gamma^\mu \not{a}\not{b} \gamma_\mu = 4(ab) \quad (\text{B.11})$$

$$\gamma^\mu \not{a}\not{b}\not{c} \gamma_\mu = -2\not{a}\not{b}\not{c} \quad (\text{B.12})$$

and for the adjoint product

$$\overline{\psi_1 \psi_2 \dots \psi_n} = \psi_n \psi_{n-1} \dots \psi_1. \quad (\text{B.13})$$

For the evaluation of the traces occurring in the transition amplitudes for the considered electroweak processes, the following general rules that can be derived from the above relations are useful:

The trace over an odd number of γ -matrices vanishes,

$$\text{tr}(\psi_1 \psi_2 \dots \psi_{2n+1}) = 0. \quad (\text{B.14})$$

Since the trace over a product of matrices is generally invariant under cyclic permutations, from Eq. (B.1) follows

$$\text{tr}(\psi_1 \psi_2) = 4(u_1 u_2) \quad (\text{B.15})$$

$$\text{tr}(\psi_1 \psi_2 \psi_3 \psi_4) = 4(u_1 u_2)(u_3 u_4) - 4(u_1 u_3)(u_2 u_4) + 4(u_1 u_4)(u_2 u_3) \quad (\text{B.16})$$

and in general

$$\begin{aligned} \text{tr}(\psi_1 \psi_2 \dots \psi_{2n}) &= (u_1 u_2) \text{tr}(\psi_3 \psi_4 \dots \psi_{2n}) \\ &\quad - (u_1 u_3) \text{tr}(\psi_2 \psi_4 \dots \psi_{2n}) \\ &\quad \pm \dots \\ &\quad + (u_1 u_{2n}) \text{tr}(\psi_2 \psi_3 \dots \psi_{2n-1}). \end{aligned} \quad (\text{B.17})$$

Another very useful relation is

$$\text{tr}(\psi_1 \psi_2 \dots \psi_n) = \text{tr}(\psi_n \psi_{n-1} \dots \psi_1). \quad (\text{B.18})$$

In the calculation of the transition amplitude for $\ell^+ \ell^- \rightarrow H Z^0$, there also occur traces over matrix products containing the fifth γ -matrix. For their evaluation, the following relations are useful:

$$\gamma_\mu \gamma^5 = \frac{i}{6} \epsilon_{\mu\nu\sigma\rho} \gamma^\nu \gamma^\sigma \gamma^\rho \quad (\text{B.19})$$

$$\text{tr}(\gamma^5) = \text{tr}(\gamma^\mu \gamma^5) = \text{tr}(\gamma^\mu \gamma^\nu \gamma^5) = \text{tr}(\gamma^\mu \gamma^\nu \gamma^\sigma \gamma^5) = 0 \quad (\text{B.20})$$

$$\text{tr}(\gamma^\mu \gamma^\nu \gamma^\sigma \gamma^\rho \gamma^5) = 4i \epsilon^{\mu\nu\sigma\rho} \quad (\text{B.21})$$

with the Levi-Civita symbol $\epsilon_{\mu\nu\sigma\rho}$.

Appendix C

Properties of the Bessel Functions

We now list some of the properties of the Bessel functions $J_n(x)$ that occur in the expansion of the leptonic currents in Chs. 6 and 10 and of which the generalized Bessel functions of Chs. 7 and 11 are composed. They are regular cylindrical Bessel functions of integer order¹ [AS65] and thus are solutions $y(x)$ to the differential equation

$$x^2 \frac{d^2 y}{dx^2} + x \frac{dy}{dx} + (x^2 - n^2)y = 0. \quad (C.1)$$

Their generating function, of which we made use in the said Fourier expansions, is

$$e^{-ix \sin \kappa} = \sum_{n=-\infty}^{\infty} J_n(x) e^{in\kappa}. \quad (C.2)$$

We now re-consider the expansion of the function $f(\kappa) = \exp(-i(\alpha_1 \sin \kappa - \alpha_2 \cos \kappa))$ occurring in Chs. 6 and 10. with $\bar{\alpha} = \sqrt{\alpha_1^2 + \alpha_2^2}$ and an angle κ_0 for which $\sin \kappa_0 = \alpha_2/\bar{\alpha}$ and $\cos \kappa_0 = \alpha_1/\bar{\alpha}$, we can write

$$\begin{aligned} \alpha_1 \sin \kappa - \alpha_2 \cos \kappa &= \bar{\alpha} \left(\frac{\alpha_1}{\bar{\alpha}} \sin \kappa - \frac{\alpha_2}{\bar{\alpha}} \cos \kappa \right) \\ &= \bar{\alpha} (\sin \kappa \cos \kappa_0 - \cos \kappa \sin \kappa_0) \\ &= \bar{\alpha} \sin(\kappa - \kappa_0). \end{aligned} \quad (C.3)$$

In the last step, we made use of the well-known addition theorem [AS65]

$$\sin(a - b) = \sin a \cos b - \cos a \sin b. \quad (C.4)$$

With this, we can write the function $f(\kappa) = \exp(-i\bar{\alpha} \sin(\kappa - \kappa_0))$ which has the form of the left side of Eq. (C.2) and therefore

$$f(\kappa) = \sum_{n=-\infty}^{\infty} J_n(\bar{\alpha}) e^{-in(\kappa - \kappa_0)}. \quad (C.5)$$

With

$$\cos \kappa = \frac{1}{2}(e^{i\kappa} + e^{-i\kappa}) \quad \text{and} \quad \sin \kappa = \frac{1}{2i}(e^{i\kappa} - e^{-i\kappa}) \quad (C.6)$$

¹Since the orders of the Bessel functions correspond to the respective number of absorbed or emitted photons, they must be integers.

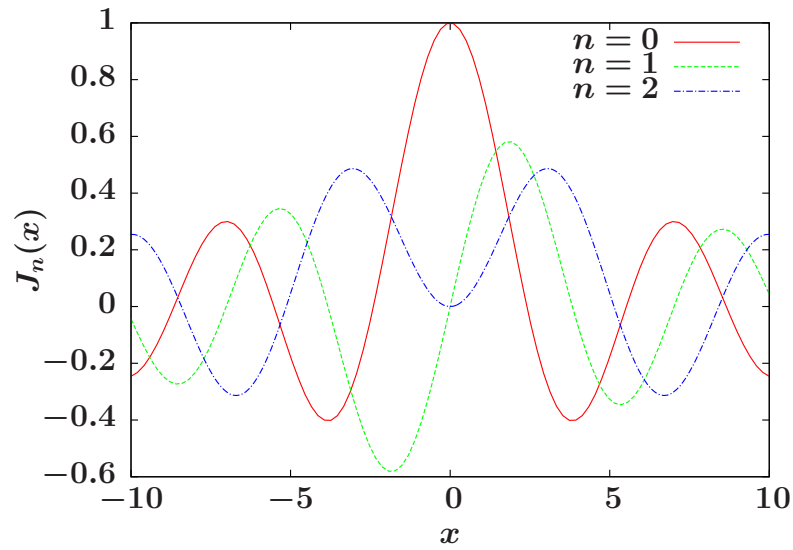


Figure C.1: Regular cylindrical Bessel functions $J_n(x)$ of orders $n = 0, 1$ and 2 (red solid, green dashed and blue dashed-dotted lines, respectively). The only Bessel function with a finite value at $x = 0$ is J_0 with $J_0(0) = 1$.

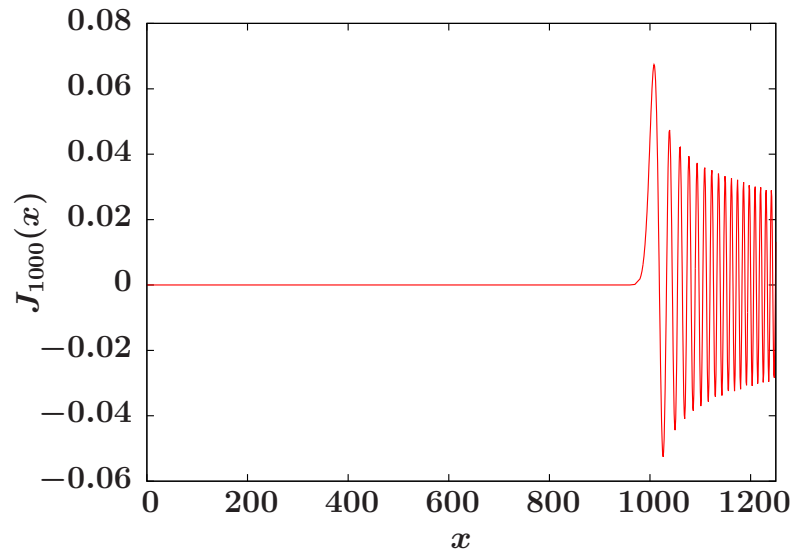


Figure C.2: Regular Bessel function $J_{1000}(x)$. As can be seen, the values of J_{1000} for $x \lesssim 1000$ are negligible.

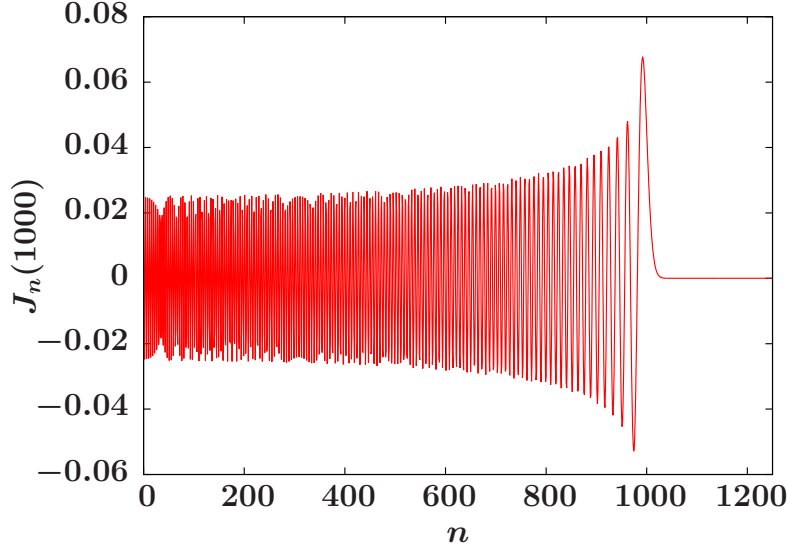


Figure C.3: Value of the regular Bessel functions for fixed argument $x = 1000$ as function of the order n . The maximum is at $n = x$ and for $n > x$, the value is negligibly small.

and since the summation goes from $n = -\infty$ to ∞ , we find

$$\begin{aligned}\cos \kappa f(\kappa) &= \sum_{n=-\infty}^{\infty} \frac{1}{2} (J_{n+1}(\bar{\alpha})e^{i(n+1)\kappa_0} + J_{n-1}e^{-i(n-1)\kappa_0}), \\ \sin \kappa f(\kappa) &= \sum_{n=-\infty}^{\infty} \frac{1}{2i} (J_{n+1}(\bar{\alpha})e^{i(n+1)\kappa_0} - J_{n-1}e^{-i(n-1)\kappa_0}).\end{aligned}\quad (\text{C.7})$$

The expansion of the function $F(\eta)$ in Ch. 10 is analogous.

Fig. C.1 shows the Bessel functions of orders 0, 1, and 2. The only order for which $J_n(0) \neq 0$ is $n = 0$, for which $J_0(0) = 1$. As can be seen in Fig. C.2, the value of a Bessel function $J_n(x)$ of large order n is negligible for $x \lesssim n$. This means, on the other hand, that for a fixed argument x , the value of $J_n(x)$ is negligible if the order n exceeds the argument x . This can be seen in Fig. C.3 where the Bessel functions $J_n(x)$ are displayed as a function of the order n for $x = 1000$.

The function $\tilde{f}(\kappa) = \exp(-i(\tilde{\alpha}_1 \sin \kappa + \tilde{\alpha}_2 \sin 2\kappa))$ from Chs. 7 and 11 can be expanded in a similar way. With (C.2), we can write

$$\begin{aligned}\tilde{f}(\kappa) &= e^{-i(\tilde{\alpha}_1 \sin \kappa + \tilde{\alpha}_2 \sin 2\kappa)} = \sum_m J_m(\tilde{\alpha}_1)e^{-im\kappa} \sum_{\ell} J_{\ell}(\tilde{\alpha}_2)e^{-i2\ell\kappa} \\ &= \sum_{\ell} \sum_m J_m(\tilde{\alpha}_1)J_{\ell}(\tilde{\alpha}_2)e^{-i(m+2\ell)\kappa} \\ &= \sum_{\ell} \sum_n J_{n-2\ell}(\tilde{\alpha}_1)J_{\ell}(\tilde{\alpha}_2)e^{-in\kappa} \\ &= \sum_n \left(\sum_{\ell} J_{n-2\ell}(\tilde{\alpha}_1)J_{\ell}(\tilde{\alpha}_2) \right) e^{-in\kappa}.\end{aligned}\quad (\text{C.8})$$

The structure of this equation is very similar to the one in (C.5). Therefore, the functions

$$\tilde{J}_n(\tilde{\alpha}_1, \tilde{\alpha}_2) = \sum_{\ell=-\infty}^{\infty} J_{n-2\ell}(\tilde{\alpha}_1) J_{\ell}(\tilde{\alpha}_2) \quad (\text{C.9})$$

are commonly referred to as *generalized Bessel functions* [Rei80]. Note that, unlike the regular Bessel functions of which they are composed, the generalized Bessel functions depend on two arguments. Like above, we find

$$\begin{aligned} \cos \kappa \tilde{f}(\kappa) &= \sum_{n=-\infty}^{\infty} \frac{1}{2} \left(\tilde{J}_{n-1}(\tilde{\alpha}_1, \tilde{\alpha}_2) + \tilde{J}_{n+1}(\tilde{\alpha}_1, \tilde{\alpha}_2) \right) e^{-in\kappa}, \\ \cos^2 \kappa \tilde{f}(\kappa) &= \sum_{n=-\infty}^{\infty} \frac{1}{4} \left(\tilde{J}_{n-2}(\tilde{\alpha}_1, \tilde{\alpha}_2) + 2\tilde{J}_n(\tilde{\alpha}_1, \tilde{\alpha}_2) + \tilde{J}_{n+2}(\tilde{\alpha}_1, \tilde{\alpha}_2) \right) e^{-in\kappa} \end{aligned} \quad (\text{C.10})$$

and similar expressions for $\tilde{F}(\eta)$, $\cos \eta \tilde{F}(\eta)$ and $\cos^2 \eta \tilde{F}(\eta)$ the expansion of the muonic current in Ch. 11.

In the setup we considered in Ch. 7 where the incident leptons are traveling perfectly (anti)parallel to the laser field, the argument $\tilde{\alpha}_1 = 0$ and, because $\sum_n J_n(0) = J_0(0) = 1$, the generalized Bessel functions reduce to

$$\tilde{J}_r(0, \tilde{\alpha}_2) = \sum_{\ell=-\infty}^{\infty} J_{r-2\ell}(0) J_{\ell}(\tilde{\alpha}_2) = J_{r/2}(\alpha_2) \quad (\text{C.11})$$

with the regular Bessel function $J_{r/2}$. In the case of muon pair production studied in Ch. 11, we have products of generalized Bessel functions,

$$\tilde{J}_n(\tilde{\alpha}_1, \tilde{\alpha}_2) \tilde{J}_{r-n}(\tilde{\beta}_1, \tilde{\beta}_2). \quad (\text{C.12})$$

For the electronic contribution, we have again $\tilde{\alpha}_1 = 0$ and the generalized Bessel functions are $\tilde{J}_n(0, \tilde{\alpha}_2)$. We find that for $\xi = 1$ and thus $\Xi \sim 1/200$, photon absorption or emission at the muon vertex is negligible and therefore $n = n' = r$. In addition, only the term with \tilde{B}_0 containing $\tilde{J}_0(\tilde{\beta}_1, \tilde{\beta}_2)$ is important in the trace product (11.13). Because $\tilde{\beta}_2 \propto \Xi^2 \approx 0$, we can express the muonic Bessel function as

$$\tilde{J}_0(\tilde{\beta}_1, \tilde{\beta}_2) \approx \tilde{J}_0(\tilde{\beta}_1, 0) = \sum_{\ell=-\infty}^{\infty} J_{-2\ell}(\tilde{\beta}_1) = \sum_{\ell \text{ even}} J_{\ell}(\tilde{\beta}_2). \quad (\text{C.13})$$

Numerical Implementation

The numerical implementation of the Bessel functions has been carried out as described in [PTVF07], namely by making use of the recurrence relation

$$J_{n+1}(x) = \frac{2n}{x} J_n(x) - J_{n-1}(x). \quad (\text{C.14})$$

The Bessel functions of orders 0 and 1 are taken from the GNU Scientific Library (GSL) [GSL]. Bessel functions of negative orders (corresponding to photon emission) are derived via

$$J_{-|n|} = (-1)^{|n|} J_{|n|}(x). \quad (\text{C.15})$$

The computation time for such a recursive routine becomes very large for large Bessel orders n . For very large arguments and orders, we therefore made use of the relation [AS65]

$$J_n(x) \approx J_n(n + zn^{\frac{1}{3}}) = 2^{\frac{1}{3}} n^{-\frac{1}{3}} \text{Ai}(-2^{\frac{1}{3}} z) + \mathcal{O}(n^{-1}) \quad (\text{C.16})$$

with $z = (x - n)n^{-1/3}$ and the Airy functions Ai (whose implementation in the GSL has been employed). This relation holds for small values of $(x - n)$. For the many photon orders that have to be taken into account in the computation of the cross sections in Part II, however, the recursive routine has to be employed for the vast majority of orders and therefore, the computation time is still very long. Thus, in some cases, we only calculated the partial cross sections for a certain number of photon orders and multiplied the result by the number of omitted orders per interval.

Bibliography

- [AAA⁺03] M. M. Alsharo'a, C. M. Ankenbrandt, M. Atac, et al. *Recent progress in neutrino factory and muon collider research within the Muon Collaboration*. Phys. Rev. STAB, Vol. 6, p. 081001, 2003.
- [ALE03] ALEPH, DELPHI, L3 and OPAL Collaborations. The LEP Working Group for Higgs Boson Searches. *Search for the standard model Higgs boson at LEP*. Phys. Lett. B, Vol. 565, p. 61, 2003.
- [ALE06] ALEPH, DELPHI, L3 and OPAL Collaborations. The LEP Electroweak Working Group, the SLD Electroweak and Heavy Flavour Groups. *Precision electroweak measurements on the Z resonance*. Phys. Rep., Vol. 427, p. 257, 2006.
- [Ale12] Y. Alexahin. *Muon collider design status*. arXiv:1202.2155v1 [physics.acc-ph], 2012.
URL:<http://arxiv.org/pdf/1202.2155v1.pdf>.
- [ALE13] ALEPH, DELPHI, L3 and OPAL Collaborations. The LEP Electroweak Working Group. *Electroweak measurements in electron-positron collisions at W-boson-pair energies at LEP*. Phys. Rep., in press, available online 26 August 2013, 2013.
URL:<http://www.sciencedirect.com/science/article/pii/S0370157313002706>.
- [Alt05] G. Altarelli. *The standard model of particle physics*. arXiv:hep-ph/0510281v1, 2005.
URL:<http://arXiv.org/abs/hep-ph/0510281v1>.
- [AMP87] G. Altarelli, B. Mele, and F. Pitolli. *Heavy Higgs production at future colliders*. Nucl. Phys. B, Vol. 287, p. 205, 1987.
- [AS65] M. Abramowitz and I. A. Stegun. *Handbook of Mathematical Functions*. Dover Publications, Inc., New York, 1965.
- [ATL12a] ATLAS Collaboration. *Combined search for the standard model Higgs boson in pp collisions at $\sqrt{s} = 7\text{ TeV}$ with the ATLAS detector*. Phys. Rev. D, Vol. 86, p. 032003, 2012.
- [ATL12b] ATLAS Collaboration. *Observation of a new particle in the search for the Standard Model Higgs boson with the ATLAS detector at the LHC*. Phys. Rev. B, Vol. 716, p. 1, 2012.

- [BBB⁺86] H. Baer, J. Berdugo, F. Bianchi, et al. *New particles*. CERN Report 86-02, Vol. 1, p. 297, 1986.
URL:<http://cds.cern.ch/record/166310/files/CERN-86-02-V-1.pdf>.
- [BBC93] D. L. Borden, D. A. Bauer, and D. O. Caldwell. *Higgs boson production at a photon linear collider*. Phys. Rev. D, Vol. 48, p. 4018, 1993.
- [BBGH95] V. Barger, M. S. Berger, J. F. Gunion, and T. Han. *s-channel Higgs boson production at a muon-muon collider*. Phys. Rev. Lett., 75, p. 1462, 1995.
- [BBGH97] V. Barger, M. S. Berger, J. F. Gunion, and T. Han. *Higgs boson physics in the s-channel at $\mu^+\mu^-$ colliders*. Phys. Rep., 286, p. 1, 1997.
- [BCD⁺07] I. Blumenfeld, C. E. Clayton, F. J. Decker, et al. *Energy doubling of 42 GeV electrons in a metre-scale plasma wakefield accelerator*. Nature, 445, p. 741, 2007.
- [BCE⁺04] C. Blöchinger, M. Carena, J. Ellis, et al. *Physics opportunities at $\mu^+\mu^-$ Higgs factories*. In EFCA/CERN studies of a European neutrino factory complex, p. p. 337, 2004. CERN Report 2004-002, URL:<https://cds.cern.ch/record/735196/files/ECFA-04-230.pdf?version=1>.
- [BCS57] J. Bardeen, L. N. Cooper, and J. R. Schrieffer. *Microscopic theory of superconductivity*. Phys. Rev., Vol. 106, p. 162, 1957.
- [BD64] J. D. Bjorken and S. D. Drell. *Relativistic Quantum Mechanics*. McGraw-Hill, New York, 1964.
- [BEGM87] A. S. Bagdasaryan, R. Sh. Egorian, S. G. Grigorian, and S. G. Matinyan. *Some peculiarities of conjoined hadroproduction of standard Higgs boson and heavy quark pair*. Sov. J. Nucl. Phys., Vol. 46, p. 315, 1987. [Yad.Fiz., Vol. 46, p. 572, 1987].
- [BFHS⁺97] D. L. Burke, R. C. Field, G. Horton-Smith, et al. *Positron production in multiphoton light-by-light scattering*. Phys. Rev. Lett., Vol. 79, p. 1626, 1997.
- [BFMvdB04] C. P. Buszello, I. Fleck, P. Marquard, and J. J. van der Bij. *Prospective analysis of spin- and CP-sensitive variables in $H \rightarrow ZZ \rightarrow l(1)^+l(1)^-l(2)^+l(2)^-$ at the LHC*. Eur. Phys. J. C, Vol. 32, p. 209, 2004.
- [BH34] H. Bethe and W. Heitler. *On the stopping of fast particles and on the creation of positive electrons*. Proc. Roy. Soc. London A, Vol. 146, p. 83, 1934.

- [BHS87] R. M. Barnett, H. E. Haber, and D. E. Soper. *Ultra-heavy particle production from heavy partons at hadron colliders*. Nucl. Phys. B, Vol. 306, p. 697, 1987.
- [Bjo76] J. D. Bjorken. *Weak interaction theory and neutral currents*. In Proceedings of Summer Institute on Particle Physics: Weak Interactions at High Energy and the Production of New Particles, August 2-13, 1976, p. 1, 1976. Also available as SLAC Report 198, URL:<http://slac.stanford.edu/pubs/slacreports/reports03/slac-r-198.pdf>.
- [BSH02] A. Butler, D. J. Spence, and S. M. Hooker. *Guiding of high-intensity laser pulses with a hydrogen-filled capillary discharge waveguide*. Phys. Rev. Lett., Vol. 89, p. 185003, 2002.
- [BW34] G. Breit and J. A. Wheeler. *Collision of two light quanta*. Phys. Rev., Vol. 46, p. 1087, 1934.
- [BZ95] S. J. Brodsky and P. M. Zerwas. *High energy photon-photon collisions*. Nucl. Instrum. Methods A, Vol. 355(1), p. 19, 1995.
- [CAB⁺08] C. C. Ankenbrandt, Y. Alexahin, V. Balbekov, et al. *Muon collider task force report*. FERMILAB-TM-2399-APC, 2008. https://mctf.fnal.gov/annual-reports/mctf-report-2007_v9.doc.
- [CD84] R. N. Cahn and S. Dawson. *Production of very massive Higgs bosons*. Phys. Rev. B, Vol. 136, p. 196, 1984. Phys. Rev. B, Vol. 138, p. 464, 1984 (Erratum).
- [CDF95] CDF Collaboration. *Observation of top quark production in $\bar{p}p$ collisions with the collider detector at Fermilab*. Phys. Rev. Lett., Vol. 74, p. 2626, 1995.
- [CDF13] CDF and D0 Collaborations. The TEVNPH Working Group. *Combined CDF and D0 upper limits on standard model Higgs boson production with up to 8.6 fb⁻¹ of data*. arXiv:1107.5518 [hep-ex], 2013.
URL:<http://arxiv.org/pdf/1107.5518v2.pdf>.
- [CER] CERN timelines. The large electron-positron collider.
URL:<http://timeline.web.cern.ch/timelines/The-Large-Electron-Positron-Collider>.
- [CER13] CERN press release. *New results indicate that particle discovered at CERN is a Higgs boson*. March 2013.
URL:<http://press.web.cern.ch/press-releases/2013/03/new-results-indicate-particle-discovered-cern-higgs-boson>.
- [CGC⁺09] J. P. Chambaret, P. Georges, G. Chériaux, et al. *The Extreme Light Infrastructure project ELI and its prototype APOLLON/ILE*.

- the associated laser bottlenecks*. In *Frontiers in Optics*, p. p. FMI2, Washington, DC, 2009. Optical Society of America.
- [Cha71] Y. W. Chan. *Ultra-intense laser radiation as a possible energy booster for relativistic charged particle*. *Phys. Lett. A*, Vol. 35, p. 305, 1971.
- [CHL07] C. Csaki, J. Hubisz, and S. J. Lee. *Radion phenomenology in realistic warped space models*. *Phys. Rev. D*, Vol. 76, p. 125015, 2007.
- [CLIC] CLIC study. Compact Linear Collider.
URL:<http://clic-study.org/>.
- [CLI04] CLIC Physics Working Group. *Physics at the CLIC multi-TeV linear collider*. arXiv:hep-ph/0412251v1, 2004.
URL:<http://arXiv.org/abs/hep-ph/0412251v1>.
- [CLI13] CLIC Detector and Physics Study. *Physics at the CLIC e^+e^- linear collider*. arXiv:1307.5288, 2013.
URL:<http://arxiv.org/pdf/1307.5288.pdf>.
- [CM99] J. L. Chaloupka and D. D. Meyerhofer. *Observation of electron trapping in an intense laser beam*. *Phys. Rev. Lett.*, Vol. 83, p. 4538, 1999.
- [CMS12a] CMS Collaboration. *Combined results of searches for the standard model Higgs boson in pp collisions at $\sqrt{s} = 7$ TeV*. *Phys. Lett. B*, Vol. 710, p. 26, 2012.
- [CMS12b] CMS Collaboration. *Observation of a new boson at a mass of 125 GeV with the CMS experiment at the LHC*. *Phys. Lett. B*, Vol. 716, p. 30, 2012.
- [CPK⁺99] T. E. Cowan, M. D. Perry, M. H. Key, et al. *High energy electrons, nuclear phenomena and heating in petawatt laser-solid experiments*. *Laser Part. Beams*, Vol. 17, p. 773, 1999.
- [CWB⁺09] Hui Chen, Scott C. Wilks, James D. Bonlie, Edison P. Liang, Jason Myatt, Dwight F. Price, David D. Meyerhofer, and Peter Beiersdorfer. *Relativistic positron creation using ultraintense short pulse lasers*. *Phys. Rev. Lett.*, Vol. 102, p. 105001, 2009.
- [CWM⁺10] Hui Chen, S. C. Wilks, D. D. Meyerhofer, et al. *Relativistic quasimonoenergetic positron jets from intense laser-solid interactions*. *Phys. Rev. Lett.*, Vol. 105, p. 015003, 2010.
- [DDHI98] A. Djouadi, V. Driesen, W. Hollik, and J. I. Illana. *The coupling of the lightest SUSY Higgs boson to two photons in the decoupling regime*. *Eur. Phys. J. C*, Vol. 1, p. 149, 1998.

- [DGH96] J. F. Donoghue, E. Golowich, and B. R. Holstein. *Dynamics of the standard model*. In Cambridge monographs on particle physics, nuclear physics, and cosmology. Cambridge University Press, Cambridge, 1996.
- [DHL⁺04] M. Duhrssen, S. Heinemeyer, H. Logan, D. Rainwater, G. Weiglein, and D. Zeppenfeld. *Extracting Higgs boson couplings from LHC data*. Phys. Rev. D, Vol. 70, p. 113009, 2004.
- [Djo08] A. Djouadi. *The anatomy of electroweak symmetry breaking. Tome I: The Higgs boson in the standard model*. Phys. Rep., Vol. 457, p. 1, 2008.
- [DMC⁺99] F. Dorchies, J. R. Marquès, B. Cros, G. Matthieussent, C. Courtois, T. Vélakorousov, P. Audebert, J. P. Geindre, S. Rebibo, G. Hamoniaux, and F. Amiranoff. *Monomode guiding of 10^{16} W/cm² laser pulses over 100 Rayleigh lengths in hollow capillary dielectric tubes*. Phys. Rev. Lett., Vol. 82, p. 4655, 1999.
- [DO 95] DO Collaboration. *Search for high mass top quark production in $p\bar{p}$ collisions at $\sqrt{s} = 1.8$ TeV*. Phys. Rev. Lett., Vol. 74, 2422, 1995.
- [DP08] A. Di Piazza. *Exact solution of the Landau-Lifshitz equation in a plane wave*. Lett. Math. Phys., Vol. 83, p. 305, 2008.
- [DPMHK12] A. Di Piazza, C. Müller, K. Z. Hatsagortsyan, and C. H. Keitel. *Extremely high-intensity laser interactions with fundamental quantum systems*. Rev. Mod. Phys., Vol. 84, p. 1177, 2012.
- [Dun09] G. V. Dunne. *New strong-field QED effects at extreme light infrastructure*. Eur. Phys. J. D, Vol. 55, p. 327, 2009.
- [DW85] D. A. Dicus and S. S. D. Willenbrock. *Higgs bosons from vector-boson fusion in e^+e^- , ep , and pp collisions*. Phys. Rev. D, Vol. 32, p. 1642, 1985.
- [DW89] D. A. Dicus and S. Willenbrock. *Higgs-boson production from heavy-quark fusion*. Phys. Rev. D, Vol. 39, p. 751, 1989.
- [EB64] F. Englert and R. Brout. *Broken symmetry and the mass of gauge vector mesons*. Phys. Rev. Lett., Vol. 13, p. 321, 1964.
- [EEG⁺09] J. R. Ellis, J. R. Espinosa, G. F. Giudice, A. Hoecker, and A. Riotto. *The probable fate of the Standard Model*. Phys. Lett. B, Vol. 679, p. 369, 2009.
- [EGN76] J. R. Ellis, M. K. Gaillard, and D. V. Nanopoulos. *A phenomenological profile of the Higgs boson*. Nucl. Phys. B, Vol. 106, p. 292, 1976. CERN preprint Nov. 1975.

- [EHLQ84] E. Eichten, I. Hinchliffe, K. Lane, and C. Quigg. *Supercollider physics*. Rev. Mod. Phys., Vol. 56, p. 579, 1984. Rev. Mod. Phys., Vol. 58, p. 1065, 1986 (Erratum).
- [EKK09] F. Ehlotzky, K. Krajewska, and J. Z. Kamiński. *Fundamental processes of quantum electrodynamics in laser fields of relativistic power*. Rep. Prog. Phys., Vol. 72, p. 046401, 2009.
- [ELIa] ELI - The Extreme Light Infrastructure. Home page of the Extreme Light Infrastructure.
URL:<http://www.extreme-light-infrastructure.eu/>.
- [ELIb] ELI beamlines. Lasers.
URL:<http://www.eli-beams.eu/science/lasers/>.
- [ER01] J. R. Ellis and D. Ross. *A light Higgs boson would invite supersymmetry*. Phys. Lett. B, Vol. 506, p. 331, 2001.
- [EZL98] P. A. Eminov, K. V. Zhukovskii, and K. G. Levchenko. *Production of Higgs with Z-boson by an electron in external fields*. arXiv:hep-ph/9804314, 1998.
URL:<http://arxiv.org/pdf/hep-ph/9804314.pdf>.
- [FGS79] J. Finjord, G. Girardi, and P. Sorba. *The needle in the large p_τ haystack: Higgs versus quark or gluon jets together with Z^0 in hadronic reactions*. Phys. Lett. B, Vol. 89, p. 99, 1979.
- [Fin80] J. Finjord. *A light Higgs boson: the decay $Z^0 \rightarrow H^0 l^+ l^-$* . Physica Scripta, Vol. 21, p. 143, 1980.
- [GGMN78] H. M. Georgi, S. L. Glashow, M. E. Machacek, and D. V. Nanopoulos. *Higgs bosons from two-gluon annihilation in proton-proton collisions*. Phys. Rev. Lett., Vol. 40, p. 692, 1978.
- [GH93] J. F. Gunion and H. E. Haber. *Higgs-boson production at the photon-photon collider mode of a high-energy e^+e^- linear collider*. Phys. Rev. D, Vol. 48, p. 5109, 1993.
- [GHK64] G. S. Guralnik, C. R. Hagen, and T. W. B. Kibble. *Global conservation laws and massless particles*. Phys. Rev. Lett., Vol. 13, p. 585, 1964.
- [GHKD00] J. F. Gunion, H. E. Haber, G. Kane, and S. Dawson. *The Higgs hunter's guide*. Front. Phys., Vol. 80, p. 1, 2000.
- [Gie09] H. Gies. *Strong laser fields as a probe for fundamental physics*. Eur. Phys. J. D, Vol. 55, p. 311, 2009.
- [Gin96] I. F. Ginzburg. *The e^+e^- pair production at $\mu^+\mu^-$ collider*. arXiv:hep-ph/9601273, 1996.
URL:<http://arxiv.org/pdf/hep-ph/9601273v1.pdf>.

- [GKP⁺84] I. F. Ginzburg, G. L. Kotkin, S. L. Panfil, V. G. Serbo, and V. I. Telnov. *Colliding γe and $\gamma\gamma$ beams based on single-pass e^+e^- accelerators II. polarization effects, monochromatization improvement*. Nucl. Instrum. Methods, Vol. 219(1), p. 5, 1984.
- [GKST81] I. F. Ginzburg, G. L. Kotkin, V. G. Serbo, and V. I. Telnov. *Production of high-energy colliding $\gamma\gamma$ and γe beams with a high luminosity at VLEPP accelerators*. Zh. Eksp. Teor. Fiz., Vol. 34, p. 514, 1981. [JETP Lett., Vol. 34, p. 491, 1982.].
- [GKST83] I. F. Ginzburg, G. L. Kotkin, V. G. Serbo, and V. I. Telnov. *Colliding γe and $\gamma\gamma$ beams based on the single-pass $e^\pm e$ colliders (VLEPP type)*. Nucl. Instrum. Methods, Vol. 205, p. 47, 1983.
- [GNY78] S. L. Glashow, D. V. Nanopoulos, and A. Yildiz. *Associated production of Higgs bosons and Z particles*. Phys. Rev. D, Vol. 18, p. 1724, 1978.
- [GSL] GNU Operating System. GSL - GNU Scientific Library.
URL:<http://www.gnu.org/software/gsl/>.
- [Hig64a] P. W. Higgs. *Broken symmetries and the masses of gauge bosons*. Phys. Rev. Lett., Vol. 13, p. 508, 1964.
- [Hig64b] P. W. Higgs. *Broken symmetries, massless particles and gauge fields*. Phys. Lett., Vol. 12, p. 132, 1964.
- [HMK06] K. Z. Hatsagortsyan, C. Müller, and C. H. Keitel. *Microscopic laser-driven high-energy colliders*. Europhys. Lett., Vol. 76, p. 29, 2006.
- [IK78] B. L. Ioffe and V. A. Khoze. *What can be expected from experiments on colliding e^+e^- beams with E approximately equal to 100-GeV?* Sov. J. Part. Nucl., Vol. 9, p. 50, 1978. [Fiz. Elem. Chast. Atom. Yadra, Vol. 9, p. 118, 1978.].
- [ILC] Linear Collider Collaboration. Home page of the International Linear Collider.
URL:<http://www.linearcollider.org/ILC>.
- [ILC07] ILC Global Design Effort and World Wide Study. *International Linear Collider Reference Design Report*. arXiv:0712.1950 [physics.acc-ph], 2007.
URL:<http://arxiv.org/pdf/0712.1950v1.pdf>.
- [IZ80] C. Itzykson and J.-B. Zuber. *Quantum Field Theory*. McGraw-Hill, Inc., New York, 1980.
- [Jac75] J. D. Jackson. *Classical Electrodynamics*. John Wiley & Sons, Inc., New York, 2nd edition, 1975.

- [JP79] D. R. T. Jones and S. T. Petcov. *Heavy Higgs bosons at LEP*. Phys. Lett. B, Vol. 84, p. 440, 1979.
- [Kei96] E. Keil. *The CERN Large Hadron Collider LHC*. LHC Project Report 83, 1996.
URL:<http://cds.cern.ch/record/321820/files/lhc-project-report-83.pdf>.
- [KKZ96] W. Kilian, M. Krämer, and P. M. Zerwas. *Higgs-strahlung and WW fusion in e^+e^- collisions*. Phys. Lett. B, Vol. 373, p. 135, 1996.
- [KMK⁺04] Q. Kong, S. Miyazaki, S. Kawata, K. Miyauchi, K. Sakai, Y. K. Ho, K. Nakajima, N. Miyanaga, J. Limpouch, and A. A. Andreev. *Electron bunch trapping and compression by an intense focused pulse laser*. Phys. Rev. E, Vol. 69, p. 056502, 2004.
- [KP05] A. E. Kaplan and A. L. Pokrovsky. *Fully relativistic theory of the ponderomotive force in an ultraintense standing wave*. Phys. Rev. Lett., Vol. 95, p. 053601, 2005.
- [Kun84] Z. Kunszt. *Associated production of heavy Higgs boson with top quarks*. Nucl. Phys. B, Vol. 247, p. 339, 1984.
- [LE09] W. P. Leemans and E. Esarey. *Laser-driven plasma-wave electron accelerators*. Phys. Today, Vol. 62, p. 44, 2009.
- [LJK08] E. Lötstedt, U. D. Jentschura, and C. H. Keitel. *Laser channeling of Bethe-Heitler pairs*. Phys. Rev. Lett., Vol. 101, p. 203001, 2008.
- [LL91] L. D. Landau and E. M. Lifschitz. *Lehrbuch der theoretischen Physik - Band 4: Quantenelektrodynamik*. Akademie Verlag, Berlin, 7th edition, 1991.
- [LNG⁺06] W. P. Leemans, B. Nagler, A. J. Gonsalves, Cs. Tóth, K. Nakamura, C. G. R. Geddes, E. Esarey, C. B. Schroeder, and S. M. Hooker. *GeV electron beams from a centimetre-scale accelerator*. Nat. Phys., Vol. 2, p. 696, 2006.
- [LQT77a] B. W. Lee, C. Quigg, and H. B. Thacker. *The strength of weak interactions at very high energies and the Higgs boson mass*. Phys. Rev. Lett., Vol. 38, p. 883, 1977.
- [LQT77b] B. W. Lee, C. Quigg, and H. B. Thacker. *Weak interactions at very high energies: the role of the Higgs boson mass*. Phys. Rev. D, Vol. 16, p. 1519, 1977.
- [Mül04] C. Müller. *Nichtlineare Paarerzeugung im Stoss eines relativistischen Kerns mit einem intensiven Laserstrahl*. PhD thesis, Universität Giessen, 2004.

- [Mal12] V. Malka. *Laser plasma accelerators*. Phys. Plasmas, Vol. 19, p. 055501, 2012.
- [Mes07] D. Meschede. *Optics, Lights and Lasers: The Practical Approach to Modern Aspects of Photonics and Laser Physics*. Wiley-VCH, Weinheim, 2nd edition, 2007.
- [ML09] M. Marklund and J. Lundin. *Quantum vacuum experiments using high intensity lasers*. Eur. Phys. J. D, Vol. 55, p. 319, 2009.
- [MMH⁺06] A. I. Milstein, C. Müller, K. Z. Hatsagortsyan, U. D. Jentschura, and C. H. Keitel. *Polarization-operator approach to electron-positron pair production in combined laser and Coulomb fields*. Phys. Rev. A, Vol. 73, p. 062106, 2006.
- [MO79] E. Ma and Y. Okada. *Possible means of detecting the Higgs boson in e^+e^- annihilation*. Phys. Rev. D, Vol. 20, p. 1052, 1979.
- [MS99] K. T. McDonald and K. Shmakov. *Temporary acceleration of electrons while inside an intense electromagnetic pulse*. Phys. Rev. STAB, Vol. 2, p. 121301, 1999.
- [MSK00] M. Melles, W. J. Stirling, and V. A. Khoze. *Higgs boson production at the Compton collider*. Phys. Rev. D, Vol. 61, p. 054015, 2000.
- [MTN08] P. J. Mohr, B. N. Taylor, and D. B. Newell. *CODATA recommended values of the fundamental physical constants: 2006*. Rev. Mod. Phys., Vol. 80, p. 633, 2008.
- [Nac86] O. Nachtmann. *Phänomene und Konzepte der Elementarteilchenphysik*. Friedr. Vieweg & Sohn, Braunschweig/Wiesbaden, 1986.
- [NIF] The National Ignition Facility. NIF home page.
URL:<https://lasers.llnl.gov/about/nif>.
- [Nol93] W. Nolting. *Grundkurs: Theoretische Physik - Band 3: Elektrodynamik*. Springer, Heidelberg and others, 1993.
- [NZ84] J. N. Ng and P. Zakarauskas. *QCD-parton calculation of conjoined production of Higgs bosons and heavy flavors in $p\bar{p}$ collisions*. Phys. Rev. D, Vol. 29, p. 876, 1984.
- [OT88] F. I. Olness and W. K. Tung. *When is a heavy quark not a parton? Charged Higgs production and heavy quark mass effects in the QCD-based parton model*. Nucl. Phys. B, Vol. 308, p. 813, 1988.
- [PS95] M. E. Peskin and D. V. Schroeder. *An introduction to Quantum Field Theory*. Addison-Wesley, Reading, Ma, 1995.
- [PTVF07] W. H. Press, S. A. Teukolsky, W. T. Vetterling, and B. P. Flannery. *Numerical Recipes in C++*. Cambridge University Press, Cambridge, 3rd edition, 2007.

- [Rei80] H. R. Reiss. *Effect of an intense electromagnetic field on a weakly bound system*. Phys. Rev. A, Vol. 22, p. 1786, 1980.
- [Rit85] V. I. Ritus. *Quantum effects of the interaction of elementary particles with an intense electromagnetic field*. J. Russ. Laser Res., Vol. 6, p. 497, 1985.
- [RRS06] R. Rabadán, A. Ringwald, and K. Sigurdson. *Photon regeneration from pseudoscalars at X-ray laser facilities*. Phys. Rev. Lett., Vol. 96, p. 110407, 2006.
- [RW79] R. Raitio and W. W. Wada. *Higgs-boson production at large transverse momentum in quantum chromodynamics*. Phys. Rev. D, Vol. 19, 941, 1979.
- [Sal68] A. Salam. *Weak and electromagnetic interactions*. In Proceedings Of The Nobel Symposium Held 1968 At Lerum, Sweden: Elementary Particle Theory, p. p. 367, 1968.
- [SH00] D. J. Spence and S. M. Hooker. *Investigation of a hydrogen plasma waveguide*. Phys. Rev. E, Vol. 63, p. 015401, 2000.
- [SLS⁺06] H. Schwoerer, B. Liesfeld, H.-P. Schlenvoigt, K.-U. Amthor, and R. Sauerbrey. *Thomson-backscattered X rays from laser-accelerated electrons*. Phys. Rev. Lett., Vol. 96, p. 014802, 2006.
- [SRJ01] S. Söldner-Rembold and G. Jikia. *Light Higgs production at a photon collider*. Nucl. Instrum. Methods A, Vol. 472, p. 133, 2001.
- [STF] STFC Central Laser Facility. The Vulcan 10 petawatt project.
URL:<http://www.clf.rl.ac.uk/New+Initiatives/The+Vul-can+10+Petawatt+Project/14684.aspx>.
- [SZ01] G. V. Stupakov and M. S. Zolotarev. *Ponderomotive laser acceleration and focusing in vacuum for generation of attosecond electron bunches*. Phys. Rev. Lett., Vol. 86, p. 5274, 2001.
- [Tan13] R. Tanaka. SM Higgs production cross sections at $\sqrt{s}=7$ TeV (update in CERN Report 3).
URL:<https://twiki.cern.ch/twiki/bin/view/LHCPhysics/CERNYellowReportPageAt7TeV>, 2013.
- [TD79] T. Tajima and J. M. Dawson. *Laser electron accelerator*. Phys. Rev. Lett., Vol. 43, p. 267, 1979.
- [Tel01] V. Telnov. *Photon collider at TESLA*. Nucl. Instrum. Methods A, Vol. 472, p. 43, 2001.
- [tH71] G. 't Hooft. *Renormalizable Lagrangians for massive Yang-Mills fields*. Nucl. Phys. B, Vol. 35, p. 167, 1971.

- [tHV72] G. 't Hooft and M. Veltman. *Regularization and renormalization of gauge fields*. Nucl. Phys. B, 44, p. 189, 1972.
- [UA183a] UA1 Collaboration. *Experimental observation of isolated large transverse energy electrons with associated missing energy at $\sqrt{s} = 540$ GeV*. Phys. Lett. B, Vol. 122, p. 103, 1983.
- [UA183b] UA1 Collaboration. *Experimental observation of lepton pairs of invariant mass around 95 GeV/c² at the CERN SPS collider*. Phys. Lett. B, Vol. 126, p. 398, 1983.
- [Vol35] D. M. Volkov. *Exact solution of Diracs equation for a plane wave of determined frequency*. Z. Phys., Vol. 94, p. 250, 1935.
- [Wei67] S. Weinberg. *A model of leptons*. Phys. Rev. Lett., Vol. 19, p. 1264, 1967.
- [Wei76] S. Weinberg. *Implications of dynamical symmetry breaking*. Phys. Rev. D, Vol. 13, p. 974, 1976.
- [WZ74a] J. Wess and B. Zumino. *A lagrangian model invariant under supergauge transformations*. Phys. Lett. B, Vol. 49, p. 52, 1974.
- [WZ74b] J. Wess and B. Zumino. *Supergauge transformations in four dimensions*. Phys. Lett. B, Vol. 70, p. 39, 1974.
- [YCK⁺08] V. Yanovsky, V. Chvykov, G. Kalinchenko, et al. *Ultra-high intensity-300-TW laser at 0.1 Hz repetition rate*. Opt. Express, Vol. 16, p. 2109, 2008.
- [Yar89] A. Yariv. *Quantum Electronics*. John Wiley & Sons, New York, 3rd edition, 1989.

Acknowledgments

I would like to conclude by expressing my gratitude and appreciation to a number of people without whom I would not have been able to finish this work.

Most prominently, I would like to thank Christoph H. Keitel for accepting me as a PhD student in the first place and for taking an interest in my research efforts, as well as for funding of several conferences and trips to the Düsseldorf University.

Carsten Müller might well be the world's best supervisor. I am deeply grateful for countless discussions, repeated encouragements, infinite patience, and not least of all intense proofreading. Thank you for always finding time for helping me out, even with the difficulties arising from your move to Düsseldorf.

I thank Karl-Tasso Knöpfle for agreeing to be my third supervisor and for helping me out when I was stuck while trying to familiarizing with the weak interaction processes.

To Carlo Ewerz I am grateful for writing the second review of this thesis.

I thank Felix Mackenroth for fruitful discussions, proofreading of this thesis and indispensable assistance over the years and in particular during the last couple of days. To my office mate Sven Augustin I am also indebted for many fruitful discussions as well as proofreading of the thesis and for countless instances of computer troubleshooting. Without you I would have probably been stuck with a mechanical typewriter. Other current and former group members that have contributed to the development of my thesis are Omri Har-Shemesh, Matthias Ruf, and Karen H. Hatsagortsyan.

I thank Adriana Pálffy-Buß, Stefano Cavaletto, Felix Mackenroth, Norman Neitz, Matthias Ruf, and Michael Ruggenthaler and everybody I probably forgot in this list for being more than just colleagues. I will never forget our theater plays, role playing games, weekend trips, and countless other private activities. The overall atmosphere provided by the work group made all these years a very enjoyable period of my life. I am very grateful for this and I hope to find people like you in my next employment as well.

There are so many other people I am indebted to that I do not even know where to start. I will therefore maybe just stick to the “order-of-appearance” approach.

I am forever grateful to my parents for their infinite support on so many levels I will not even try to list them all. But I would like to particularly thank you for lending me your car during the last couple of weeks and, maybe even more so, for enjoying doing it. And for always being there for me. I would also like to thank my sisters and their husbands for being in my life.

Chronologically next would be my friend Silf. When we met twenty-something years ago, I would have never thought that our friendship would grow so deep and last so long that I could not even try to imagine my life without her. Thank you for being just the way you are and for your emotional support during all these years. And for proofreading snippets of this thesis.

I would like to thank my current (and former) roommates for being my second family, for supporting me emotionally and for bearing with my negligence regarding the household chores during the final weeks of my thesis writing.

Last but not least, I wish to thank my boyfriend Konstantin for being there for me, for feeding me vitamins, for letting me use his kitchen table as a desk in many a night shift, and most of all, for never losing his patience despite his own thesis completion stress. You truly transformed one of the most stressful periods of my life into one of the most enjoyable ones.